Nucleation Process of the 2011 *Mw* 6.2 Northern Nagano Earthquake

January 2018

Kengo Shimojo

Nucleation Process of the 2011 *Mw* 6.2 Northern Nagano Earthquake

A Dissertation Submitted to
the Graduate School of Life and Environmental Sciences,
University of Tsukuba
In Partial Fulfilment of Requirements
for the Degree of Doctor of Philosophy in Science
(Doctoral Program in Earth Evolution Sciences)

Kengo Shimojo

Contents

Abstract

The seismicity in Japan after the 2011 Tohoku-Oki earthquake changed dramatically (e.g., Hirose et al., 2011). Most of these changes can be explained either by static (Ishibe et al., 2011; Toda et al., 2011a,b; Enescu et al., 2012) or dynamic (e.g., Yukutake et al., 2011; Miyazawa, 2011) stress changes due to the 2011 Tohoku-Oki earthquake.

The seismicity in a few inland regions of northeast Japan was also clearly activated following the M9.0 event (e.g., Toda et al., 2011). Given the compressional tectonic regime in northeast Japan, the seismicity in such areas, after the megathrust event, should have been inhibited rather than activated, if we assume the Coulomb failure criterion (Terakawa et al., 2012). Thus, the static stress transfer from the Tohoku-oki earthquake cannot explain this seismicity increase. It may be possible to relate such activation with dynamic stress changes caused by the passage of surface waves from the 2011 Tohoku-oki earthquake. However, based on the Japan Meteorological Agency (JMA) earthquake catalog, the seismicity in these inland areas was activated with a delay of more than several hours after the Tohoku-oki earthquake. Such a delay, if real, would make the dynamic triggering unlikely.

One of the inland areas in northeast Japan where the seismicity was clearly activated following the 2011 Tohoku-oki earthquake is the northern part of Nagano region. An Mw6.2 earthquake occurred here after about 13 hours from the Tohoku-Oki earthquake. A few sparse events started occurring earlier in the region, however according to the JMA earthquake catalog there is no recorded seismicity in the first 7 hours after the M9.0 event. To understand the triggering mechanism in the region, it is essential to have an earthquake dataset as complete as possible. Unfortunately, the seismicity immediately after large earthquakes is incompletely recorded in earthquake catalogs (Kagan, 2004).

In Chapter 2, as seismic catalogues are usually incomplete after large earthquakes, I have applied the Matched Filtered Technique (Peng and Zhao, 2009) to detect missing events within the first 13 hours after Tohoku-oki earthquake, using continuous waveforms and template events recorded at Hi-net seismic stations in Northern Nagano. As a result, I have identified 139 new events in the study area, with M1.0~3.0. Few of these events are located close to the hypocenter of the Mw6.2 earthquake, and many

others locate about 10km to the south, in an area where an Mw5.4 earthquake occurred about one month later.

In the northern area (around the Mw6.2 hypocenter) the activation of seismicity is relatively weak and there is no detection in the first 3h after the Tohoku-oki earthquake. However, a few earthquakes (foreshocks) occur very close to the hypocenter of the Northern Nagano earthquake, at short times before the Mw6.2 event. In the southern area, around the hypocenter of the Mw5.4 quake, the seismicity starts immediately after the megathrust event and shows episodic activation that consists in small events occurring in tight spatio-temporal clusters. In several of these clusters I have identified events that occur within the incoming surface-wave train from the Tohoku-oki earthquake, so were likely triggered dynamically. The seismicity in the south is shallower and shows an overall swarm-type behavior, although no clear migration could be identified. Furthermore, the early activation occurs in areas of relatively high near-surface fluid temperature, indicating that the dynamic triggering is likely caused by excitation of geothermal crustal fluids. These results bring detailed evidence on the essential role of geothermal activity, as revealed by shallow-depth fluid temperature data, as well as crustal fluid excitation to modulate seismicity activation.

In Chapter 3, I take advantage of the data recorded by a dense temporary seismic network operated by NIED from 2008 to 2012 to reveal with an unprecedented resolution the nucleation process that culminated with the occurrence of the Northern Nagano earthquake.

I have detected a total of 285 earthquakes in the source region of the Mw6.2 event. The earthquakes are relatively small, with magnitudes less than 2.5, and distribute within two spatially distinct clusters: one of these clusters was located close to the hypocenter of the Mw6.2 event (western cluster), the other about 5 km to the east (eastern cluster).

In the eastern cluster the seismicity starts within one hour after the Tohoku-oki earthquake. The events occur off the Mw6.2 fault and expand with time from shallow towards deep locations. In the western cluster the seismicity starts immediately after the passage of surface waves excited by a moderate earthquake in the Tohoku-oki aftershock area, which occurred 21 minutes after the Mw9.0 megathrust; most of these events distribute along the fault line of the Mw6.2 mainshock. Within the western seismicity area, a tight sub-cluster that occurred in the immediate vicinity (within about 2 km) of the Mw6.2 hypocenter was strongly activated thrice: about 9 hours before, 3 hours before and 50 minutes before the mainshock, respectively. In particular, about 9-

hours before and 3-hours before the Nagano earthquake, micro-seismicity migrated towards its epicenter, and just about 1-hour before, micro-seismicity accelerated within about several hundred meters of the M_w 6.2 epicenter. Migration speeds indicate potential underlying slow-slip culminating with the occurrence of the large inland earthquake, but fluids might have also played a triggering role at a broader, regional scale.

In both western cluster and eastern cluster some events occurred during or immediately after the passage of surface waves from some $M_{JMA} \geq 5.5$ Tohoku-oki aftershocks. I show that the local seismicity continued intermittently until the occurrence of the M6.2 event, being likely 'modulated' by the arrival of surface waves from larger teleseismic aftershocks off-shore Tohoku.

Key words: Matched-Filter Technique, Hi-net, Hizumi, Win system, 2011 Mw 6.2 Northern Nagano Earthquake, dynamic stress changes, fluid flow, aseismic slip, nucleation process

List of Figures

Chapter 1

Chapter 2

Chapter 3

Appendix

List of Tables

Chapter 3

Chapter 1

Introduction

1.1. Background of the research

The seismicity in many areas of central and northeastern Japan was activated following the M_w9.0 2011 Tohoku-oki earthquake (e.g., Hirose *et al*., 2011). While most seismicity changes are consistent with the static stress triggering hypothesis (e.g., Ishibe *et al*., 2011; Toda *et al.*, 2011; Enescu *et al*., 2012), there are areas in northeast Japan where the seismicity increase may not be due to static stress transfer. Considering the compressional tectonic regime of northeast Japan, the seismicity in these areas, after the megathrust event, should have been inhibited rather than activated, if we assume the Coulomb failure criterion (Terakawa *et al*., 2013). Two other physical mechanisms may have played an important role in the triggering of seismicity in northeast Japan.

One of them is dynamic triggering - a process where earthquakes are triggered by transient stress perturbations due to the passage of seismic waves from large earthquakes (Hill *et al.*, 1993). Because the attenuation of the dynamic stress changes as a function of distance from the source region of a large earthquake is smaller than that of the static stress changes, the dynamic stress changes play an important role for remote triggering. Dynamically-triggered remote earthquakes were observed immediately following the Landers (California), Hector Mine (California) and Denali (Alaska) earthquakes (Hill *et al*., 1993; Gomberg *et al*., 2001; Prejean *et al*., 2004); most of the triggered sites were located within areas of volcanic/geothermal activity. In Japan, although it is well known that deep low-frequency tremors on the subducting slab in west Japan are triggered by the seismic waves from distant earthquakes (e.g. Obara, 2003; Miyazawa and Mori,

2005), it has been assumed that remotely triggered crustal events, associated with dynamic stress changes, are inhibited to some extent due to a number of factors, including the compressional tectonic stress regime in Japan (Harrington and Brodsky, 2006). However, several recent studies that focused particularly on the earthquake triggering following the *M* 9.0 Tohoku-oki earthquake found relatively widespread seismicity activation likely due the strong shaking associated with the 2011 megathrust earthquake. Thus, Yukutake *et al*. (2011) found that dynamically-triggered earthquakes occurred during the passage of the surface waves of Tohoku-oki earthquake in the Hakone volcanic area. Miyazawa (2011) showed that dynamically-triggered earthquakes occurred in various regions including volcanic/geothermal areas and systematically propagated along the Japanese Islands; these events were associated with the surface wave propagation from the source area of the Tohoku-oki earthquake.

The other mechanism is fluid-related triggering - a process where earthquakes are triggered by fault weakening caused by the accumulation of pore fluid pressure (Sibson, 1990). It has long been known that crustal fluids play an important role in earthquake generation (e.g. Nur and Booker, 1972). In some studies, a diffusion process of pore fluids is associated with seismicity triggering or migration of seismicity, and the pore fluid pressure fields can be changed by the occurrence of large earthquakes (e.g. Miller *et al*., 2004). The changes of pore fluid pressure following large earthquake may be interpreted as the changes of permeability related to static or dynamic stress changes from large earthquake (e.g. Muir-Wood and King, 1993; Brodsky *et al*., 2003). Terakawa *et al*. (2013), as a result of analysis of the focal mechanism solutions of local seismicity in some inland regions in northeast Japan (e.g. the Northern Nagano region), showed that pore fluid pressure is increased following Tohoku-oki earthquake, and indicate that such

seismicity activation is caused by the over-pressured fluid flow from a deep reservoir or increase in fault-confined fluid pressure.

However, one of the major problems in assessing the role of various triggering factors is the relatively large earthquake catalog incompleteness in the hours following the megathrust event (Lengliné *et al*., 2012; Kato *et al*., 2013). The direct investigation of high-pass filtered waveforms (e.g., Peng *et al*., 2006; Enescu *et al*., 2007, 2009; Peng and Zhao, 2009; Kato *et al.*, 2012; Marsan and Enescu, 2012; Sawazaki and Enescu, 2014) to detect missing events in the aftermath of a large earthquake is essential for an unbiased interpretation of the seismicity pattern. Note that waveform-based methods can also contribute to a more accurate and complete detection of foreshocks (e.g., Doi and Kawakata, 2012), which are sometimes too small and thus missing from the earthquake catalogues.

Here, in this study, I reveal the detailed local seismicity of a specific area located at northern Nagano region, central Japan, where a moment-magnitude (Mw) 6.2 crustal earthquake occurred at shallow depth, 13 h after the megathrust event by applying Matched-filter technique (MFT) (Shelly *et al*., 2006; Peng and Zhao, 2009) to regional seismic network.

1.2. Seismicity in the Northern Nagano region

At first, I focus on the Northern Nagano region, central Japan, where an M_w6.2 earthquake occurred about 13 hours after the Tohoku-oki event. The study area is located about 400 km west of the Tohoku-oki epicentral region. According to the Japan Meteorological Agency (JMA) catalogue, 8 sparse events started occurring earlier in the region, however there is no recorded seismicity in the first 6 hours after the *M* 9.0 event (Figure 1). To understand the triggering mechanism in the region, it is essential to have an earthquake dataset as complete as possible.

Unfortunately, the seismicity immediately after large earthquakes is incompletely recorded in earthquake catalogs (e.g., Kagan, 2004; Enescu *et al*., 2007, 2009; Peng and Zhao, 2009). Therefore, by applying MFT to the waveform data recorded at the permanent and temporary stations in the region, I was able to obtain a much more complete event history, compared with the one catalogued by the JMA. Using such improved catalogue. I reveal distinct spatial seismicity activation patterns, which were otherwise impossible to decipher. The results presented in this thesis bring detailed evidence on the essential role of crustal fluid excitation to modulate seismicity activation.

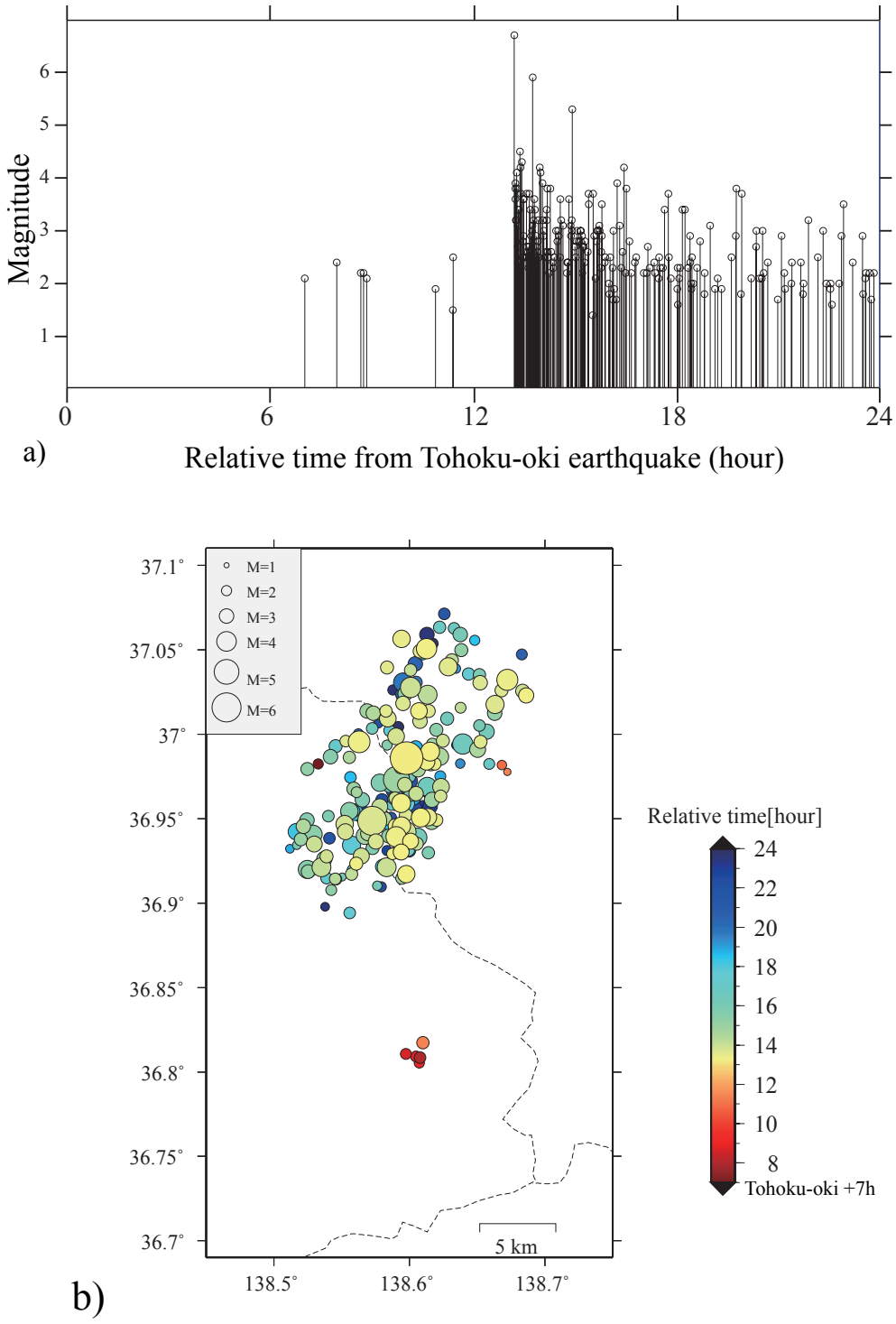

Figure 1. Spatio-temporal distribution of earthquakes (JMA catalogue, M>0) within 1 day from the M 9.0 Tohoku-oki earthquake: (a) Earthquakes magnitude versus time plot (b) Spatial distribution of earthquakes, colored as a function of time from the Tohoku-oki megathrust event.

Chapter 2

Fluid-driven Seismicity Activation in Northern Nagano Region After the 2011 M9.0 Tohoku-oki Earthquake: MFT-analysis to Hi-net Observation Network

2.1. History of Matched-filterMethod

It is known that earthquake catalogues are incomplete immediately after large earthquakes because the *P*- and *S*-wave phases of smaller aftershocks are usually obscured by the overlapping, relatively large-amplitude coda waves of the mainshocks, as well as the wave-phases of other aftershocks (Kagan, 2004). In some previous studies, the high-pass filtering of waveform data helped the detection and quantification (time, magnitude) of missing early aftershocks (e.g. Peng *et al*., 2006; Enescu *et al*., 2007; Marsan and Enescu, 2012), which were otherwise "hidden" by the lower-frequency coda waves. However, this method does not provide hypocenter locations for the missing events.

A powerful technique that has been used in many recent studies (e.g., Peng and Zhao, 2009; Bouchon *et al*., 2011; Kato *et al*., 2012, 2013; Lengline *et al.*, 2012) uses cross-correlations between waveforms of already catalogued events and continuous waveform data to detect additional new earthquakes (this method will be described in detail below). Other techniques that are currently being applied to produce more complete early-aftershock datasets include the back-projection method (e.g., Kiser and Ishii, 2013) and an inversion method that uses continuous high-frequency seismogram envelopes to image the energy radiation process (Sawazaki and Enescu, 2014).

In this study, I used the Matched-Filter Technique (MFT) (Peng and Zhao, 2009) – a method where undetected events are identified by cross-correlating template waveforms (of cataloged

events with known occurrence times, locations and magnitudes) and continuous waveforms at recording stations in the area. All waveforms are high-pass filtered, so the influence of longer-period mainshock coda waves is attenuated. Shelly *et al*. (2006) first applied this method to continuous waveform records during non-volcanic tremor activity, and detected many low-frequency earthquakes in western Shikoku. Peng and Zhao (2009) applied it to the continuous waveforms recorded after the 2004 Parkfield earthquake, and detected 11 times more aftershocks than listed in the standard catalogue, which helped them reveal migration of early aftershocks. In addition, the Matched-Filter Technique is also used to detect and recover foreshocks (e.g. Bouchon *et al*., 2011; Kato *et al.*, 2012) and remotely triggered earthquakes (e.g. Meng *et al*., 2012). The detailed analysis procedure is described below.

2.2. Data and Methods

I use continuous three-component seismic velocity recordings from 10 borehole stations (Figure 1) of the Japanese High Sensitivity Seismograph Network (Hi-net), operated by the National Research Institute for Earth Science and Disaster Prevention (NIED), in the northern Nagano region. All stations are recording at a sampling rate of 100 Hz. Continuous waveforms are 13 hours and 15 minutes long and start on March 11, 2011 at 14:46:00 local time (18 seconds before the Tohoku-oki mainshock origin time) and end on March 12, 2011 at 4:01 local time (about 2 minutes after M_w6.2 Northern Nagano earthquake). I applied a two-way 10–30 Hz Butterworth filter to the data to reduce the influence of the low frequency coda wave of the Tohoku-oki mainshock, as well as that of aftershocks that occurred at remote distances from northern Nagano (Figure 2). Figure 2 shows that clear local seismicity can be seen on the continuous waveforms

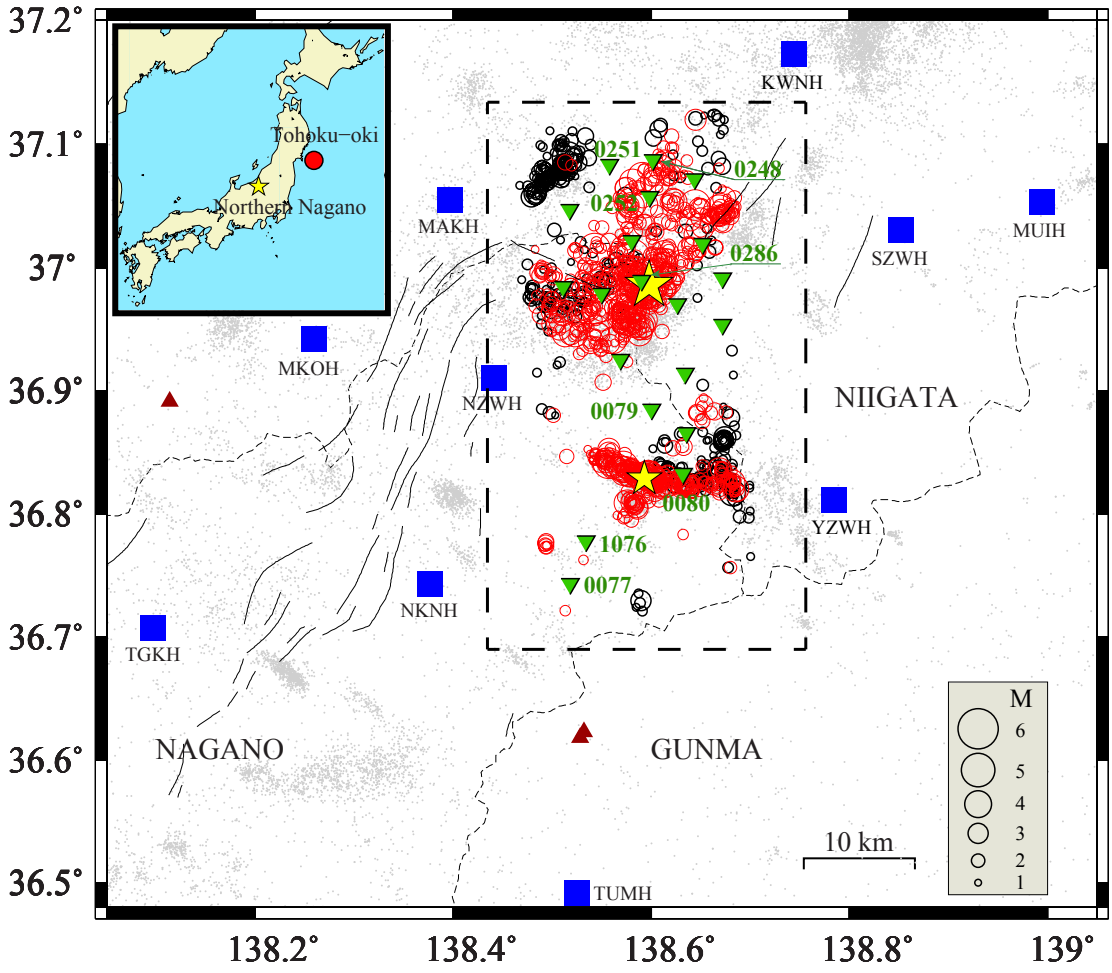

Figure 1. Earthquake and station distributions in Northern Nagano. The time span of earthquake data is January 2001 to February 2013. Red and black circles indicate relocated template events ($M \geq 1.0$) occurred before and after the 2011 Tohoku-oki earthquake, respectively; the gray circles show all JMA events in a broader region. The blue squares and inverted green triangles represent Hi-net borehole and temporary surface stations, respectively. Yellow stars show the Northern Nagano earthquake and the April 12, 2011 M_w5.4 event to the south. Brown triangles show volcanoes. Dotted rectangle delimits the study area. Inset shows the Japanese Islands and the epicenters of the 2011 Tohoku-oki and Northern Nagano earthquakes by a red circle and yellow star, respectively. The light dashed lines and thin solid lines show prefecture borders and faults respectively.

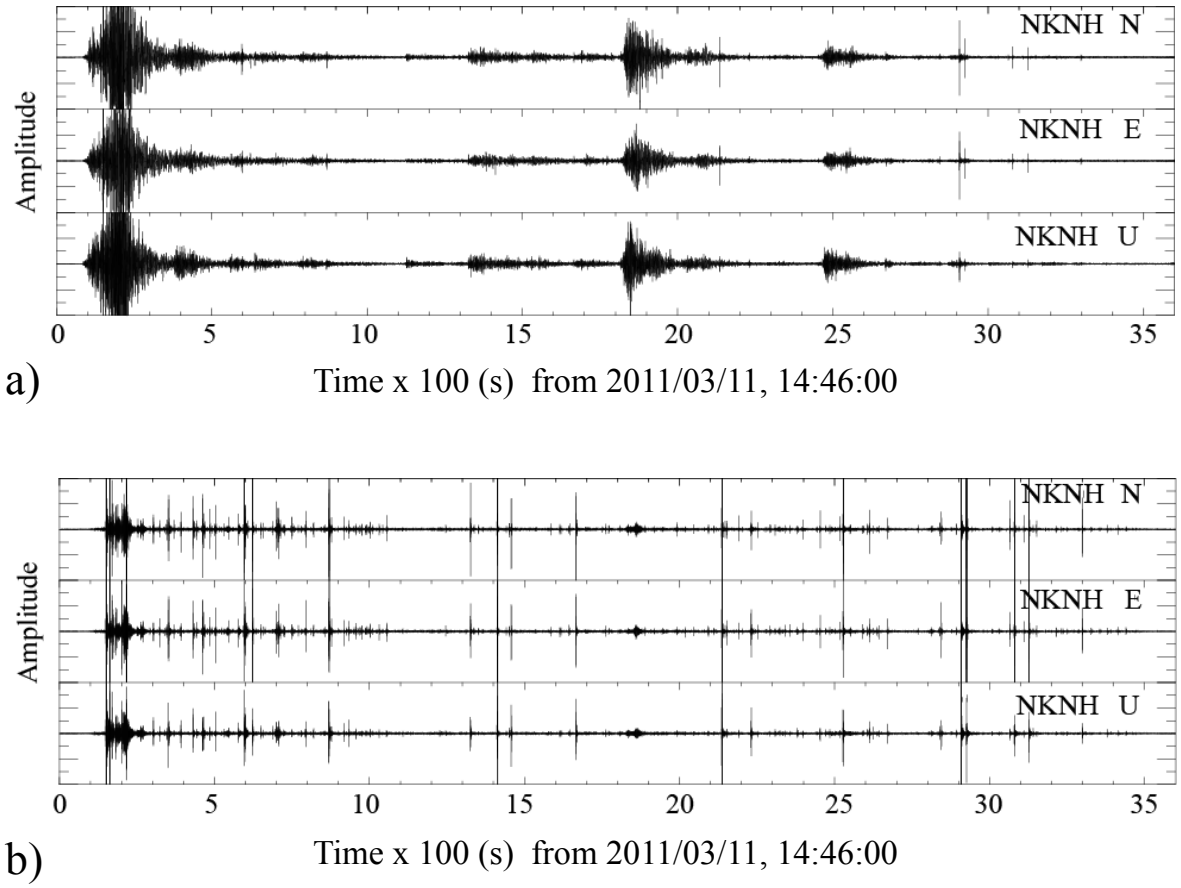

Figure 2. Comparison the unfiltered and filtered waveforms: (a) The unfiltered three component waveforms recorded at the Hi-net station NKNH. (b) The waveforms at the same station, band-pass filtered between 10 to 30 Hz, which shows local triggered events.

by band-pass filtering.

I use all 1278, $M \geq 1.0$, events of the Hi-net catalogue that occurred between January 2001and February 2013 in the study region (36.70-37.12°N; 138.44-138.74°E; Figure 1) as template events. To improve the accuracy of the routine earthquake locations, the template earthquakes were relocated using a double-difference approach (Zhang and Thurber, 2003). The earthquakes become shallower by a few kilometers after relocation and more clustered in space. The RMS of the double-difference time residual was reduced from 257 ms to 52 ms. Most events in the hypocentral region of the Northern Nagano earthquake are deeper than 5 km, while those clustered about 10 km to the south (Figure 1) locate in majority between 2 to 5 km depth. I used 4-seconds long waveform windows for each template event, recorded at each station component, starting 2 seconds before the *S*-wave arrival time, and applied the same filtering as for the continuous data. Only waveforms for which the signal to noise (measured as the average waveform amplitude from -6 to -2 seconds before the *P*-wave arrival) ratio is larger than 5 were used for further processing.

I look for events in the continuous data that strongly resemble the template events (Figure 3 and 4). In Figure 3, I show a simple example of the Matched-Filter Technique analysis. The correlation coefficient between the continuous waveforms and templates, at each recording station (and for each of the three components), is calculated by shifting the template window in increments of 0.01 seconds (Figure 3, top and center). The correlation coefficient value obtained at each time point is assigned to its origin time by subtracting the *S*-wave arrival time. Next, I stack the correlation coefficient values for all stations and three components, and compute the mean correlation coefficient value at each time point (Figure 3, bottom). I then compute the Median Absolute Deviation (MAD) of the mean correlation coefficient trace for each template

event and use 9 times the MAD-value as the detection threshold (Peng and Zhao, 2009). The location of each waveform-detected event was assigned to be the same as that of the corresponding template earthquake. I end up with a catalogue of 139 events, compared with only 8 in the JMA catalogue, for the 13-hour time period following the Tohoku-oki mainshock.

The magnitude of each MFT-detected event was estimated by comparing the waveform amplitudes of detections and templates, assuming that a tenfold increase in amplitude corresponds to one unit increase in magnitude. To minimize the underestimation of larger event magnitudes at high frequencies (e.g., Shearer, 2009; Figure 9.24), I use 5 Hz high-pass filtered waveforms for magnitude calibrations.

Since the start of earthquake activation is of primary interest for understanding the triggering mechanism, I have scrutinized continuous waveforms recorded by a dense, regional seismograph network (Figure 1) in the first ~30 minutes after Tohoku-oki earthquake. Although these stations are installed at the surface and their recordings are relatively noisy, their proximity to the events occurred in the study area helps the detection of smaller earthquakes. Based on the identified *P*- and *S*-wave arrival times at both the regional network and Hi-net stations, I have located 7 events that occurred from 130 s to 590 s after the Tohoku-oki earthquake, corresponding roughly with the time period of the mainshock surface wave arrivals in Northern Nagano.

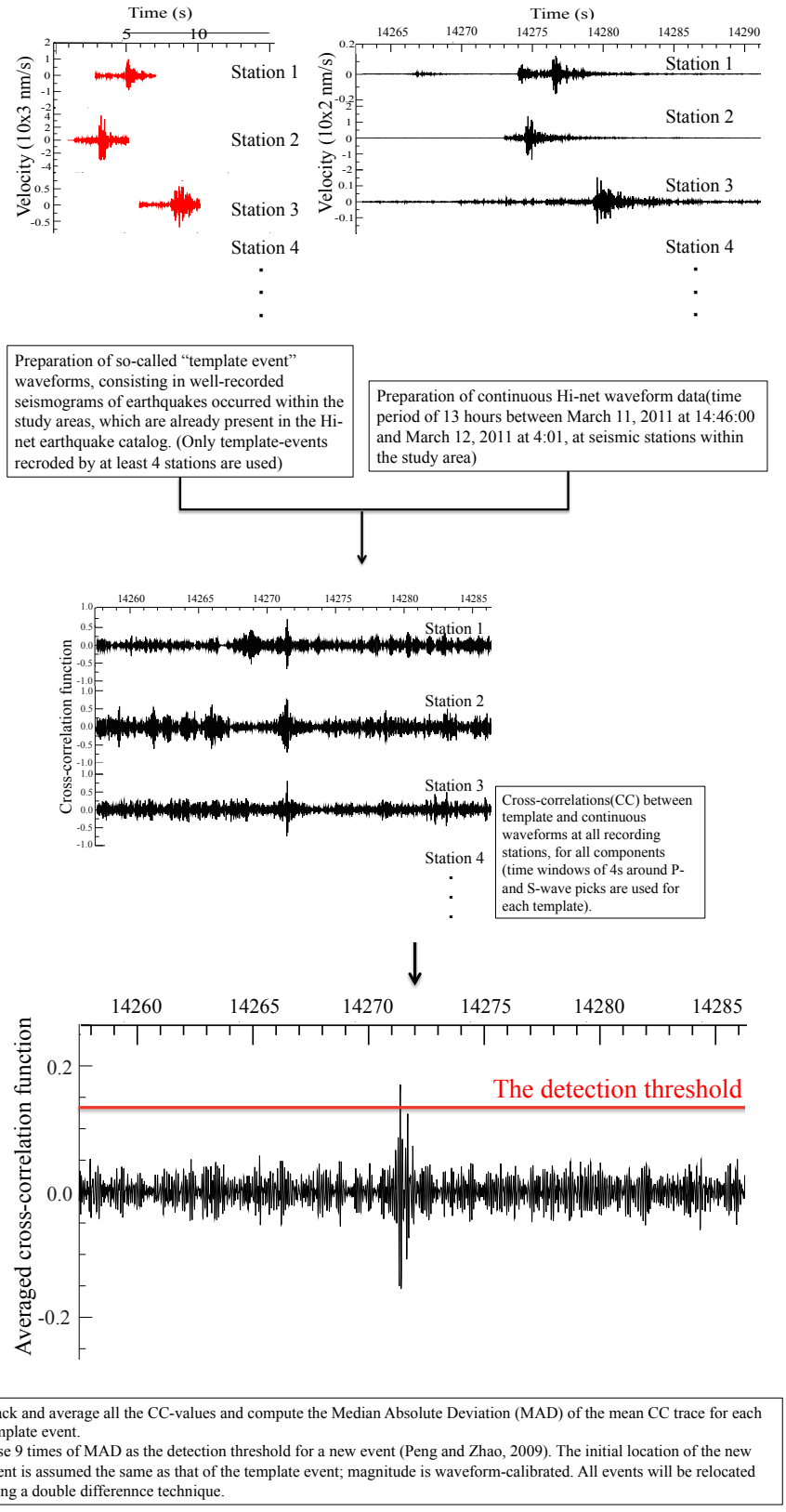

Figure 3. Step-by-step description of the Matched-Filter Technique

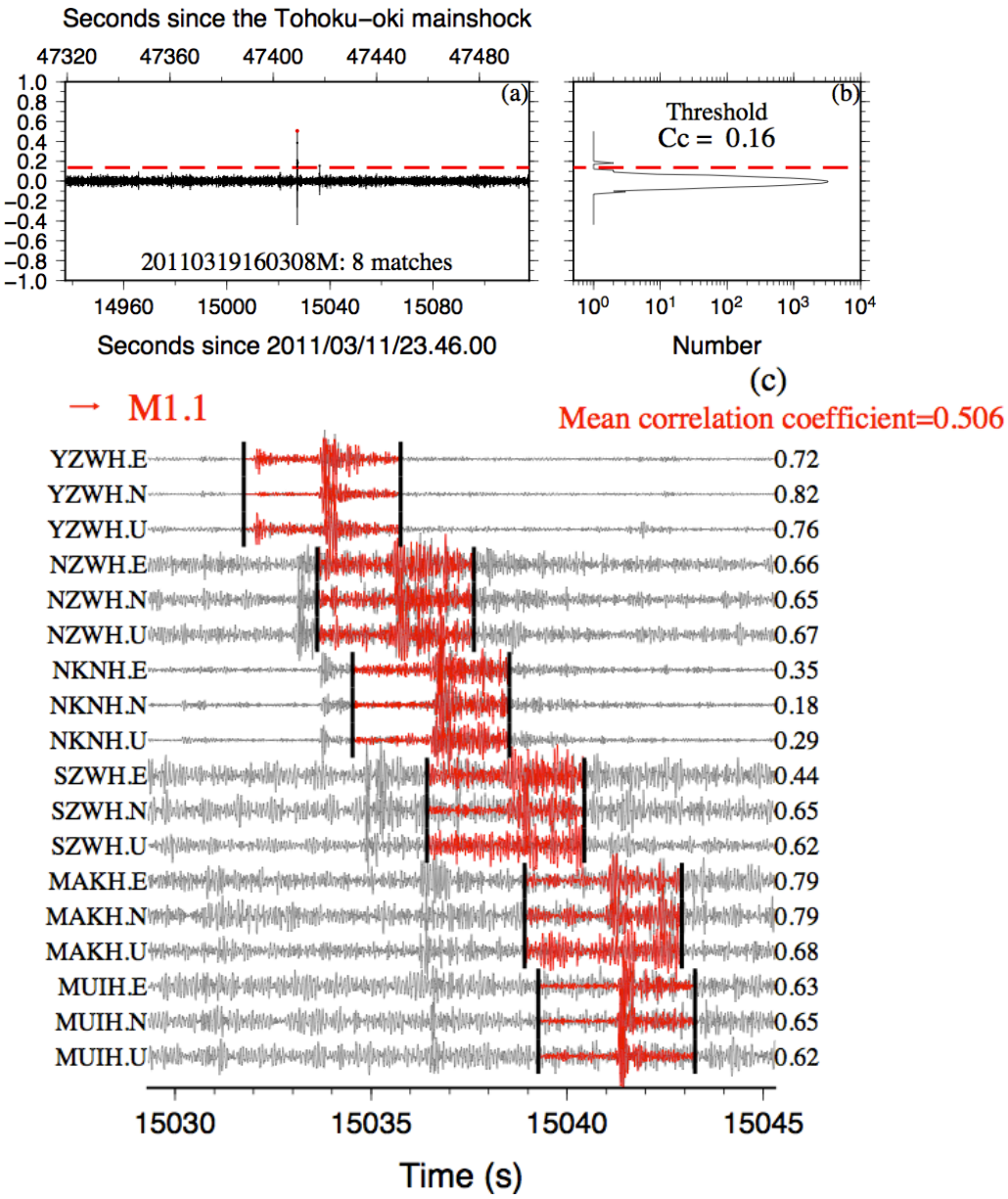

Figure 4. Example of earthquake detection, using MFT: (a) Stacked, continuous cross-correlation function, between one template event (20110311172306M) and the continuous waveform data, recorded at Hi-net stations in the region; (b) Histogram of stacked cross-correlation values in (a). The horizontal dotted line corresponds to the threshold CC-coefficient used in this study; (c) Continuous waveforms (gray) together with the superposed template seismograms (red) at a position corresponding to an average CC-coefficient of 0.39, recorded at Hi-net stations (vertical, north and east components) in the region

2.3 Results

Among the 139 MFT-detections, only 13 were located in the aftershock area of the M_w6.2 earthquake ("North" area), while the majority of the rest located about 10 km to the south ("South" area) (Figure 5a). Since the station coverage (Figure 1) is about the same for both regions, I am confident that the relatively intense activation in the "South" is genuine.

The temporal distribution of events (Figures 5b-d), does not show the characteristic Omori law decay following the occurrence time of Tohoku-oki earthquake. Indeed, a modified Omori law fit (Figure 5b) to the earthquake data in the whole study area, above the completeness magnitude (M1.2 – Figure 6), has an unusually low p-value (the slope of the modified Omori law distribution) of 0.11, indicating a quasi-constant occurrence rate of events in the Nagano region, during the 13h observation period (Figure 5b).

In the "North" area the seismicity is relatively weak and there are no detections in the first three hours following the Tohoku-oki earthquake (Figure 5b). A few isolated events occurred within this area three to seven hours after the Tohoku-oki mainshock, but at a distance from the M_w6.2 hypocenter. Two small foreshocks occurred close to the hypocenter of the M_w6.2 event, within one hour of its origin time.

In the "South" the seismicity activation is sudden and relatively strong. Note that I have applied the MFT method using the continuous Hi-net waveforms 4 hours prior the Tohoku-oki mainshock and found no evidence of local seismicity. The seismicity in the "South" starts immediately after the megathrust event and shows episodic activation, mainly associated with the

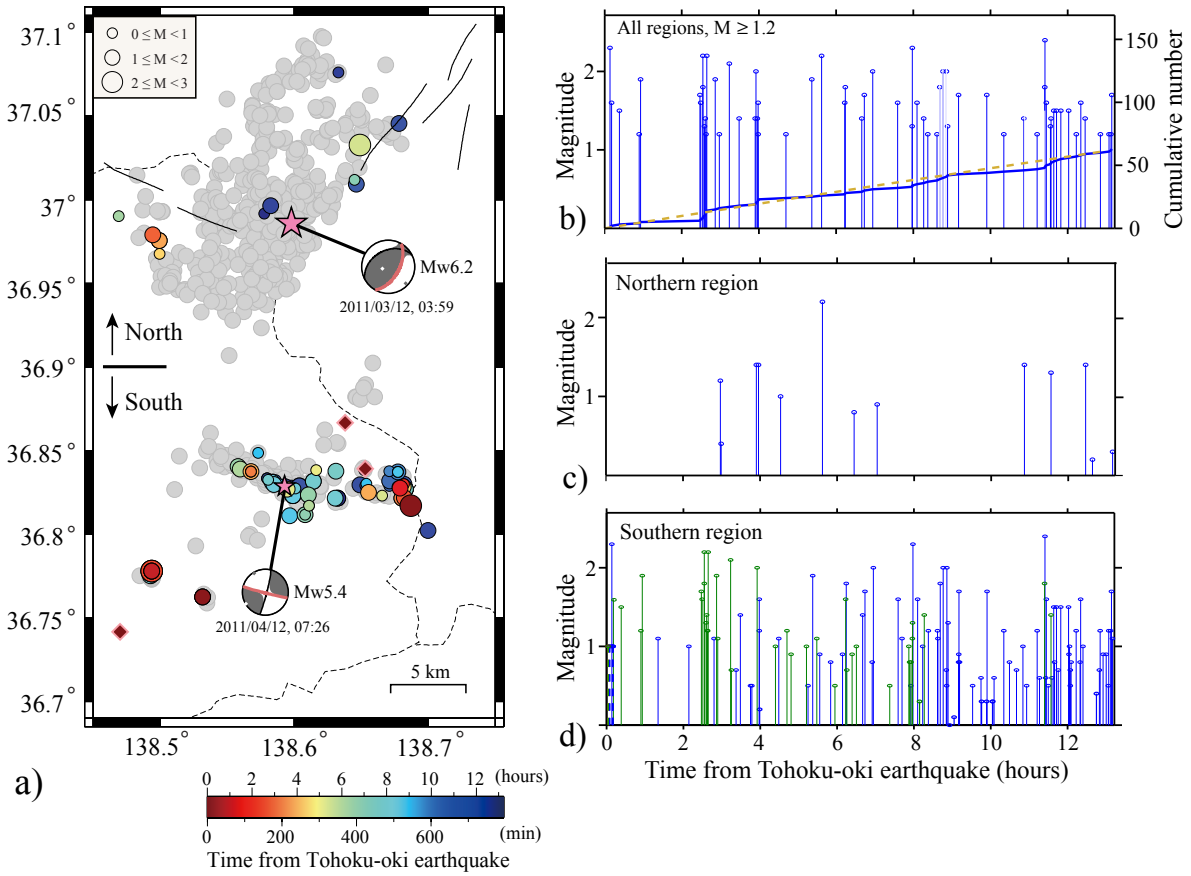

Figure 5. Seismicity distribution in the study region: (a) Map view showing the MFT-detected earthquakes, colored as a function of time from the Tohoku-oki megathrust event; the one-month relocated Hi-net aftershocks are shown in gray. Diamonds represent early events detected by inspecting the temporary seismic stations in the region; The focal mechanisms of the March 12, 2011 Northern Nagano earthquake and April 12, 2011 event are also shown. The nodal planes on which static stress changes are calculated are colored in red. "North" and "South" indicate the two regions referred in the text. (b), (c) and (d) Time history of seismicity for the whole region in (a) and for the "North" and "South" areas, respectively. Solid blue lines in (b) show the cumulative number of events for detections, and the dotted line represents an Omori-Utsu law fit to the data, as explained in the text. The stems shown in green, in (d), are earthquakes occurred in the southernmost area of the study region, and the dotted stems show events with locations determined by picking *P*- and *S*-wave arrivals on the temporary and Hi-net seismograms.

occurrence of a few larger events ($M \geq 2.0$) (Figure 5d, blue stems). The majority of detected earthquakes align along an E-W direction, likely associated with a fault plane of similar strike. Both the strike and dip angles of the southern cluster are consistent with one of the nodal planes of the M_w5.4 earthquake, which occurred about one month later (Figure 7).

As previously mentioned, I have inspected the seismograms recorded by stations of a regional seismic network (installed temporary in the region before Tohoku-oki event) at early times after the megathrust. Figure 8 shows an example of early event activation recorded in the southernmost area of the study region; the high-pass filtered seismogram (Figure 8a, bottom) at "0077" station (Figure 1) reveals the occurrence of nearby small earthquakes. The earliest event in this area that I was able to locate occurred 131 s after the origin of the Tohoku-oki earthquake, during the passage of the mainshock surface waves. Activation at similar early times was also observed within the main "South" cluster (at station "0080"). The earliest event located here occurred ~292 s after the megathrust event. The events located using arrival times observed at both the temporary network and Hi-net stations are plotted as diamonds in Figure 5a. The magnitudes are around 1.0, however have relatively large uncertainties. I did not observe similar early activation in the "North", despite the very good station coverage. The seismicity in southernmost area of the study region continued after the passage of the mainshock surface waves, and most events occurred at a same site around an event triggered during surface wave (Figure 5a and 5d, green stems). There is a relative sparseness of seismicity in the first ~2.5 hours after Tohoku-oki earthquake: I attribute it to the difficulty of detecting events of $M \sim 1.0$ due to the very "noisy" waveforms immediately after the M 9.0 event.

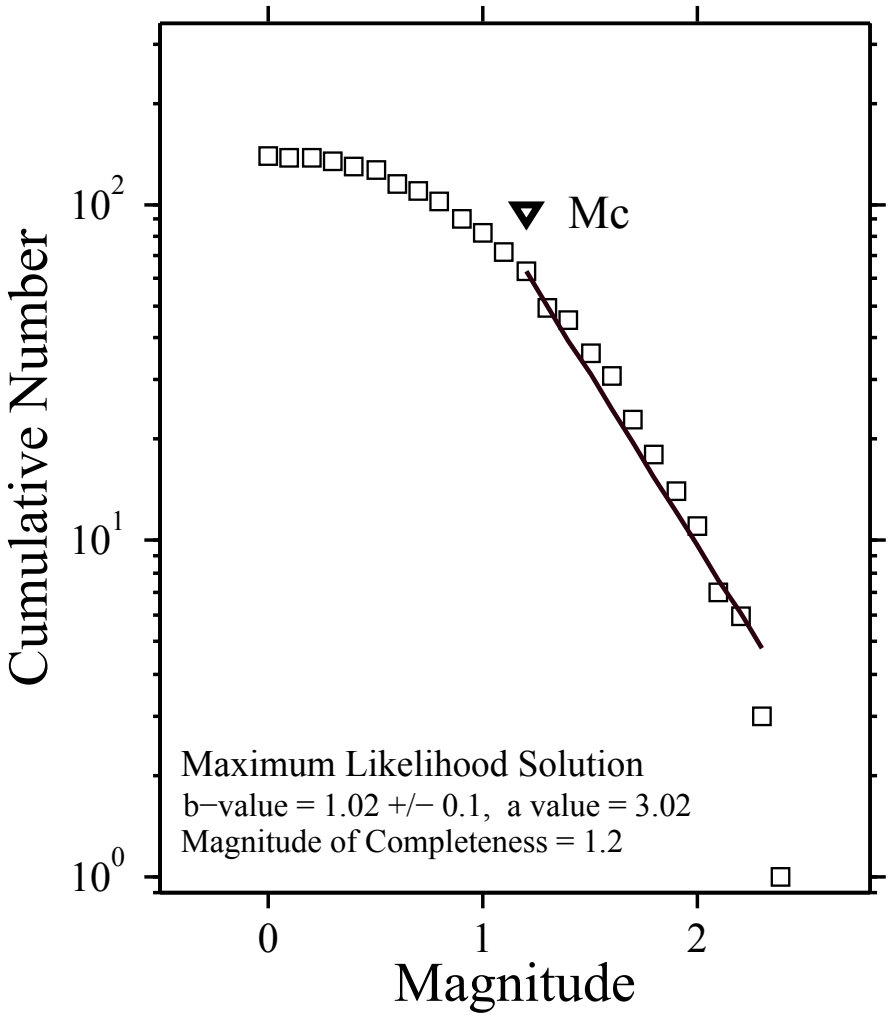

Figure 6. Frequency-magnitude distribution of MFT-detected earthquakes (Figure 6) in the Northern Nagano region

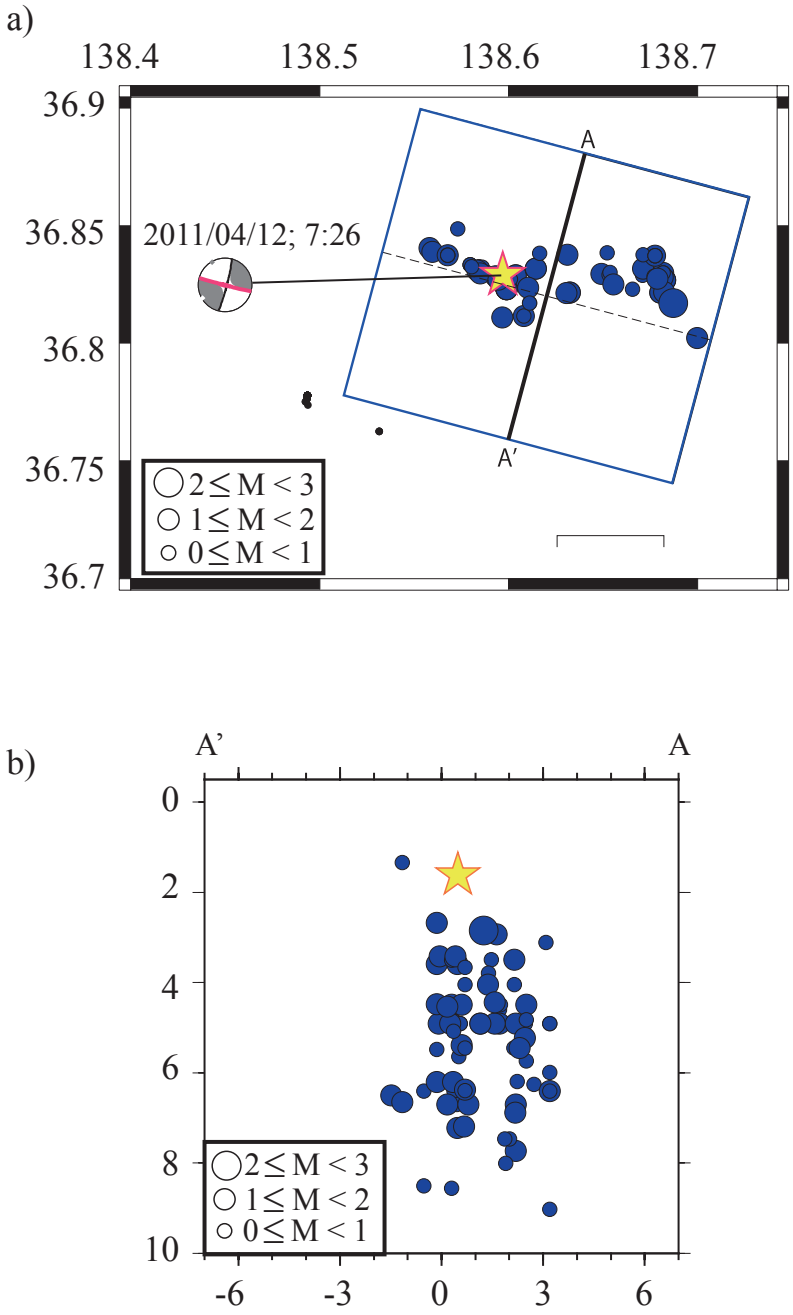

Figure 7. (a) Map view of events in the southern region and (b) cross-section along the profile AA' in (a). The focal mechanism shown in (a) corresponds to the *M* 5.4 April 12, 2011 earthquake. The AA' direction corresponds to the strike of one of the *M* 5.4 nodal planes (shown as a thick red line).

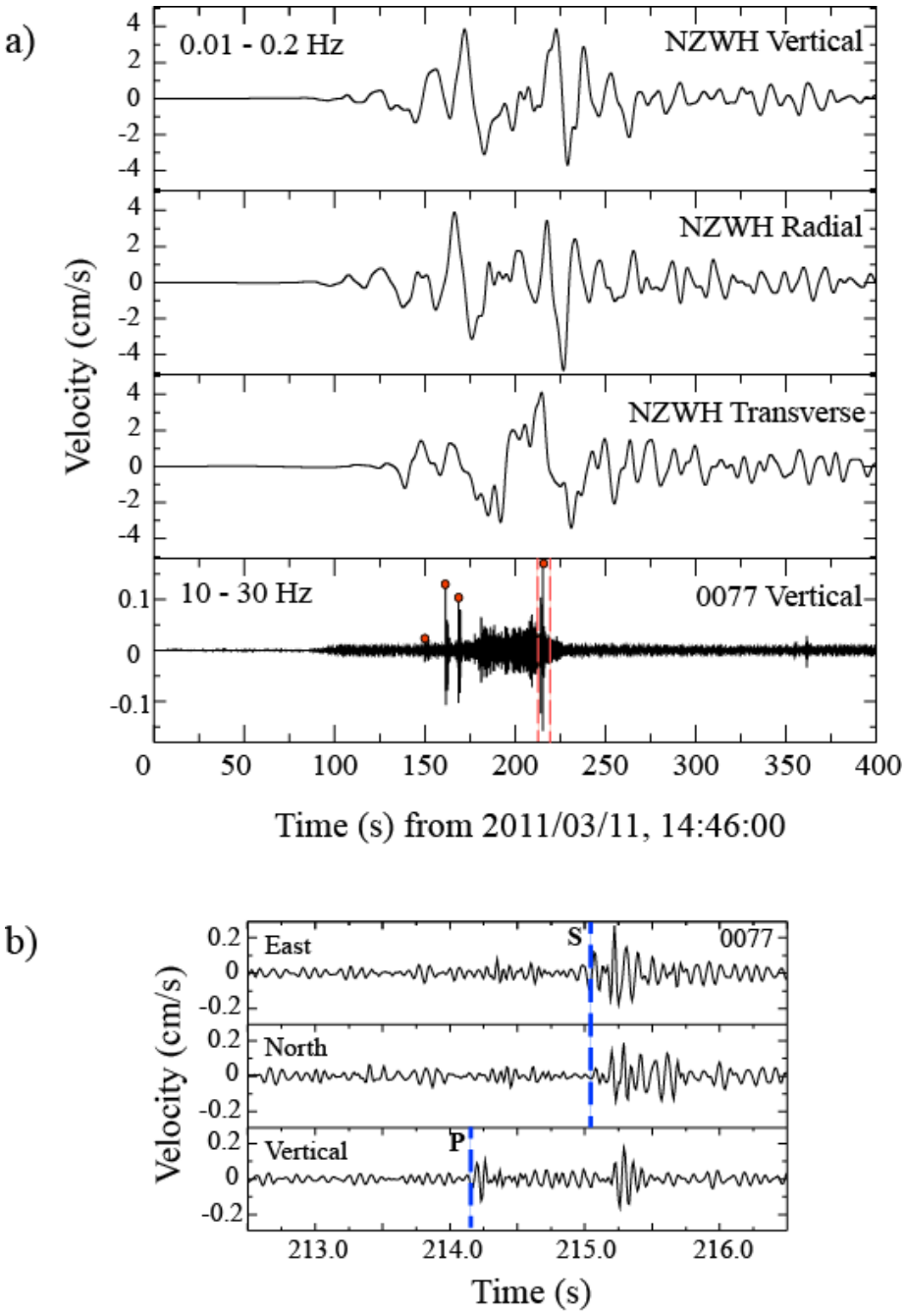

Figure 8. Earthquakes detected during the passage of surface waves from the Tohoku-oki earthquake. (a) From top to bottom: low-frequency seismograms (0.01 – 0.2 Hz) at the NZWH station (Vertical, Radial and Transverse components) and high-frequency waveform (10 – 30 Hz) at the temporary station 0077; locally triggered events are marked by small red circles; discontinuous red lines indicate the time interval used for zooming in (b). (b) Enlarged high-frequency seismogram showing *P*- and *S*-wave arrivals from one of the triggered events

2.4. Discussion

2.4.1. Dynamic triggering and fluid-related seismicity activation

Several events occurred in the southernmost part of the study region (Figure 5a) during the passage of surface waves (Figure 8a) from the Tohoku-oki earthquake. I estimate the peak dynamic stress changes associated with the passage of Love and Rayleigh waves in the area from the amplitudes of the surface wave ground velocities (e.g., Peng *et al*., 2009) recorded by the NZWH station (Figure 1). Assuming plane wave propagation for teleseismic waves, the peak dynamic stress σ_d is proportional to Gu'/v_{ph} (Jaeger and Cook, 1979), where G is the shear modulus, u' is the peak particle velocity, and v_{ph} is the phase velocity. Using a nominal G value of 30 GPa, v_{ph} = 4.1 km/s for the Love waves, and v_{ph} = 3.5 km/s for the Rayleigh waves, I estimated maximum dynamic stress change values of 300 kPa and 417 kPa, for the Love and Rayleigh waves, respectively. The occurrence of the southernmost earthquakes during the passage of Tohoku-oki surface waves, as well as the significant dynamic stress level, indicate that they were triggered dynamically.

Since there are no broad-band F-net stations close to the area where dynamic triggering was observed in northern Nagano, the waveform data at the Hi-net station NZWH, band-pass filtered between 0.01 to 0.2 Hz, was used instead for surface-wave dynamic stress calculations. Although Maeda *et al*. (2011) showed that the Hi-net waveform data can be successfully used to retrieve long-period ground motions after applying an appropriately designed recursive filter to the data (such a processing was done in this study), some limitations may exist due to the fact that the Hi-net seismometers are not truly broad-band. Here I briefly investigate such possible limitations,

for the study area, by comparing Hi-net and F-net recordings. In the upper three panels of Figure 9 I show superposed band-pass filtered waveforms at the NZWH station (Hi-net) and ONS station (F-net). Since stations NZWH and ONS are located 412 km and 406 km away from the Tohoku-oki epicenter, respectively, the waveform amplitudes should not differ significantly taking into account the relatively slow surface-wave attenuation with distance ($\sim r^{2/3}$). As Figure 9 confirms, the waveform amplitudes observed at the Hi-net and F-net stations are of the same order. The maximum absolute amplitude values for the vertical, radial and transverse waveform components are of 4.70 cm/s, 5.23 cm/s, and 7.14 cm/s, at the ONS station, respectively. The corresponding dynamic stress changes are 403 kPa, 448 kPa and 522 kPa, at the ONS station. The phases are in rather good agreement at the beginning of the surface-wave signal (note that the surface waveforms are shifted in such a way as they were recorded at the station 0077, assuming propagation velocities of 4.1 km/s and 3.5 km/s for the Love and Rayleigh wave velocities, respectively), however, later on, the phase mismatch is more significant, probably because of dispersion effects. The maximum waveform amplitudes at the Hi-net station are smaller than those observed at the F-net station, which might be caused by the limitations of Hi-net data at low frequencies.

Two main classes of models (Hill and Prejean, 2006) are used to explain the triggering by dynamic stresses: 1) direct triggering by frictional failure, and 2) triggering through excitation of crustal fluids. With regard to the latter, some previous research modeled hydrous fluid transfer caused by opening permeable fractures clogged by accumulating detritus (e.g. Brodsky *et al*., 2003), or bubble excitation during the dilatational phase of the surface wave from distant

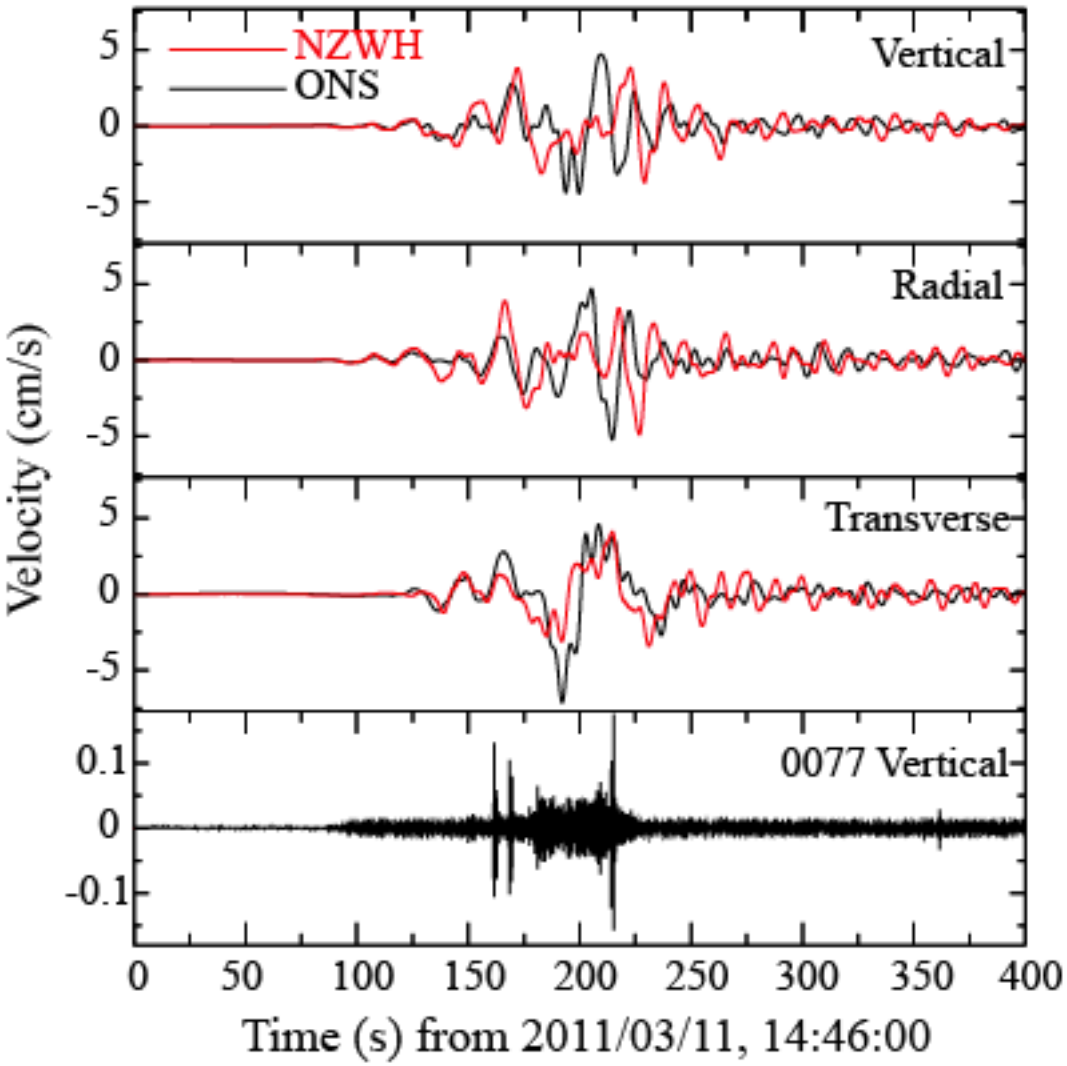

Figure 9. Earthquakes detected during the passage of surface waves from the Tohoku-oki earthquake. From top to bottom: low-frequency seismograms (0.01 – 0.2 Hz) at the NZWH station (red) and ONS station (black) (Vertical, Radial and Transverse components) and high-frequency waveform (10 – 30 Hz) at the temporary station 0077; locally triggered events are marked by small red circles. The ONS broad-band station is located at coordinates (138.9822, 36.1557), south of the area plotted in Figure 1.

earthquake (e.g. Sturtevant *et al*., 1996). As documented in such studies, fluids are active agents in geothermal and volcanic areas, which appear to be particularly susceptible to dynamic triggering (Hill and Prejean, 2006). To quantify the degree of geo-thermal activity in the study region, I use fluid temperature (Figure 10a) and flux data (Figure 10b) (Geological Survey of Japan, 2009) measured at the shallowest part of the crust (depth between 0 to 900 m).

As seen in Figure 10a, the activated area close to stations "0077" and "1076" is characterized by high fluid temperatures, indicating the presence of a geothermal field. I therefore interpret the dynamically triggered shallow events located close to "0077" station as being caused by a sudden excitation of fluids due to the strong shaking by the Tohoku-oki surface waves. In addition to the temperature data, I have extracted from the same database the fluid flux values (Figure 10b) of the study region, measured as water flowing to the surface. The largest such values (~3000 liters/minute) are observed at the well closest to station "0077", where the most remarkable immediate seismicity activation has occurred (Figure 8 and 11).

The seismicity activation around station "0080" also started very early after the Tohoku-oki earthquake, although it is only detectable after the passage of the largest-amplitude surface waves. This slight onset delay and the likely weaker early earthquake activation (Figure 11) may be due to the fact that the area in and around the main "South" cluster is only mildly geothermal (Figure 10a). However, the relatively shallow fault-like structure that is revealed by the alignment of seismicity (Figure 5a and 7) may constitute a favorable permeable environment for geofluid circulation and episodic seismic activity. The results of Kumazawa and Ogata (2013), who analyzed the JMA earthquake catalog after the Tohoku-oki mainshock, support the swarm-like

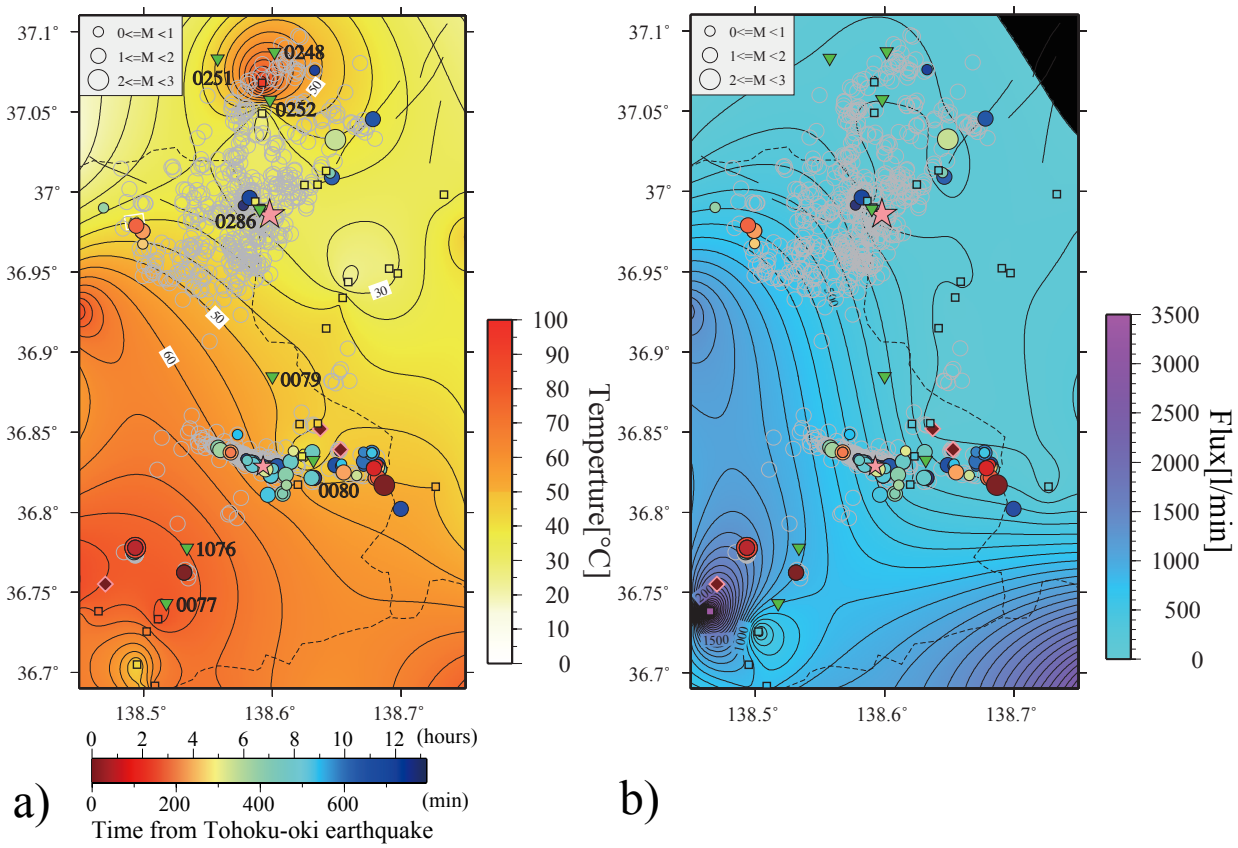

Figure 10. Fluid temperature and flux map of the study area, with seismicity superposed: (a) the temperature distribution (shown by the yellow-to-red color scale in the right side of the map) and (b) the flux distribution (shown by the sky blue-to-purple color scale in the right side of the map) were obtained by smoothly interpolating locally measured values from locations of small rectangles available all-over Japan. The superposed seismicity is the same as in Figure 5. Inverted green triangles show select temporary seismic stations. The light dashed lines and thin solid lines show prefecture borders and faults respectively.

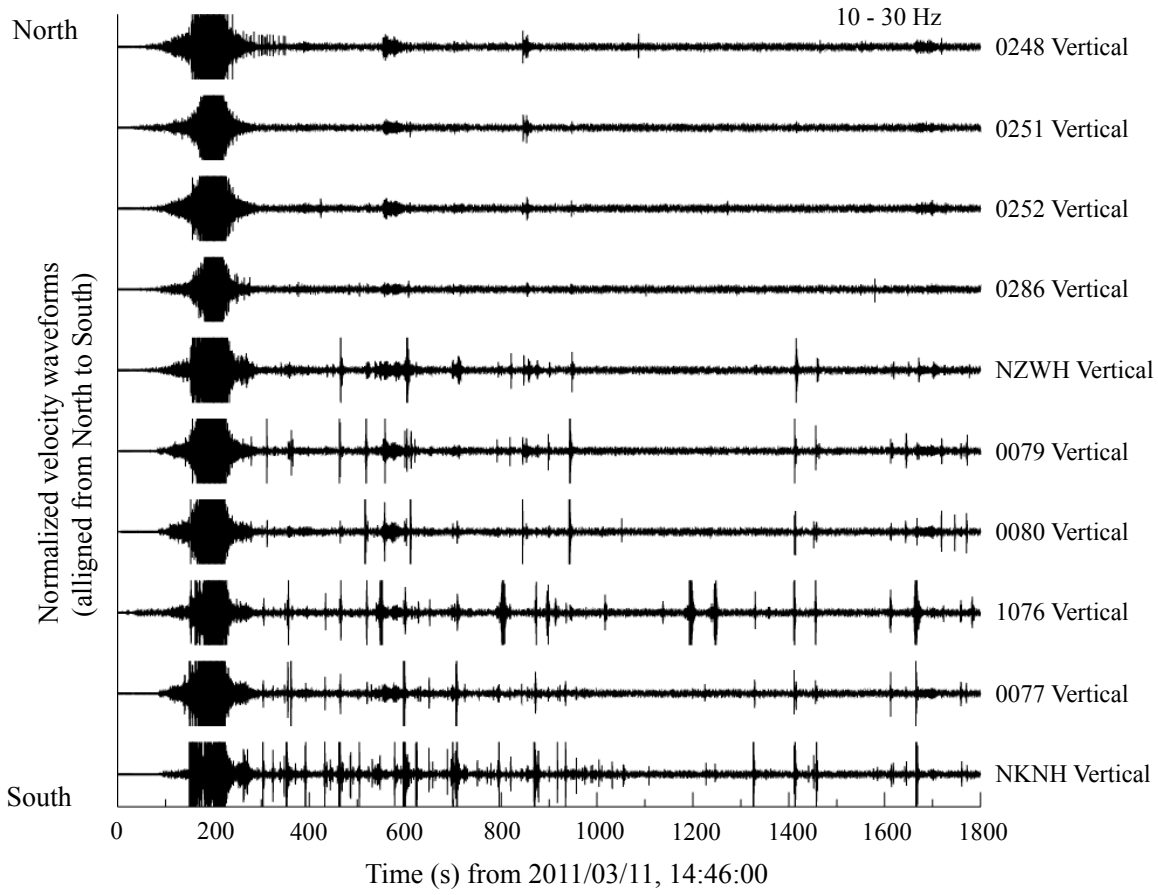

Figure 11. Continuous vertical-component waveform data recorded at Hi-net stations (NZWH, NKNH) and temporary, local-network stations (0248, 0251, 0252, 0286, 0079, 0080, 1076 and 0077) in the study region, band-pass filtered from 10 to 30 Hz. The origin time is March 11, 2011; 14:46:00. For the location of stations, please see Figure 1. The waveform data is normalized and the stations are arranged from North (upper part of plot) to South (lower part of plot). Note the relative absence of early triggering at seismic stations located to the north (0248, 0251, 0252 and 0286) in contrast with the very early activation of seismicity that can be seen at the stations (NKNH, 0077 and 1076), in the vicinity of the southernmost hotspot, as well as at the stations 0080 and 0079, which are located close to seismically activated fault-like structure in the "South", characterized by average temperatures (Figure 10a). Note that the Hi-net station NZWH is located close to another 'hotspot' (Figure 10a, left of map, between 36.9 – 36.95 degrees latitude).

behavior of seismicity in the “South”.

Although the geothermal data used in this study is measured at or close to the surface, there is evidence supporting its relation to thermal properties of the deeper crust. The southern study area lies in a region where the volcanoes Naeba and Torikabuto-yama were active in the middle Pleistocene; such geologically-recent volcanic structures are usually warm enough to provide the necessary heat supply for the hot-spring activity (e.g., Fukutomi, 1961). Note also that the geothermal gradient (Tanaka, 2004) is particularly high (~150 K/km) at one observation point in the “South” in contrast to several locations in the “North”, however the measurements are too sparse for interpolations. Although the geothermal gradient data is measured near the surface, it shows correlations with properties of the seismogenic layer (e.g., Tanaka *et al*., 2004).

The dynamically-initiated triggering of seismicity in the “South” due to crustal fluid excitation is supported also by independent findings (Terakawa *et al*., 2013) based on the analysis of focal mechanism data in several regions in Northeast Japan, which suggest fault-confined fluid pressure increase in this area, following the Tohoku-oki earthquake. Specifically, Terakawa *et al*. (2013) report a median over-pressure coefficient increase of more than 6.0 times in the “South” Nagano region, following the Tohoku-oki earthquake, which is the largest of all the areas they investigated.

As I have already pointed out, there is no evidence of early seismicity activation in the “North” region; both the MFT analysis and direct examination of waveform data (Figure 11) support this result. One may question whether the seismicity in the “North” is causally related with the Tohoku-oki earthquake. The strongest argument in favor of a triggering relationship is given by

the pre-Tohoku seismicity in the "North": there are no earthquakes of $M \geq 5.5$ from January 1st, 1923 (the beginning of the JMA catalogue) until the March 12, 2011 Nagano earthquake. It is therefore highly unlikely that the M_w6.2 event occurred by chance just 13 hours after the Tohoku-oki megathrust. In addition, there have been no recorded earthquakes by JMA in the "North" since March 2, 2011. As shown in Figure 10, the northern area is characterized, in general, by lower fluid temperatures than the "South". One "hotter" area can be seen close to the station "0252". However, the fluid-flux values are relatively low here and the seismogenic region is relatively deep (between 5 km to 10 km, from the relocated seismicity), so this may explain the lack of dynamically triggered events.

It is important to understand what physical mechanism might have been responsible for the delayed activation of seismicity in the "North", in particular the triggering of the M_w6.2 earthquake. Terakawa *et al*. (2013) showed that the region surrounding the Northern Nagano epicenter may have experienced an increase in regional ambient fluid pressure, caused by the flow of over-pressurized fluid from a deep reservoir, following the Tohoku-oki earthquake. A tomography study in the area (Enescu *et al*., 2011; Sekiguchi *et al*., 2013) found evidence of a high v_p/v_s structure just below the Northern Nagano hypocentral region, which has been interpreted as a fluid-like body at depth. Such independent results support qualitatively a scenario involving fluid migration from a deeper source, which upon arrival – with some delay – at seismogenic depths could have triggered earthquakes.

Although poorly constrained, the manually located earthquakes in the southernmost part of the study region are shallower than ~5 km. The MFT-detected events in the southernmost area

and the “South” also have shallower average depths compared to those in the “North” (Figure 12). The relatively shallow seismogenic areas might be closer to the failure stress threshold, likely due to the geothermal environment; as a consequence, the seismicity activation is pronounced but unlikely to develop into a larger event. The situation is opposite in the hypocentral area of the Northern Nagano earthquake.

The dynamic stress changes in this study have been estimated using only surface wave amplitudes, however the orientation of local faults relative to the incidence angle of the incoming surface wave, as well as their faulting mechanism, influence as well the dynamic stresses (Hill, 2012). It is thus possible that the fault structures in the “South” were more favorably oriented for being dynamically triggered than those in the “North”.

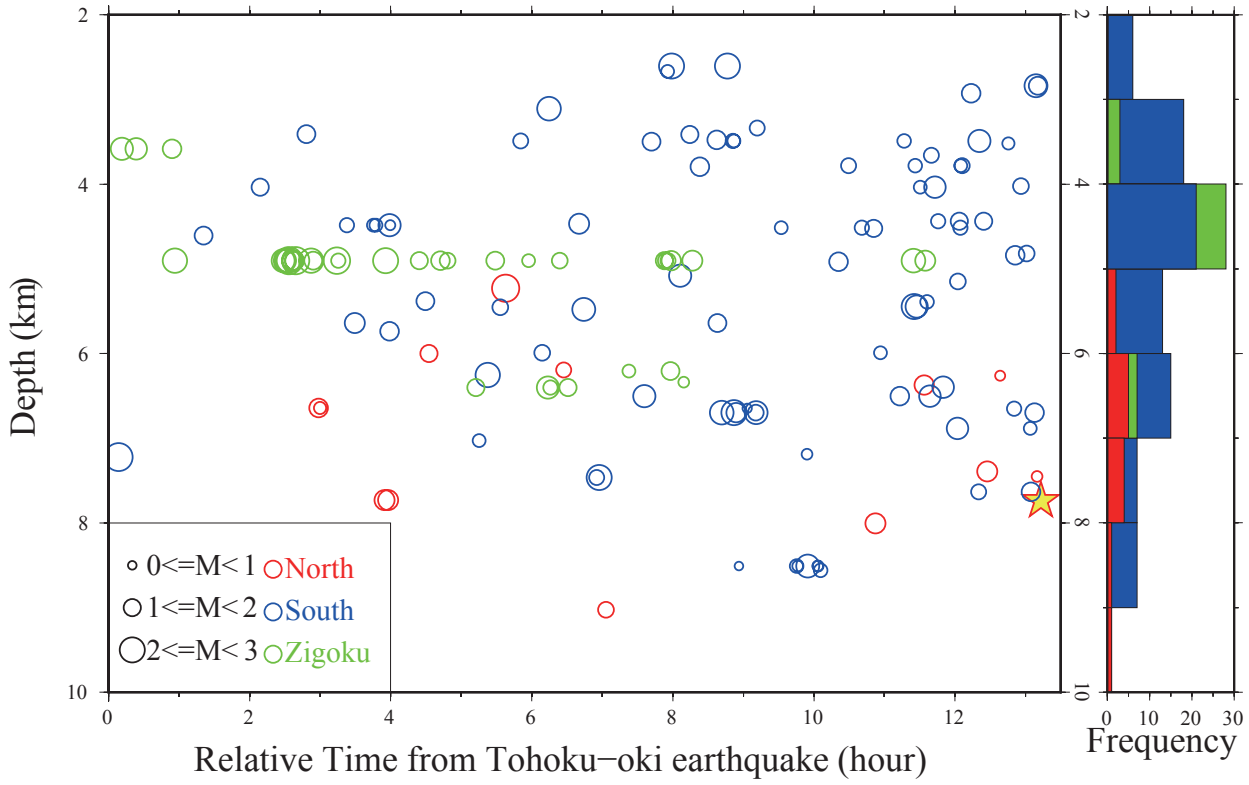

Figure 12. Left: depth versus time plot for the MFT-detected events in the study region. Red, blue and green circles correspond to the “North”, “South”, and the southernmost area of the study region respectively. The symbol sizes scale with the events magnitude; Right: Histogram plot of detected events in “North” (red), “South” (blue) and the southernmost (green) area function of their depth.

2.4.2 Possibility of static stress *triggering*

I have also calculated the static Coulomb stress change (ΔCFS) due to slip on the Tohoku-oki earthquake fault plane on two receiver faults: the fault plane of the M_w6.2 Northern Nagano earthquake in the "North" and that of the M_w5.4 earthquake in the "South", which coincides with one of the nodal planes of the F-net focal mechanism and was chosen based on the distribution of seismicity. The strike, dip, and rake for the two faults are: 29^0, 56^0, 70^0 and 105^0, 88^0, -175^0, respectively. The stress change is computed (King *et al.*, 1994) using the equation: $\Delta CFS = \Delta\tau + \mu'\Delta\sigma$, where Δτ is the shear stress change on a given fault plane (positive in the direction of fault slip), Δσ is the fault-normal stress change (positive when unclamped), and μ' is the apparent coefficient of friction. I use μ'= 0.4, which is an average value among those usually used in the literature (e.g., King *et al*., 1994). I consider three different slip models published in the literature: Yagi and Fukahata, 2011 (source model inferred from teleseismic waveform inversion); Suzuki *et al*., 2011 (source model inferred from strong-motion data) and Pollitz *et al*., 2011 (source model inferred from geodetic data).

The obtained ΔCFS values on the two receiver faults, computed for the three slip models are: 0.022 MPa and 0.134 MPa, for the Yagi and Fukahata (2011) model; 0.021 MPa and 0.142 MPa for the Suzuki *et al*. (2011) model and 0.022 MPa and 0.130 MPa, for the Pollitz *et al*. (2011) model. The similarity of these values for different slip models of the Tohoku-oki mainshock shows that they are robust to variations in the source model. I have also considered friction coefficients in the range 0.2 to 0.8 and obtain similar stress change results. Note that similar small stress change values for the *Mw* 6.2 receiver fault have been reported by Okada *et al*. (2011), who

uses yet a different Tohoku-oki slip model and an independently determined *Mw* 6.2 receiver fault.

The ΔCFS value obtained in the "North" is very small (close to the static stress threshold of 0.01 Mpa above which earthquake triggering is usually observed – Parsons *et al*, 2008 and references therein) and it is doubtful that could have induced an M_w6.2 earthquake. For the "South", the static stress changes are significant (~0.13 MPa) but still lower than the peak dynamic stresses (~0.4 MPa).

Based on all the above considerations, the contribution of static stress changes to triggering cannot be excluded, however the swarm-like characteristics of seismicity in the "South" suggest that crustal fluids, excited by the dynamic stresses associated with the Tohoku-oki surface waves, are the most important triggering factor.

Chapter 3

Nucleation Process of the 2011 Mw6.2 Northern Nagano Earthquake: MFT analysis to "Hizumi" temporal observation network at the hypocentral regions of Mw 6.2

3.1. Summary of Chapter 2 and its controversial point

In Chapter 2, by applying the matched-filter technique (MFT) (Shelly *et al*., 2006; Peng and Zhao, 2009) to waveform data recorded at 10 permanent Hi-net stations in the northern Nagano region, I detected 139 events, compared with only eight in the JMA catalogue, that occurred during the 13 h following the 2011 Tohoku-oki mainshock. Among the 139 MFT detections, only 13 were located in the aftershock area of the M_w 6.2 earthquake ("North" area), which occurred about 13 h after the Tohoku-oki event. Most other detections were located in a linear cluster about 10 km to the south ("South" area) or in isolated seismicity hotspots another 10 km farther south ("Zigokudani" area) (Figure 5, Chapter 2). In the South and Zigokudani areas, relatively shallow swarm-like seismicity started during or immediately after the passage of surface waves from the Tohoku-oki megathrust event. Comparison of shallow crustal (0–900 m depth) geothermal data, including fluid temperature and flux data (Geological Survey of Japan, 2009), in this region with the MFT event distribution indicated that the South and Zigokudani seismic areas were characterized by high fluid temperatures and fluxes. I inferred from these observations, and from the overall episodic character of seismicity in the southern region, that geothermal fluid excitation related to stress perturbation caused by the passage of surface waves from the Tohoku-oki earthquake was the underlying physical triggering mechanism. In contrast, in the North area – the hypocentral region of the M_w 6.2 earthquake – seismicity was relatively weak, and there were no

detections in the first 3 h following the Tohoku-oki earthquake (Figure 5, Chapter 2). A few isolated events occurred within this area 3–7 h after the mainshock, but at some distance from the M_w 6.2 event hypocenter and its fault plane. Two small foreshocks occurred close to the hypocenter of the M_w 6.2 event within 1 h of its origin time. To understand the physical mechanism that might have been responsible for the delayed activation of seismicity in the North area, in particular, the triggering mechanism of the M_w 6.2 event, I referred to Terakawa *et al.* (2013), who showed that the region surrounding the epicenter in Northern Nagano may have experienced an increase in regional ambient fluid pressure following the Tohoku-oki earthquake, caused by the flow of over-pressurized fluid from a deep reservoir. The tomographic study of Sekiguchi *et al*. (2013) reported a high v_p/v_s structure just below the hypocentral region, which they interpreted as indicating the presence of fluid. The independent results of Terakawa *et al.* (2013) and Sekiguchi *et al.* (2013) qualitatively support a scenario in which fluid migration from a deep source might trigger earthquakes upon arrival – after some delay – at seismogenic depths. Hence, I hypothesized that the seismicity in the North area could be explained by fluid migration from a deep source to seismogenic depths. However, no direct evidence of a causal link between fluid migration and seismicity was presented.

In addition, I used waveform data of the "Hizumi" temporary network to preliminarily identify many small events that occurred close to the hypocenter of the M_w 6.2 earthquake during a period of several hours before its origin time (Figure 1). Hizumi is a temporary dense regional network of three-component seismograph stations (station spacing about 5 km or less) operated from 2008 to 2012 by NIED that is able to detect events not detectable by the permanent Hi-net stations around the source area of the M_w 6.2 earthquake. Therefore, in this chapter, I apply the

MFT to waveform data recorded by the Hizumi network stations and examine in detail the triggering mechanism of the seismicity in the North area, that is, the epicentral region of the M_w 6.2 event.

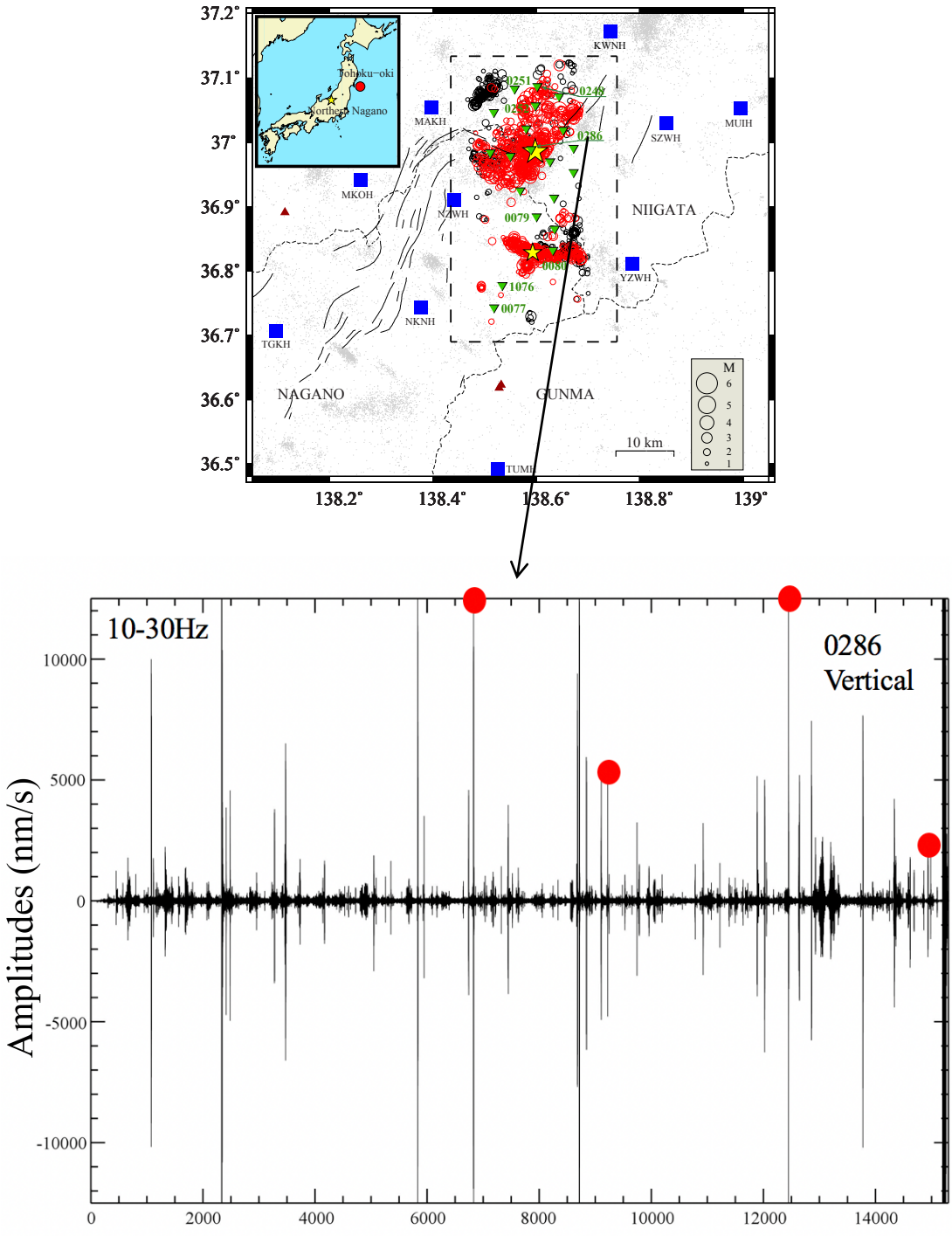

.

Figure 1. (top)Same figure as Figure 1 in Chapter 2; (bottom) Continuous vertical-component waveform data recorded at 0286 station, band-pass filtered from 10 to 30 Hz. The origin time is March 11, 2011; 23:46:00 and the end time is March 12, 2011; 4:01. Red solid circles indicate detected events in Chapter 2. For the location of stations, please see Figure 2.

3.2. Data and Methods

3.2.1. Determination of earthquake locations by MFT and the Win waveform data processing system

Before applying the MFT, I first picked earthquake P- and S-wave arrivals on continuous seismograms automatically/manually, located the events using the Win waveform data processing system (Urabe and Tsukada, 1992), and then used the located events as the first MFT templates in the study region (from –3 to 10 km in the fault strike direction (N30°E) and from –5 to 10 km in the dip direction (N120°E) from the M_w 6.2 hypocenter) (Figure 2). I applied the MFT to data from two Hizumi network stations, 0286 and 2289, using 4 s of waveform data for each template event recorded by each station component, starting 2 s before the S-wave arrival time and applying the same filtering as for the continuous data. For each component, I calculated the correlation coefficient between the continuous waveforms and the templates by shifting the template window in increments of 0.01 s. For each station, the correlation time series thus obtained was averaged throughout. I then computed the median absolute deviation (MAD) of the mean correlation coefficient trace for each template event and set the detection threshold to 9 times the MAD value. The waveforms of all newly identified events were visually checked to minimize the possibility of spurious detection. The events thus detected were relocated by applying the picked P- or S-wave arrivals to manually select waveforms from at least three stations for each event in the Win system, and were then used as new templates. Finally, the earthquakes detected by this procedure were relocated using tomoDD software (Zhang and Thurber, 2003).

I end up with a catalogue of 285 events for the 13-hour time period following the Tohoku-oki mainshock. My high-resolution earthquake data set makes it possible to further divide the seismicity in the first one hypocentral area into an eastern and western region (Figure 6a).

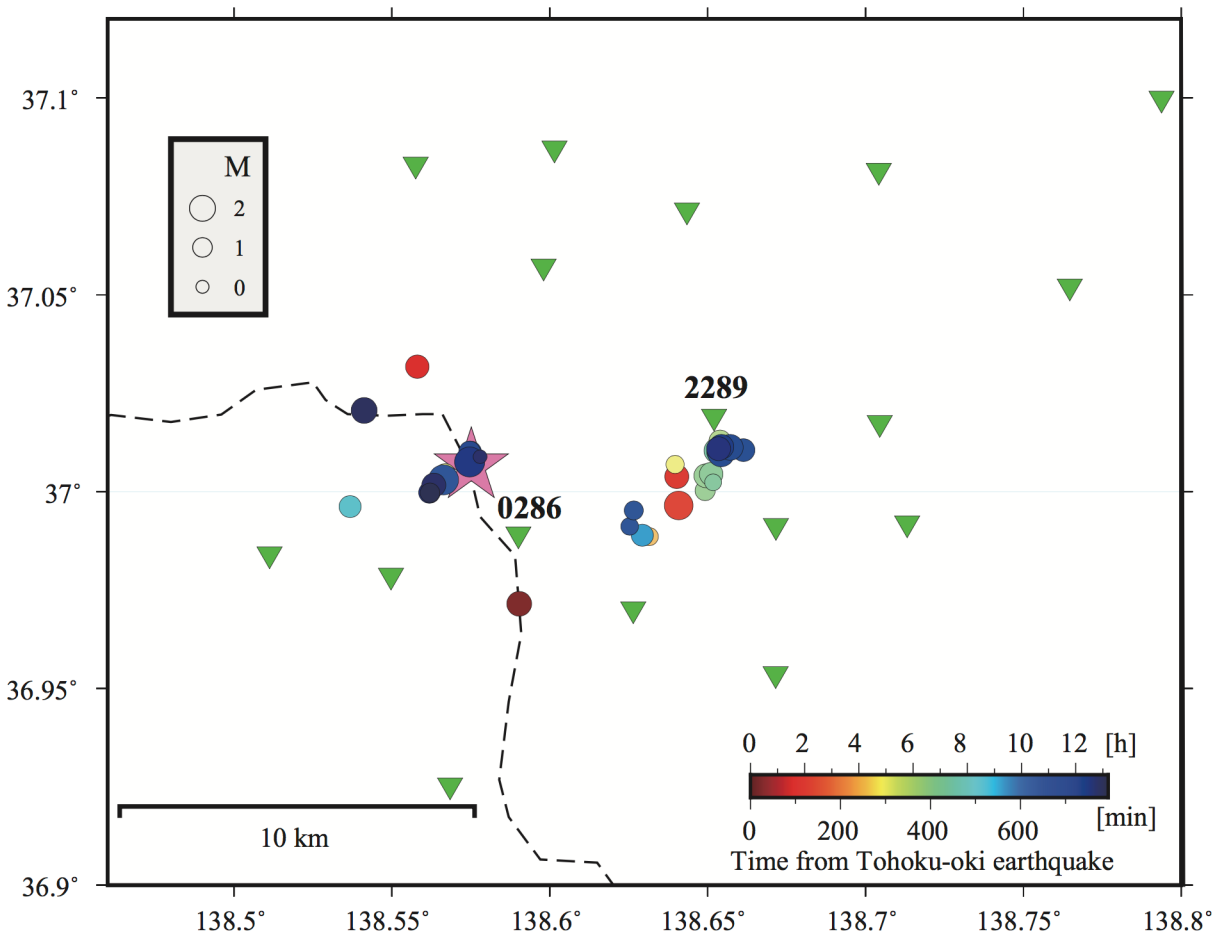

Figure 2. Map view of first template events used to MFT analysis. The symbol sizes of circles, that magnitudes are obtained, scale with the events magnitude. Colors indicate lapse time from the Tohoku-oki megathrust event. Inverted green triangles represent temporary surface stations by "Hizumi". Dashed line indicates a prefectural boundary.

3.2.2. Determining the mechanisms of detected events

For some detected events in both the western and eastern areas, and for the M_w 6.2 mainshock, I also picked P-wave first-motion polarities manually by careful inspection and then applied the HASH program (Hardbeck and Shearer, 2002) to the polarity data to define the focal mechanisms. For the M_w 6.2 mainshock, picked data recorded by the MAKH Hi-net station (Figure 1 in Chapter 2) were used to refine the result. Polarity data were picked from more than eight stations and used with the one-dimensional P-wave velocity structure determined by Ukawa *et al.* (1984). The focal mechanism of each event was classified according to quality (see Hardbeck and Shearer, 2002); mechanisms of quality A or B were considered excellently defined, those of quality C were less accurately determined, and those of quality D were only considered as possible mechanisms (Uchide *et al.*, 2015). Among 19 detected events, the focal mechanisms of two were of quality B, those of three were of quality C, and the remaining 14 were of quality D.

3.2.3. Detection of Tohoku-oki aftershocks that could dynamically trigger local seismicity

Many large aftershocks occurred immediately after the M_w 9.0 Tohoku-oki megathrust event, raising the question of whether dynamic stress changes caused by large aftershock sequences modulated local seismicity in places far from the event's epicenter. Therefore, I searched the catalogue of events for Tohoku-oki aftershocks that triggered local events in the research area.

To identify aftershocks to include in this analysis, it was necessary to determine how large of an event could dynamically trigger local seismicity. Van der Elst and Brodsky (2010), using a progressive approach, estimated that the minimum dynamic stress that can trigger an earthquake

is on the order of 0.1 kPa or even less. Peak dynamic stress σ_d is proportional to Gu'/v_{ph} (Jaeger and Cook, 1979), where G is the shear modulus (= 30 GPa), v_{ph} is the phase velocity (3.5 km/s for Rayleigh waves and 4.1 km/s for Love waves), and u' is the peak particle velocity; thus, dynamic stress changes on the order of 0.1 kPa correspond to peak velocity amplitudes on the order of a few 10^4 of nm/s. A visual check of the low-frequency envelope of the vertical component waveform at station NZWH showed that most peak amplitudes excited by events larger than M_{JMA} 5.5 that occurred in the Tohoku-oki aftershock area (34.38°–40.11°N, 137.58°–144.79°E) exceeded a few 10^4 nm/s, except those overlapped by peaks with larger amplitudes excited by earlier large events (Figure 3). Hence, I considered 113 events with $M_{JMA} \geq 5.5$ that occurred in the Tohoku-oki aftershock area during the 13 h after the Tohoku-oki mainshock to be large events with the potential to trigger local seismicity in northern Nagano.

To detect aftershocks that triggered local seismicity, I first calculated the arrival times of the Love waves emitted from the 113 $M_{JMA} \geq 5.5$ Tohoku-oki aftershocks (referred to as large events) in each research area (the eastern and western clusters in this chapter and the South and Zigokudani areas in Chapter 2). Here, I used the center of the study area (37.0226°N, 138.6193°E; the center of the black rectangle in Figure 6) as a reference point for seismicity in the western and eastern clusters, assuming the Love-wave phase velocity was 4.1 km/s. East of the reference point, where the surface waves of the Tohoku-oki earthquake aftershocks would have arrived earlier, there is a possibility that events were triggered before the arrival of surface waves at the reference point. Therefore, I calculated the difference in arrival time between the reference point and the point expected to show the largest Love-wave arrival time difference in the research area (i.e., in the easternmost corner of solid rectangle in Figure 6a). Then considering such maximum time lags of

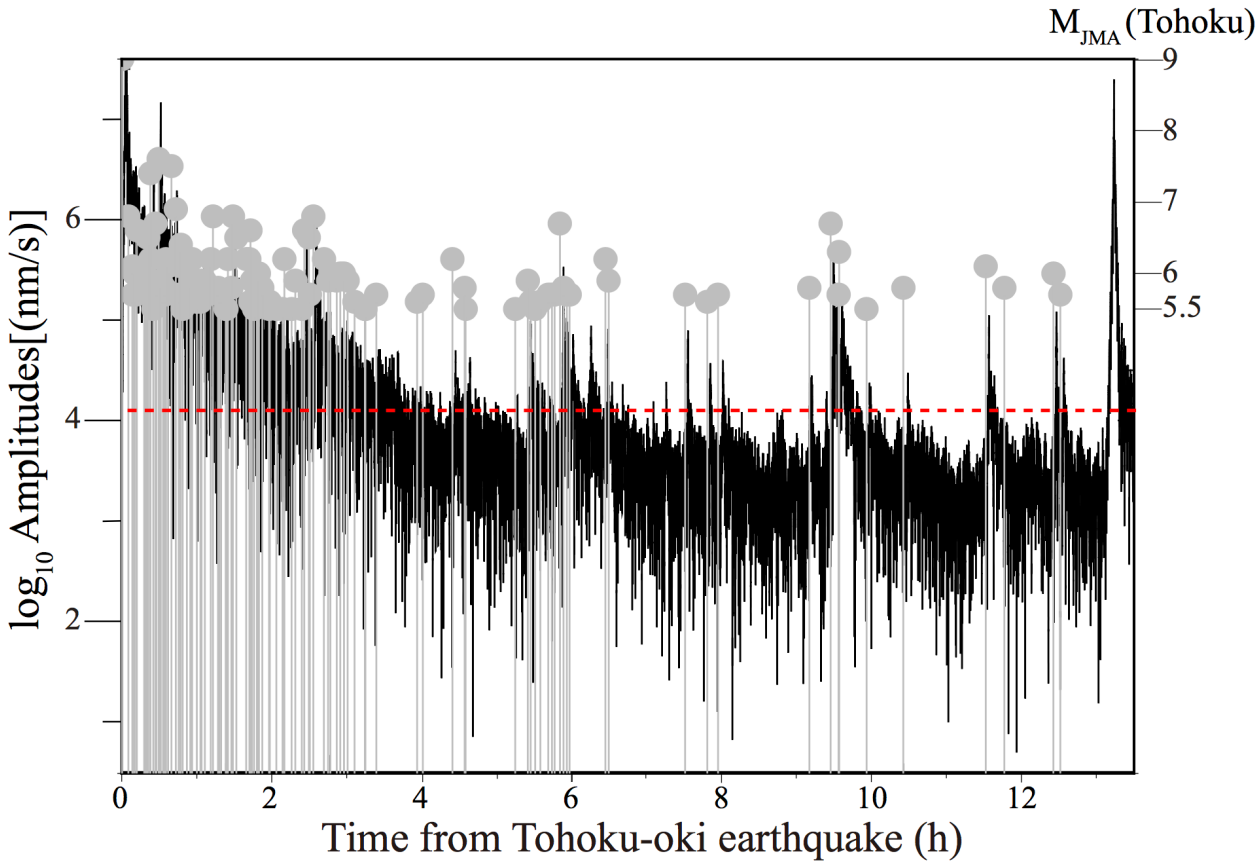

Figure 3. Time history for $M_{JMA} \geq 5.5$ Tohoku-oki aftershocks within 13 and a half hours from the origin time of Tohoku-oki earthquake superposed by low-frequency envelope seismograms (0.01 – 0.2 Hz) at the NZWH station (Vertical). Red dot line shows the values of amplitudes which coincides with the dynamic stresses of 0.1 kPa.

Love-wave arrivals, arrival times are further shifted to 2.42s before. I applied the same procedure to the estimation of the arrival times in the South and Zigokudani areas by using reference points at 36.8°N, 138.6°E and 36.776°N, 138.494°E, respectively.

Next, I searched and counted the numbers of events in 100- and 200-s windows before and after each arrival time, respectively, determined as described above. To distinguish between background events and local events triggered by the large events, I considered the number of events identified before the arrival time (b) to represent local background events, and the number of events counted after the arrival time (a) to local triggered events; thus $a - b$ represents amount of the increase in local events. Here, I exclude local events triggered by each large event from background events. For the South and Zigokudani areas, I used detected events catalogued as described in Chapter 2.

Moreover, I generated 1000 synthetic catalogues by randomizing origin times by rearranging the time difference between temporally adjacent local events listed in the real catalogue for each area. Since I used 113 Tohoku large events in this analysis, 113 large events × 1000 synthetic catalogues = 113,000 values of a and $a - b$ obtained for each area (Figure 4). Then I applied the procedure described above to these randomized synthetic catalogues. I calculated the cumulative frequency distributions of these 113,000 values of a and $a - b$ for each area and defined the upper 5% of the cumulative distribution as the threshold value for detecting remote aftershocks with significant a or $a - b$ values in the real catalogue of each area (Figure 5).

Finally, using the thresholds obtained for each area and time window, I searched large events associated with significant numbers of local events, or increased numbers of events after the Love-wave arrival, and defined such large events as triggering events. Here, I visually checked

the low-frequency waveforms at station NZWH and excluded large events for which the amplitudes could not be confirmed from the list of triggering events.

I next calculated A and $A - B$ as the sum of all values of a and $a - b$, respectively, in each real catalogue of large events ($M_{JMA} \geq 6.0$ or 6.5) to confirm the modulation of local seismicity in each area through the whole time series. I also calculated A and $A - B$ for each synthetic catalogue, thus obtaining 1000 A and $A - B$ values for each area (Figure 4). I then calculated the cumulative distributions of those values, and defined thresholds as described above (Figure 5). Values of A and $A - B$ for events larger than $M_{JMA} \geq 6.0$ or 6.5 are compiled in Table 2. In Tables 1 and 2, the threshold values for each event, area, time window, and range of magnitudes are shown at the bottom of each column.

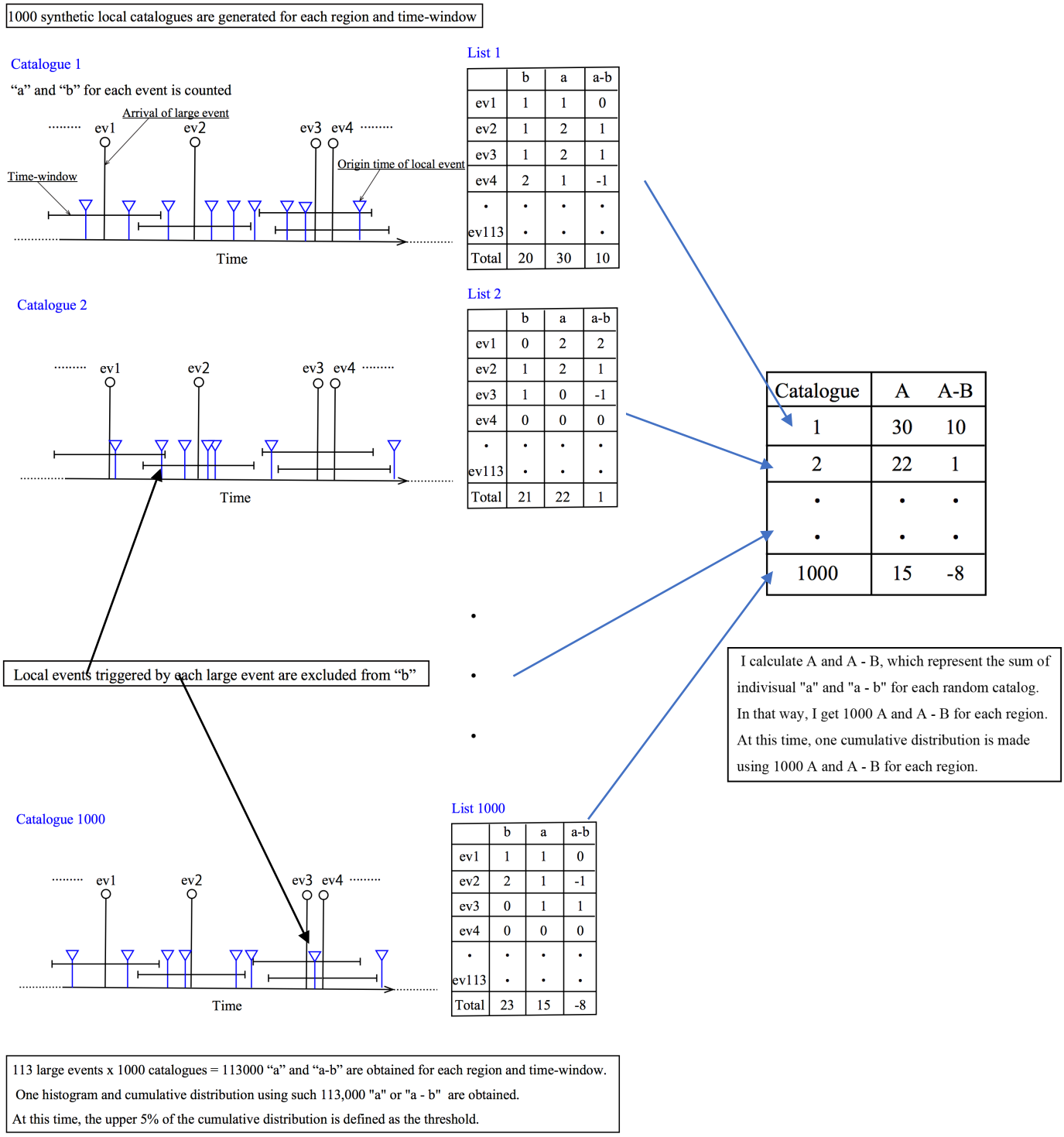

Figure 4. The description of the processing synthetic local catalogues. (left) An illustration for explaining the way to count local events in each time windows before and after the arrival of Love-waves from remote event on each synthetic local catalogue. (center) Lists of *b*, *a* and *a-b* for each catalogue. (right) List of *A* and *A-B* extracted by the process as shown in center.

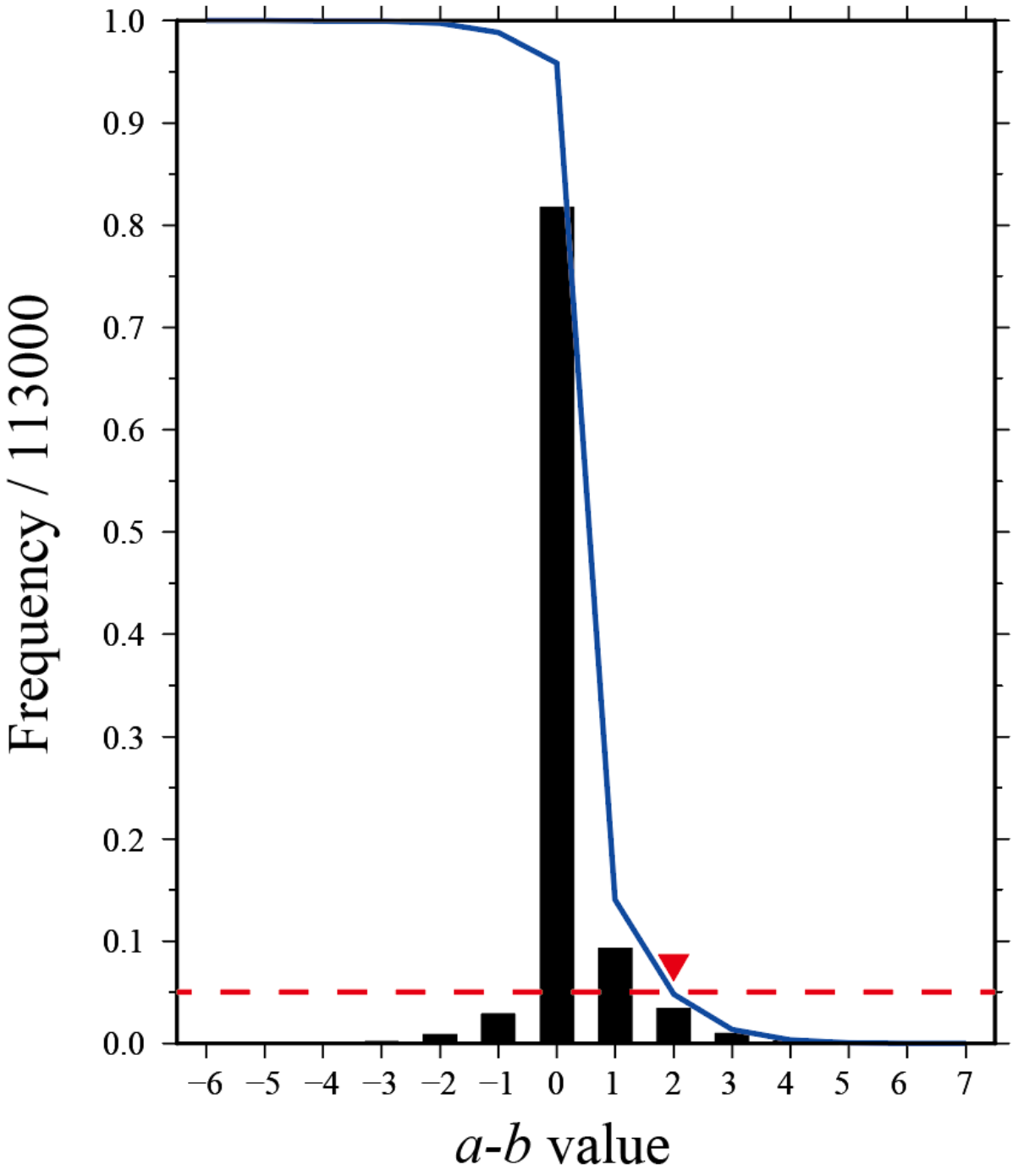

Figure 5. An example of frequency and cumulative frequency of the *a*-*b* value for the time window of 200 seconds using all 1000 synthetic catalogues for the western region. Black thick bars and blue solid line shows frequency and cumulative one in order from the larger *a*-*b*. Red dashed line indicates significant level of 5 % and red inverse triangle points out the threshold to detect remote aftershocks with significant increase in real catalogue.

3.3. Results

3.3.1. Catalogue of MFT-detections

In the previous chapter, it is clear that the seismic activity in Northern Nagano following the 2011 Tohoku-oki earthquake can be grouped in two distinct regions: the main area where the Mw6.2 earthquake occurred after about 13 h from the megathrust event, and another one, located 20 km to the south, where a M5.4 earthquake occurred about 1 month later (Figure 5 in Chapter 2).

In this chapter, I have detected a total of 285 earthquakes in the source region of the Mw 6.2 event, compared with only three in the JMA catalogue. Such high-resolution earthquake data set makes it possible to further divide the seismicity in the first area into an eastern and western region (Figure 6a). The western area defines a group of events that occurred in the immediate vicinity of the M6.2 earthquake, while the larger, more voluminous group to the eastern cluster might belong to a seismologically distinct region.

The earthquakes are relatively small, with magnitudes less than 2.5. I calculated magnitude of completeness (Mc) for all events that magnitudes are obtained, and estimated value is 0.1 (Figure 7), which is much less than 1.2 obtained by my previous study in Chapter 2. Eight of the 285 detected events were in the JMA catalogue and in the catalogue of MFT-detected events described in Chapter 2.

Note that I examined continuous waveforms for the 4-h period before the Tohoku-oki mainshock and I found no evidence of local seismicity in the study area.

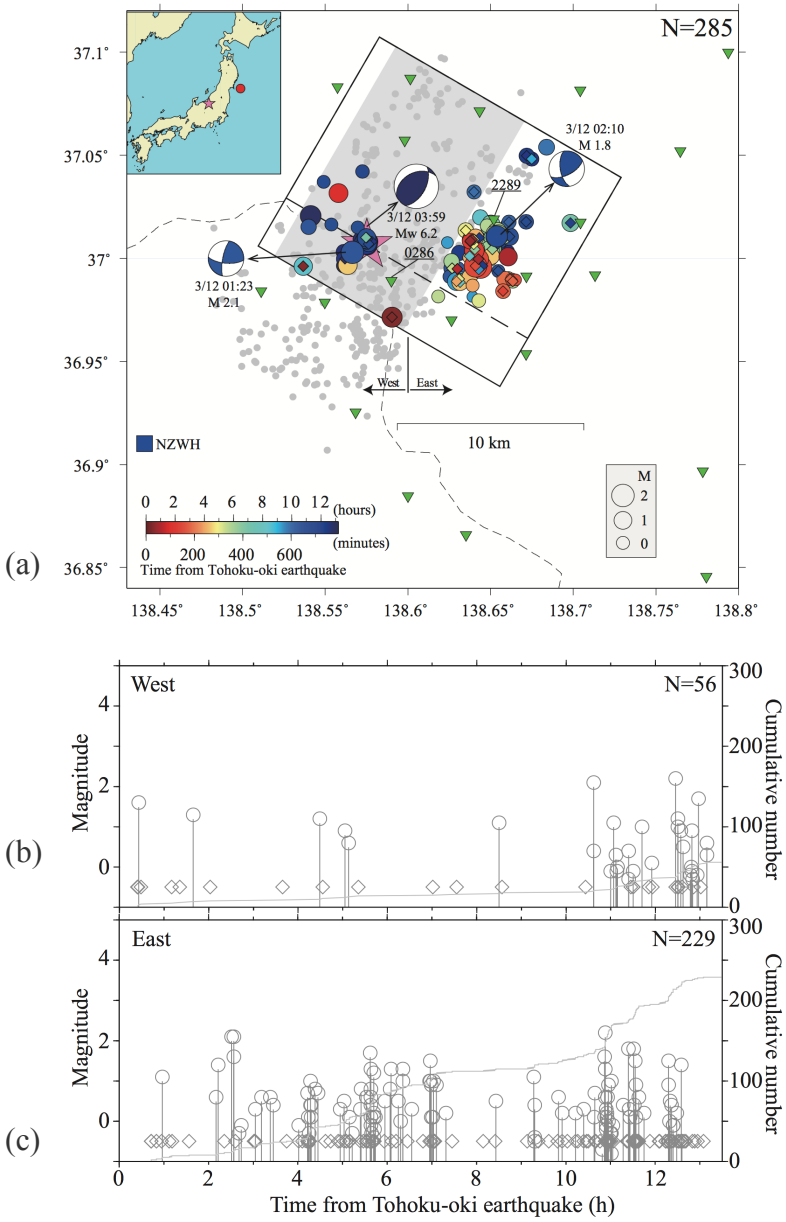

Figure 6. Seismicity distribution in the study region: (a) Map view showing the MFT-detected earthquakes. Colored circles and diamonds denote MFT-detections; their size scales with the events magnitude. Colors indicate lapse time from the Tohoku-oki megathrust event; the one-month relocated Hi-net aftershocks (M ≥ 1.0) are shown in gray. Pink star shows the March 12, 2011 Northern Nagano earthquake. Two focal mechanisms of small local events (detected in the present study) and the Centroid Moment Tensor focal mechanism of the Mw 6.2 Nagano mainshock, determined by NIED, F-net broadband network are also shown. "West" and "East" indicate the two regions referred in the text. Black thick dashed line shows the profile AA' in Figure 8a. The blue square and inverted green triangles represent Hi-net borehole and temporary surface stations, respectively. Gray rectangle indicates the fault plane of Mw 6.2 mainshock estimated by Sekiguchi et al., 2013. The light dashed line shows prefecture border. (b) and (c) Time history of seismicity for the western and eastern areas, respectively. Solid gray lines show the cumulative number of events for detections, respectively.

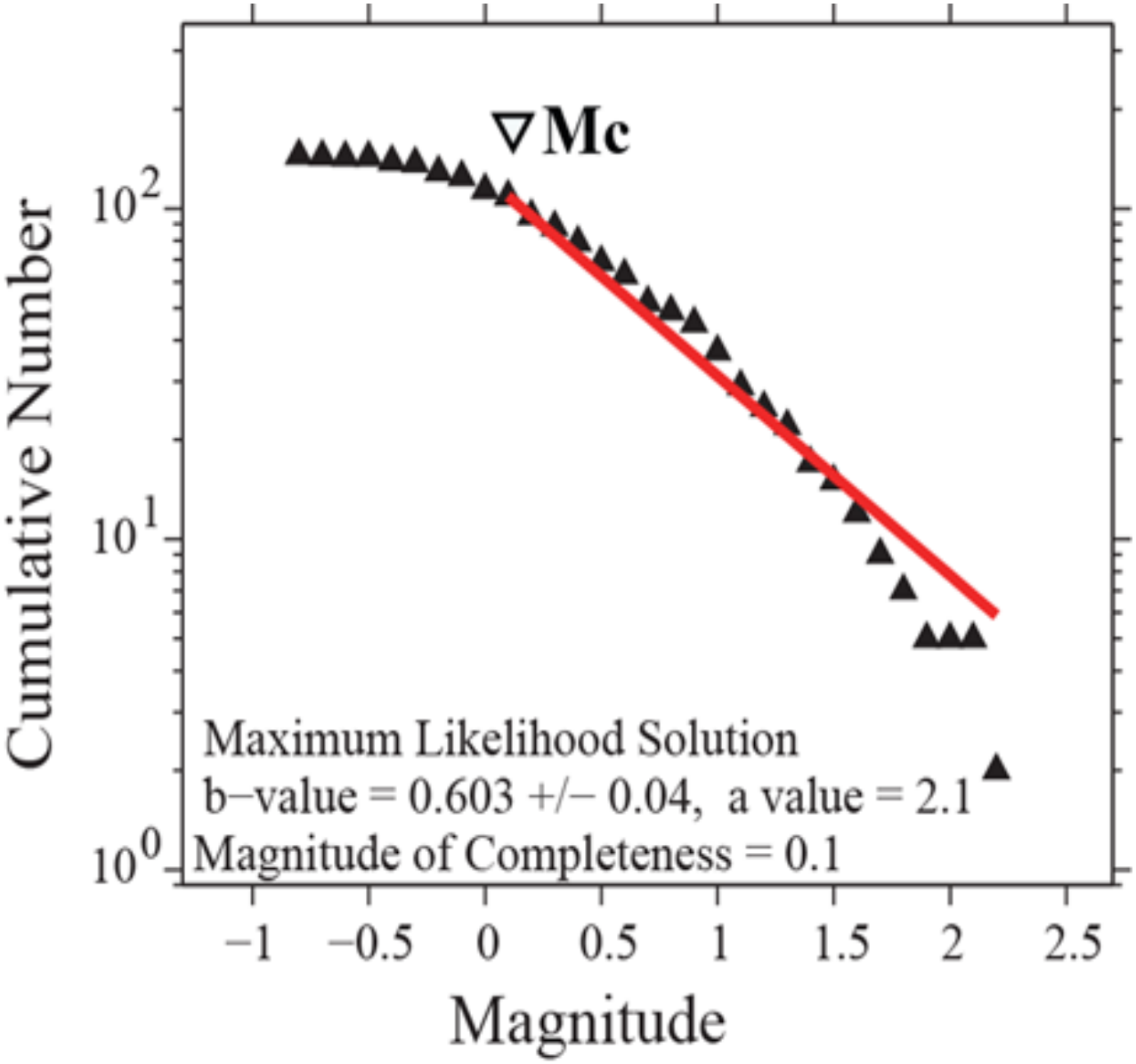

Figure 7. Frequency-magnitude distribution of all MFT-detected earthquakes. The black triangles indicate the data, while the Maximum Likelihood fit is shown as a black line. The magnitude of completeness (Mc = 0.1) is computed using the Maximum Curvature method of Wiemer and Wyss (2000). A slightly larger value of Mc (0.4) is obtained if using the Entire Magnitude Range (EMR) method of Woessner and Wiemer (2005).

The earthquake activity in the eastern cluster was more intense compared to that of the western group (Figure 1) and consisted of 229 events that cluster both temporally and spatially. In the western area, most events were distributed along the dip of the fault plane of the M_w 6.2 mainshock, as estimated by Sekiguchi *et al.* (2013), or were located in a tight subcluster in the immediate vicinity (within about 2 km) of the M_w 6.2 event hypocenter (Figure 8a). In this subcluster, seismicity migrated along the strike of the M_w 6.2 event fault from southwest of the hypocenter three times, during 4–7 h, 10–12 h, and more than 12 h after the M_w 9.0 megathrust event (Figure 9). In particular, third activation started within few hundred meters of *Mw* 6.2 event hypocenter (Figure 9a4). On the other hand, the cluster to the eastern region is almost vertical, with a discontinuity around 4 km depth (Figure 8a). As figure 8a, b indicates the seismicity in the western area started at relatively shallow depths, of about 2 km, and gradually extended towards deeper portions of the seismogenic zone.

I obtained focal mechanisms for seven events in the western area and for 12 events in the eastern area, including the M_w 6.2 mainshock, but most of them were of low quality. Two of the five most useful solutions are shown in Figure 6. The parameters obtained for the first-motion mechanism of the M_w 6.2 mainshock (classified as quality B) were as follows: strike angle = 74/337; dip angle = 66/75; and rake angle = –164/–25, for the one/another plane, respectively. Almost all P-axes in the focal mechanisms of the foreshocks were oriented roughly NW–SE, consistent with the background stress regime in the northern Nagano region (e.g. Terakawa and Matsu'ura, 2010).

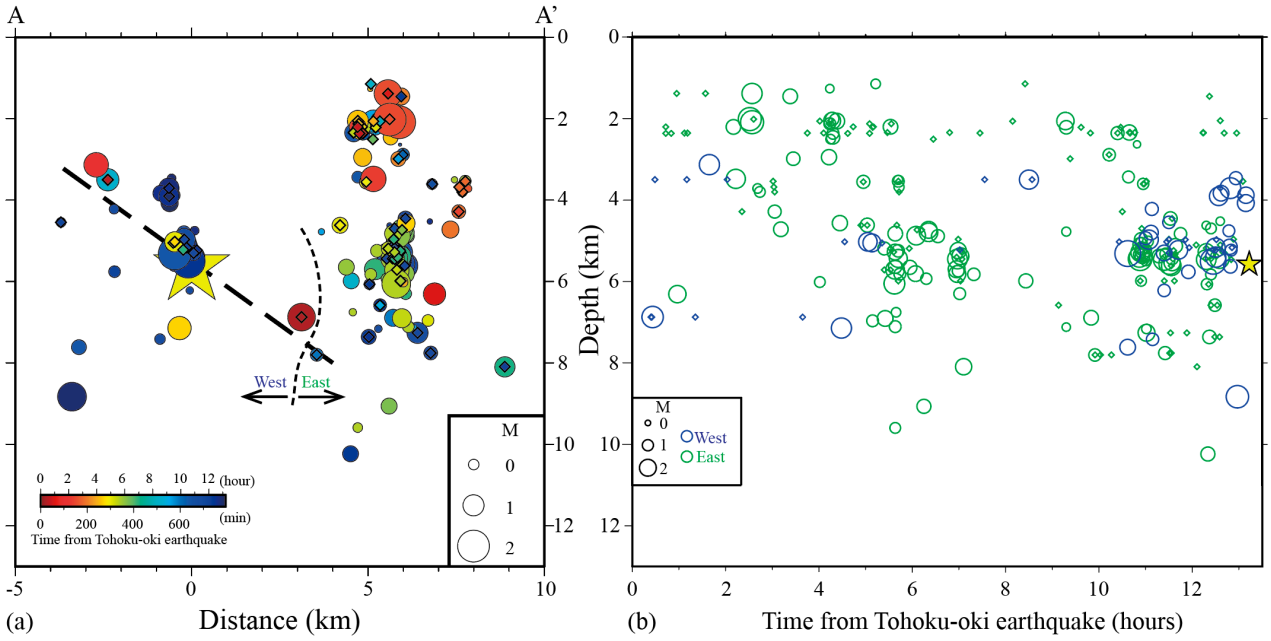

Figure 8. Space-time characteristics of seismicity. (a) Cross-section along the profile AA' in Figure 6(a). "West" and "East" indicate the two regions referred in the text and the curved line shows an approximate separation. Horizontal axis indicates the distance from the Mw 6.2 hypocenter along the AA' direction. Thick straight dashed line denotes the fault plane of the Mw6.2 earthquake, estimated by Sekiguchi et al., 2013. Yellow star shows the Mw6.2 mainshock. (b) Depth versus time plot for the MFT-detected events in the study region. Green and blue circles or diamonds correspond to the eastern and western areas, respectively. The symbol sizes of circles scale with the events magnitude. The diamonds indicate small events for which it was not possible to determine reliably their magnitudes. Yellow star shows Mw 6.2 mainshock.

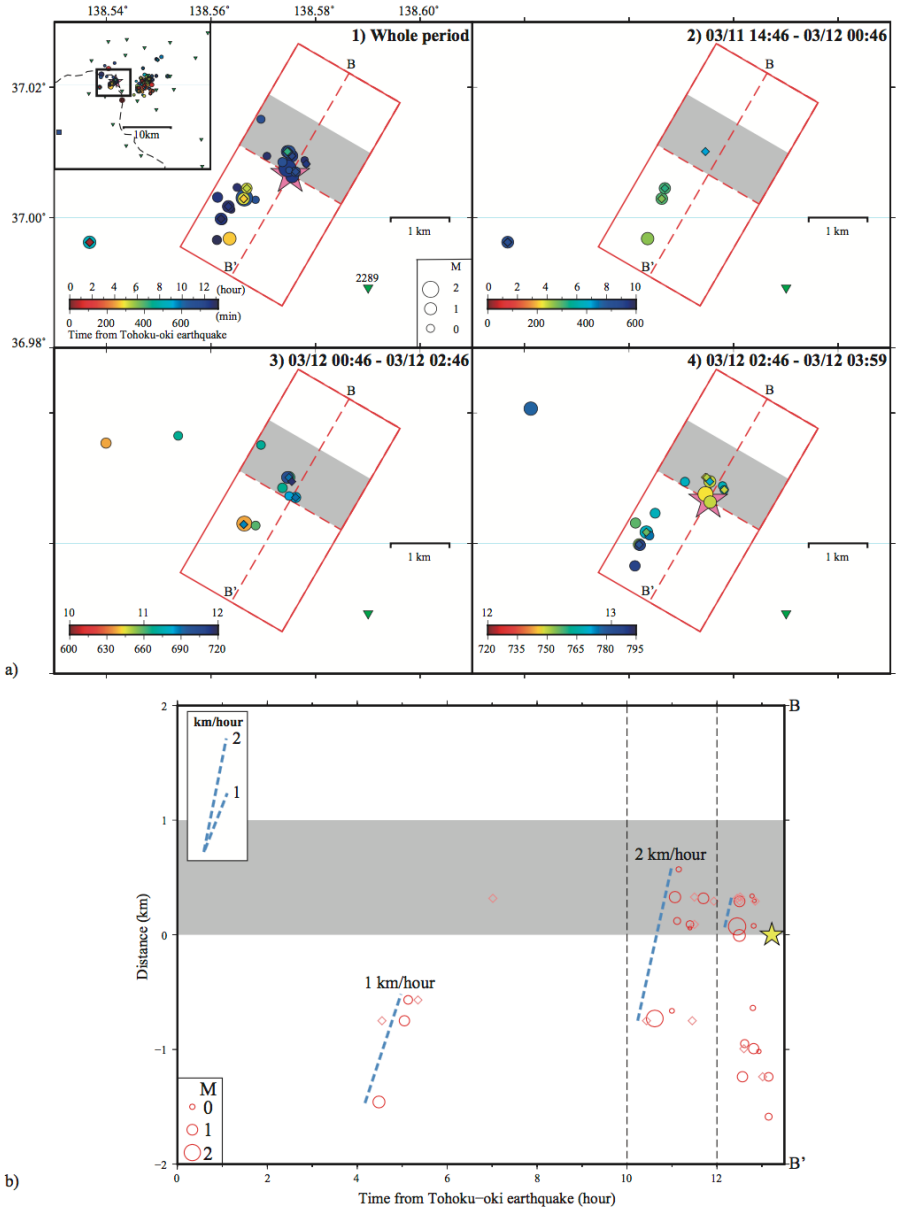

Figure 9. Space and time plots of seismicity for the western cluster. (a) Maps of detected events for different time windows. Colors indicate lapse time from the Tohoku-oki megathrust event. Pink star shows the Mw6.2 Northern Nagano earthquake. Gray rectangles indicate the ranges of 1km NE along strike from the Mw6.2 earthquake. (b) Distance versus time plot along the fault strike of the Mw6.2 earthquake. Red open circles show events of the cluster plotted as a function of time and distance from the Mw6.2 mainshock epicenter. Light-blue dashed lines indicate an approximate earthquake migration direction (a rough estimation of the migration speed is written nearby).

3.3.2. Aftershocks preceded by small local earthquakes

As mentioned above, I searched distant aftershocks that may have increased the number of local events compared with the background seismicity, and detected five in the western area and 10 in the eastern area; in both the western and eastern areas, the first local event occurred during the passage of the surface waves from the aftershocks (Figure 10 and Table 1). Only moderate or large aftershocks with $(a - b) \geq 1$ in either time window are included in Figure 10; distant events whose amplitudes could not be detected by a visual examination of the low-frequency waveforms recorded at station NZWH are excluded. As examples, seismograms of the first three local events in the western area recorded at station 0286 (Figure 6a) during or after the passage of surface waves from the M_{JMA} 6.5 event that occurred offshore of Ibaraki Prefecture (15:07:16 JST 11 March 2011) and the M_{JMA} 7.4 event that occurred offshore of Iwate Prefecture (15:08:53 JST 11 March 2011) are shown in Figure 11. All three events occurred within 100 s of each Love-wave arrival. In the subcluster in the western area, the first event of the first and third periods of activity occurred during the passage of surface waves from aftershocks. Figure 12 shows the third activity period in the subcluster during the passage of surface waves from the M_{JMA} 6.0 event that occurred offshore of Fukushima Prefecture (03:11:25 JST 12 March 2011). An M 2.2 event, which was the largest local event in both the western and eastern areas, occurred about 50 s after the Love-wave arrival from the M_{JMA} 6.0 event and was followed by relatively smaller events in the subcluster.

In the Zigokudani area, following aftershocks with $M_{JMA} \geq 6.0$, local seismicity increased significantly in all time windows (Table 2). In Chapter 2, I quantified the degree of geothermal

activity in the northern Nagano region by using published fluid temperature and flux data (Geological Survey of Japan, 2009) and compared geothermal characteristics among the North (i.e., the western and eastern areas), South, and Zigokudani areas. On the whole, the South and Zigokudani areas were characterized by relatively higher fluid temperatures and fluxes than the North area, indicating the presence of a geothermal field, and in particular, the highest fluid temperature (~80 °C) and flux (3000 L/min) were observed in the well closest to the Zigokudani area, where seismicity started during the passage of the surface waves from the Tohoku-oki earthquake. In contrast, in the South area, where activity started very soon after the passage of the Tohoku-oki surface waves, the geothermal field was relatively mild. Hence, in Chapter 2, I concluded that seismicity was dynamically triggered in the South area by the sudden excitation of geothermal fluids in the crust by strong shaking due to the Tohoku-oki surface waves. In this study, I showed that local seismicity in the Zigokudani area was modulated repeatedly by the passage of surface waves of the M_w 9.0 event and $M \geq 6.0$ aftershocks, whereas seismicity in the South area was not modulated.

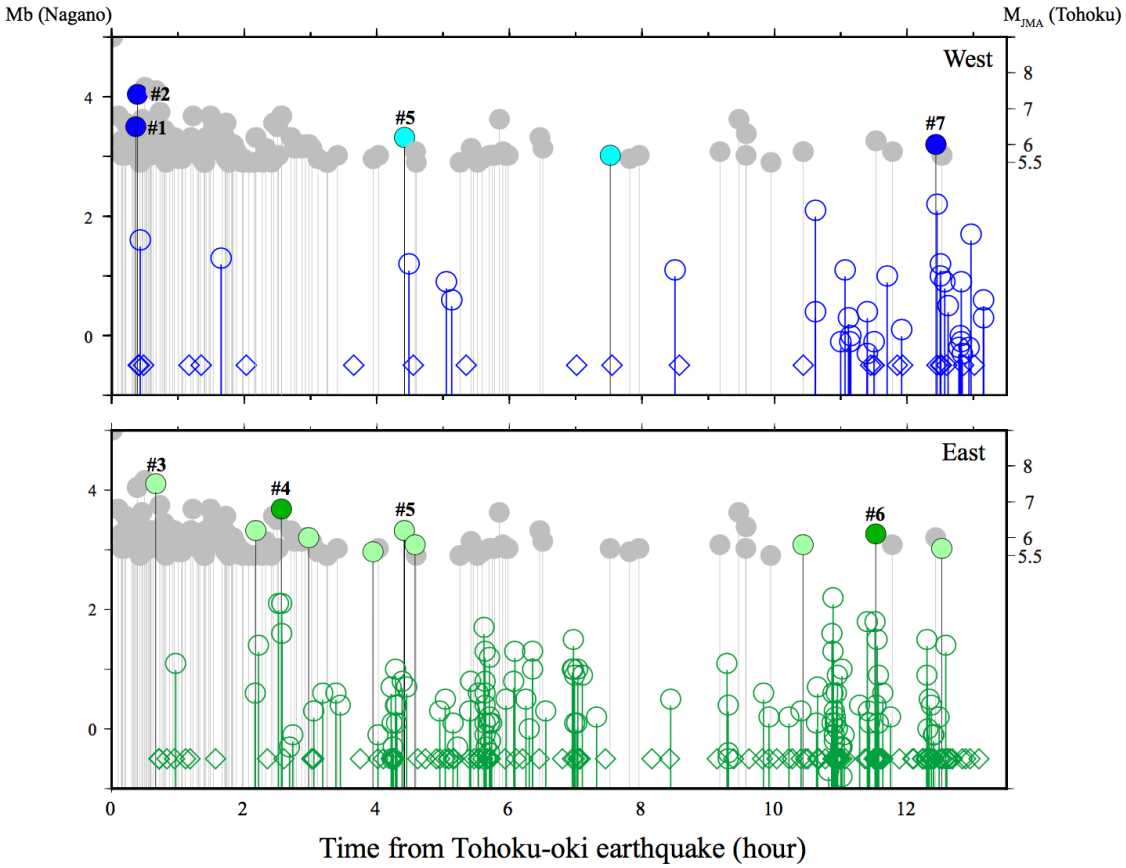

Figure 10. Time history comparison of Tohoku-oki mainshock and larger aftershocks with local (Nagano) seismicity. (a) for the western area. Gray stems indicate JMA catalog Tohoku-oki mainshock and aftershocks (M ≥ 5.5). Black stems having dark or light blue filled circles (a) on top show Tohoku-oki aftershocks that are succeeded by a relative increase of local seismicity as compared with the background seismicity. Dark-blue circles are for triggered seismicity that exceeds the statistical significance level. The numbers prefixed by "#" are consistent with the numbers of "remarkable events" of Table 3. (b) for the eastern area. Symbols have same meaning as in (a), except that blue colors are replaced by green colors.

West

Event information			100s		200s	
Origin time	Location	M_{JMA}	a	a-b	a	a-b
15:07:16	Off shore Ibaraki	6.5	1	1	2	**2**
15:08:53	Off shore Iwate	7.4	**2**	**2**	2	**2**
19:10:39	Off shore Iwate	6.2	0	0	1	1
22:16:48	Off shore Ibaraki	5.7	1	1	1	1
03:11:25	Off shore Fukushima	6.0	**2**	**2**	2	**2**
Threshold			2	2	3	2

East

Event information			100s		200s	
Origin time	Location	M_{JMA}	a	a-b	a	a-b
15:25:16	Off shore Sanriku	7.5	1	1	2	2
16:56:08	Off shore Fukushima	6.2	0	0	1	1
17:19:17	Off shore Ibaraki	6.8	3	**3**	3	2
17:43:52	Off shore Ibaraki	6.0	0	0	2	2
18:42:19	Off shore Sanriku	5.6	0	0	1	1
19:10:39	Off shore Iwate	6.2	1	1	1	0
19:20:24	Off shore Fukushima	5.8	0	0	1	1
01:11:25	Off shore Sanriku	5.8	1	1	1	-1
02:17:25	East Off shore Kanto	6.1	**5**	1	**8**	3
03:17:06	Off shore Ibaraki	5.7	1	0	3	2
Threshold			4	3	5	5

Table 1. List of larger ($M \geq 5.5$) Tohoku-oki aftershocks that have been scrutinized for possible remote triggering in the "West" and "East" Nagano regions, together with statistical-test results for their triggering significance. The tables present some event information (origin time, occurrence area and magnitude, as well as *a* and *a-b* values. The letters *b* and *a* denote the number of events, in "100s" and "200s" windows, that occurred before and after the arrival of surface waves, respectively; the difference "a-b" is reported in the table. Bold text indicates numbers that are equal or exceed each of the thresholds specified at the bottom, which have been obtained by Monte Carlo simulations.

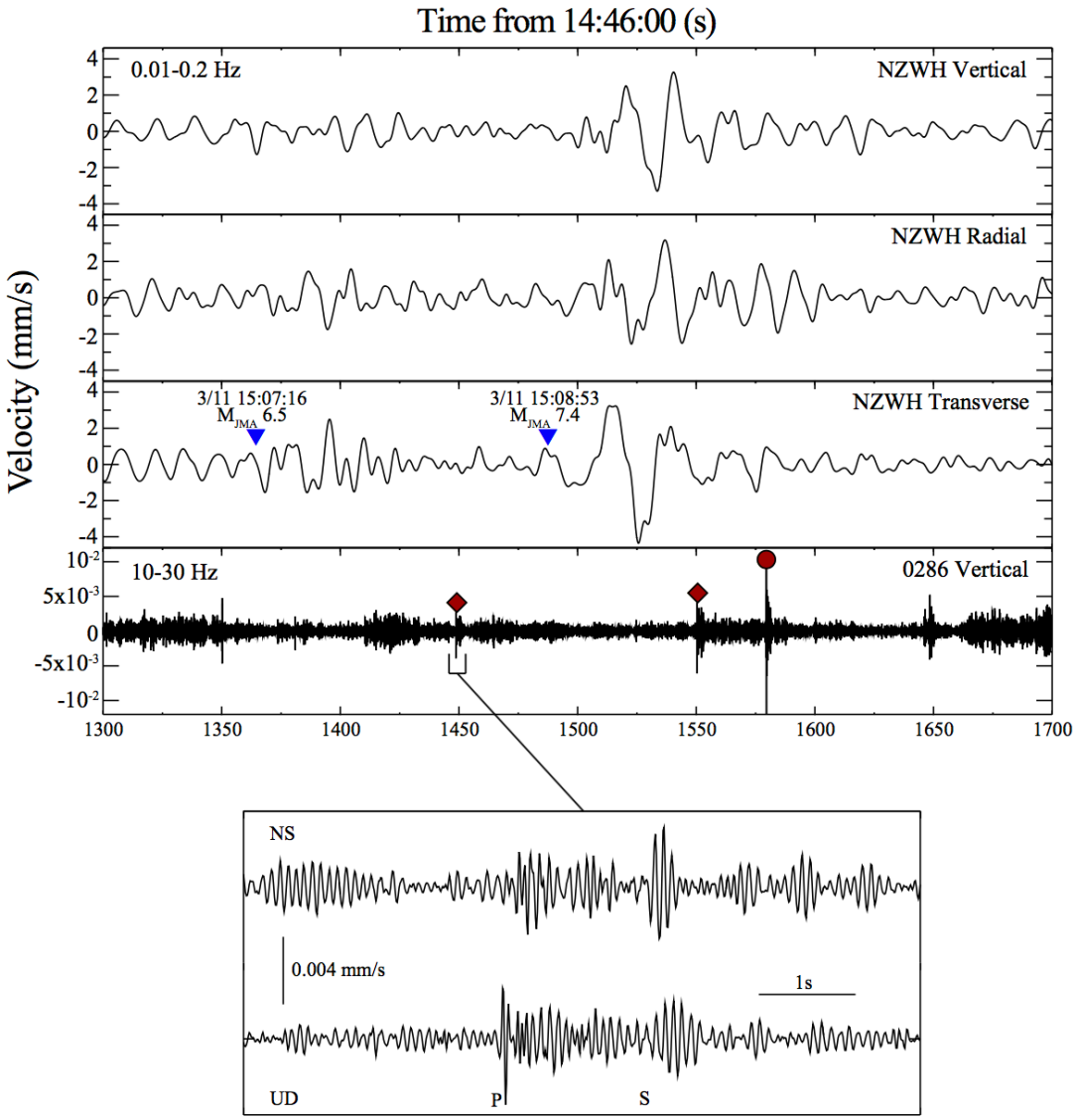

Figure 11. Earthquakes detected during the passage of surface waves from Tohoku-oki aftershocks. (a) Top to bottom: low-frequency seismograms (0.01 – 0.2 Hz) at the NZWH station (Vertical, Radial and Transverse components, around the passage of surface waves from the M(JMA) 7.4 event (#1 in Figure 10), occurred off-shore Iwate Prefecture (March 11, 2011; 15:08:53, JST)) and high-frequency waveform (10 – 30 Hz) at the temporary station 0286 (Figure 6a); locally triggered events (in the western area) are marked by small color-filled symbols (same explanations as for the MFT-detections in Figure 1). Blue inverted triangles indicate arrival of Love waves from the M(JMA)6.5 aftershock (#2 in Figure 10), occurred off-shore Ibaraki Prefecture (March 11, 2011; 15:07:16, JST) and the M(JMA) 7.4 aftershock, for a phase velocity of 4.1 km/s. (b) Enlarged high-frequency seismogram showing P- and S-wave arrivals at 0286 station from one of the triggered events.

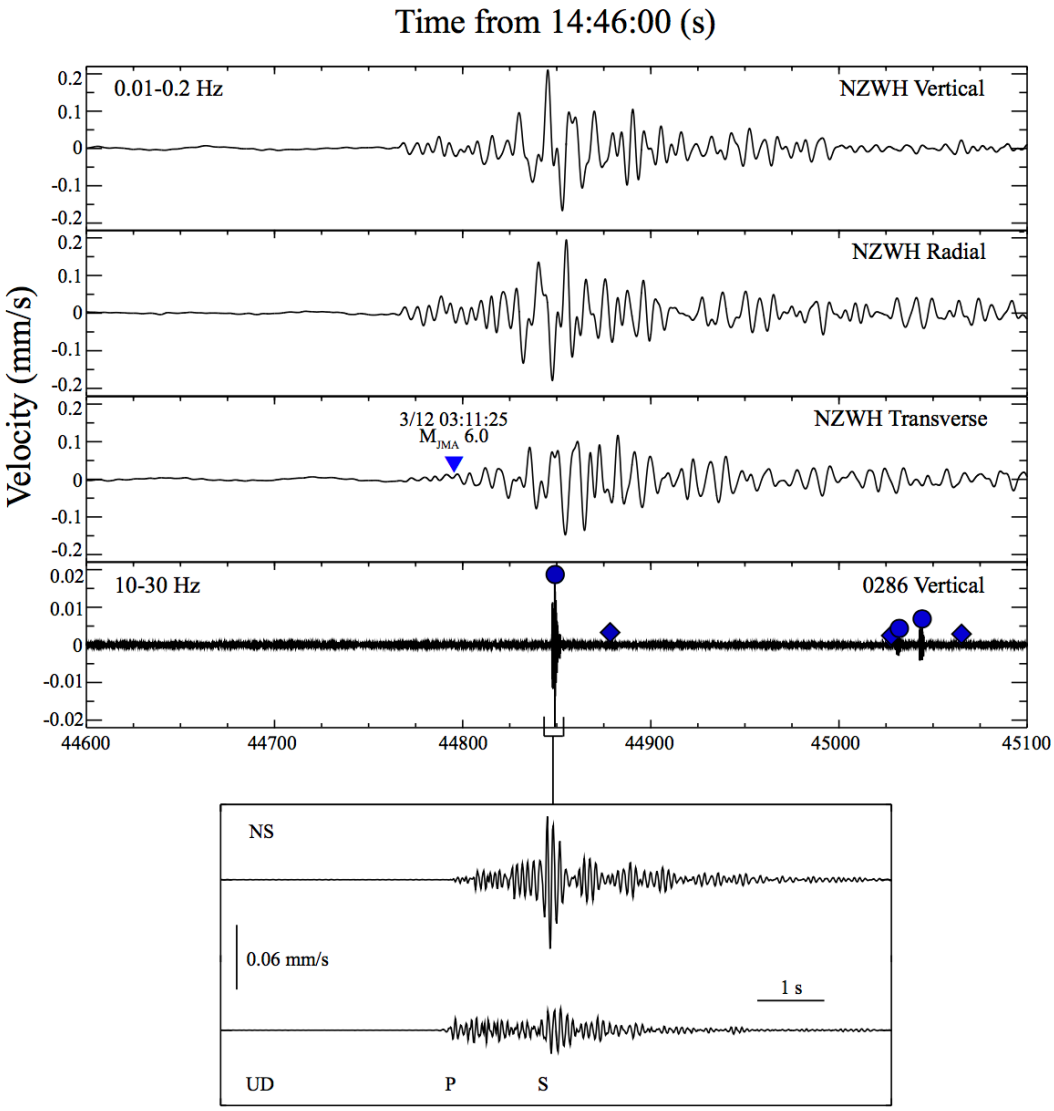

Figure 12. Local earthquakes detected during the passage of surface waves from the M(JMA)6.0 Tohoku-oki aftershock (#7 in Table 3) occurred on March 12, 2011, at 3:11:25 (JST), off-shore Fukushima Prefecture. (a) From top to bottom: low-frequency seismograms (0.01 – 0.2 Hz) at the NZWH station (Vertical, Radial and Transverse components) and high-frequency waveform (10 – 30 Hz) at the temporary station 0286; locally triggered events are marked by small circles, colored function of the lapse time from the Tohoku-oki mega-earthquake (same scale as in Figure 6). Blue inverted triangles indicate the arrival of Love waves from the Tohoku-oki aftershock, for a phase velocity of 4.1 km/s. (b) Enlarged high-frequency seismogram showing P- and S-wave arrivals from the largest event (M2.2, occurred on March 12, 2011, at 3:13:25 (JST)) among those triggered in the western region.

West

	M_{JMA} ≧6.0 100s		M_{JMA} ≧6.0 200s		M_{JMA} ≧6.5 100s		M_{JMA} ≧6.5 200s	
	A	A-B	A	A-B	A	A-B	A	A-B
Real catalogue	6	4	12	7	3	2	6	6
Threshold	11	8	20	16	7	5	12	9

East

	M_{JMA} ≧6.0 100s		M_{JMA} ≧6.0 200s		M_{JMA} ≧6.5 100s		M_{JMA} ≧6.5 200s	
	A	A-B	A	A-B	A	A-B	A	A-B
Real catalogue	14	4	28	11	4	2	8	5
Threshold	34	18	62	44	18	11	33	22

linear cluster at the South

	M_{JMA} ≧6.0 100s		M_{JMA} ≧6.0 200s		M_{JMA} ≧6.5 100s		M_{JMA} ≧6.5 200s	
	A	A-B	A	A-B	A	A-B	A	A-B
Real catalogue	1	-3	6	0	0	-1	3	1
Threshold	15	10	27	20	9	6	14	10

Zigokudani

	M_{JMA} ≧6.0 100s		M_{JMA} ≧6.0 200s		M_{JMA} ≧6.5 100s		M_{JMA} ≧6.5 200s	
	A	A-B	A	A-B	A	A-B	A	A-B
Real catalogue	**12**	**11**	16	13	**10**	**10**	**12**	**11**
Threshold	11	8	19	15	6	5	11	8

Table 2. Results of yet another statistical test to check whether the triggering of Nagano events by larger Tohoku aftershocks is significant. Besides the "East" and "West" regions, discussed in this chapter, we have also tested the triggering in a larger region, specifically for the "South" and the Zigokudani area in previous chapter, both known for geo-thermal activity. The *A* and *B* symbols represent the sum of individual *a* and *b* (Table 1), respectively, for the time windows (100s and 200s) and Tohoku-oki aftershocks magnitude thresholds (M(JMA) ≥ 6.0 and M(JMA) ≥ 6.5, reported in the head of each table. The numbers in bold indicate statistically significant triggering.

Event information				Maximum dynamic stress changes (kPa)		Significant (or not) (Table S1)	Notes
#	Origin time	Location	M_{JMA}	Love	Rayleigh		
0	14:46:18	Off shore Miyagi	9.0	300	417	-	The M9.0 megathrust event (referred as "mainshock")
1	15:07:16	Off shore Ibaraki	6.5	22	12	Significant	Suceeded by the earliest events in the “West”
2	15:08:53	Off shore Iwate	7.4	31	29	Significant	Suceeded by the earliest events in the “West”
3	15:25:16	Off shore Sanriku	7.5	44	26	Not	Suceeded by the earliest events in the “East”
4	17:19:17	Off shore Ibaraki	6.8	10	12	Signifiant	
5	19:10:39	Off shore Iwate	6.2	1.4	1.3	Not	Suceeded by first activation in the sub cluster
6	02:17:25	East Off shore Kanto	6.1	1.8	1.6	Significant	
7	03:11:25	Off shore Fukushima	6.0	1.0	1.8	Significant	Suceeded by third activation in the sub cluster

Table 3. List of dynamic stress changes associated with the 2011 Tohoku-oki earthquake and several of its aftershocks that have been discussed in the paper. The columns list the event information (origin time, location and magnitude), the maximum dynamic stresses (kPa) corresponding to the passage of the Love and Rayleigh wave trains, the statistical significance for triggering (Table 1) and some important notes.

3.4. Discussion

3.4.1. Delayed activation following the Tohoku-oki earthquake and dynamically initiated activity in the overall research region

In Chapter 2, I detected a small number of events (<10) in the western and eastern areas as defined in this chapter. Seismicity in these areas started within 6 hours after the origin time of the Tohoku-oki megathrust event. Based on the space-time distribution of the many events detected in this chapter, I confirmed that the initiation of the seismicity was delayed by few tens of minutes after the Tohoku-oki mainshock. Generally, local delayed activation following distant large earthquakes is explained by mechanisms related to acceleration of friction instability (Dieterich, 1994), subcritical crack growth (Das and Scholz, 1981), fluid flow (Hill et al., 1993), or both. In particular, the first and second mechanisms are dominated by stepwise stress perturbation such as static stress change. However, the static stress changes calculated for the *Mw* 6.2 earthquake is on the order of 0.01 MPa (see Chapter 2), which is at the level of threshold values known to be able to trigger seismic activity. Therefore, it is hard to think that the clearly activated seismicity discovered in this research was mainly driven by the increase in static stress changes, even though such slight static stress changes may trigger weak seismicity. In Chapter 2, I inferred that the delay of the seismicity in overall northern Nagano region reflected a physical process involving crustal fluid flow initiated mainly by influences from the Tohoku-oki mainshock. In particular, in the hypocentral region of the M_w 6.2 event, I inferred that the delay in the initiation of seismicity reflected the time required for the pore pressure to be increased by fluid flowing from a deep

reservoir below the M_w 6.2 event source area to the vicinity of its hypocenter at seismogenic depths.

However, there is no evidence of earthquake migration from the deeper part to shallower part, which would indicate fluid flowing from a deep-reservoir (Figure 8), and, as I will show later in section 3.4.2, there is a possibility that fluids exist widely in the seismogenic region where local events are detected in this analysis. Therefore, I assume that fluid flew from some sources located close to the locally triggered seismicity, and likely not from the inferred deep reservoir mentioned above. Furthermore, if the activation of fluid flow initiated within the seismogenic region immediately after the M9 event, one might expect a similar, immediate activation of seismicity. Nevertheless, local seismicity initiated with a delay of several tens of minutes after the M9 event (Figure 6) and immediately after some Tohoku-oki aftershocks (Table 1 and 3). Hence, it is reasonable to suppose that fluid flow, which could have triggered seismicity, initiates immediately after such aftershocks rather than Tohoku-oki mainshock.

In general, two mechanisms have been proposed to explain fluid flow in the crust due to distant large earthquakes: 1) dynamic excitation, and 2) increased permeability due to the opening of flow pathways under a static extensional stress regime.

Regarding the first mechanism, previous research has modeled permeability increase related to hydrous fluid transfer caused by the opening of fractures that have become clogged by accumulated detritus (e.g. Brodsky *et al*., 2003), shaking-induced dilatancy (Bower and Heaton, 1978), fracture of an impermeable fault (King et al., 1999) or pore pressure increase related to bubble mobilization (e.g. Sturtevant *et al*., 1996). Field observations have suggested that such changes are caused by dynamic stress changes on the order of tens of kilopascals (e.g., Elkhoury

et al., 2006). In Chapter 2, I estimated the peak dynamic stress changes excited by the Tohoku-oki earthquake to be >300 kPa by using waveform data recorded at the NZWH Hi-net station; therefore, these dynamic stress changes would be sufficient to increase permeability and pore pressure, and initiate fluid migration.

On the other hand, seismicity started during or immediately after the passage of surface waves from some Tohoku-oki aftershocks that occurred 1 h after the origin time of the Tohoku-oki mainshock. Using a nominal G value of 30 GPa and v_{ph} = 4.1 km/s for Love waves or 3.5 km/s for Rayleigh waves, I estimated the maximum dynamic stress change values for seven events that increased local seismicity significantly or were preceded by remarkable activity (Table 3) in the same way I calculated peak dynamic stress changes for the Tohoku-oki mainshock in Chapter 2. The surface waves arrivals from the M_{JMA} 6.5 and M_{JMA} 7.4 aftershocks, which were followed by the earliest local events in the western area, about 5 km south of the M_w 6.2 northern Nagano event, were associated with maximum dynamic stress changes on the order of 10 kPa. Similarly, the arrival of surface wave from the M_{JMA} 7.5 event, which was followed by the two earliest local events in the eastern area, was associated with a maximum dynamic change on the order of 10 kPa. The surface wave arrivals from the M_{JMA} 6.8 and M_{JMA} 6.1 aftershocks, which were followed by significant levels of local seismicity in the western area, were associated with maximum dynamic stress changes on the order of 10 kPa and 1 kPa, respectively. The surface waves arrivals from both the M_{JMA} 6.2 and M_{JMA} 6.0 events, which were followed by the first and third periods of activity in the subcluster in the western area, respectively, were associated with maximum dynamic stress changes of about 1 kPa.

Hence, some moderate or large aftershocks that were associated with maximum dynamic stress changes ranging from around 1 to a few tens of kilopascals might have triggered seismicity without large delay in both the eastern and western areas. These values are similar to the minimum dynamic stresses that have been shown to trigger earthquakes in geothermal regions, which are particularly susceptible to dynamic triggering, on the North American continent (on the order of 1–10 kPa; e.g., Aiken and Peng, 2014). Thus, the excitation of fluids leading up to the triggering of an earthquake can be initiated even by such small dynamic stress changes. Nevertheless, much higher values of the order of 10 or 100 kPa have been shown to be the dynamic stress thresholds for triggering earthquakes in Japan (e.g., Van der Elst and Brodsky; 2010). Moreover, the eastern and western areas, unlike the South and Zigokudani areas, are characterized by low surface-fluid temperatures, indicating the absence of a geothermal field (Figure 10 in Chapter 2).

To clarify the origin of seismicity directly triggered by small dynamic stress changes, not large stress changes from Tohoku-oki mainshock, in the eastern and western areas, I introduce a model that involves increasing permeability or pore pressures. In this model, distant seismic waves dislodge sedimentary particles blocking flow paths (Brodsky et al., 2003), fracture impermeable media (Bower and Heaton, 1978; King et al., 1999), or excite bubble during the dilatational phase of surface waves (e.g. Sturtevant *et al*., 1996), thus increasing permeability or pore pressure, leading up to initiating fluid flow. Although this fluid flow involving such increasing permeability or pore pressure stochastically expects to be much more difficult to be suddenly initiated by small dynamic stress changes than by large stress changes from Tohoku-oki mainshock, it is not necessarily impossible. In addition, even though the probability of initiating flow per one passage of surface waves is low, multiple passages, in a relatively brief time, may

rapidly increase the expected value. The preparation process of fluid flow might have been assisted by repeated high or low amplitude shaking due to the M9 event and subsequent aftershocks. In the eastern and western areas, seismicity was apparently directly triggered, long after the megathrust event followed by frequent aftershocks, by small-amplitude surface waves. The scenario outlined above suggests that the repeated passage of the amplitudes of seismic waves from the Tohoku-oki mainshock-aftershock sequences may have prepared the situation which highly facilitates fluid flow through such processes as weakening clogs, damaging impermeable pathways or exiting bubble, and slight dynamic stress changes from several aftershocks as listed in Table 1 or 3 could initiate sudden fluid flow later, possibly inducing seismicity. Moreover, it is also possible that more Tohoku-oki aftershocks not listed in Tables 1 or 3, which apparently did not trigger small local events, may have aseismically facilitated and further promoted the fluid flow.

At the same time, I cannot exclude the possibility that fluid flow was initiated under a static stress regime. In many areas of the Japanese islands, compressional stress regimes within the continental crust changed to extensional regimes following the Tohoku-oki megathrust event (Geospatial Information Authority of Japan, 2011). Under such static extensional stress regimes within the continental crust, channels in the crust may open, allowing fluid flow (e.g., Muir-Wood and King, 1993).

If the above scenario is correct, then fluid flow and accompanying seismicity in the eastern and western areas can be attributed to the influence of the Tohoku-oki mainshock. However, some delayed local events that occurred during or immediately after the passage of surface waves from distant aftershocks resulted from the repeated passage of transient seismic waves associated with

slight dynamic stress changes that helped increase permeability through opening potential flow pathways to flow fluid or pore pressure through bubble mobilization.

I confirmed whether local seismicity in the western, eastern, South, and Zigokudani areas was not only dynamically triggered by individual aftershocks but also modulated throughout the time series of seismicity. In the western, eastern, and South areas, aftershocks did not significantly increase seismicity in any time window or magnitude range (Table 2). In the Zigokudani area, however, aftershocks with magnitudes larger than M_{JMA} 6.0 clearly increased local seismicity significantly for most examined time windows. This difference between the Zigokudani and the other areas may reflect the ease with which permeability and pore fluid pressure can suddenly build up in the Zigokudani area because of, for example, high fluid temperatures and fluxes, and characteristic chemical factors due to geothermal activity.

In both the western and eastern areas, I obtained five first-motion mechanisms, for four MFT-detected local events and the M_w 6.2 event, with relatively high quality (B or C). Previous studies have included first-motion mechanisms determined by the HASH program with these quality levels in their analyses of seismicity in other regions (e.g., Katsumata *et al.*, 2015). In the western area, a quality C mechanism was obtained for one detected event, and in the eastern area, of the three mechanisms obtained, two were classified as quality C and the third was classified as quality B. All five events had strike-slip type mechanisms, different from the reverse-fault type mechanism expected from the background seismicity recorded in this area before the Tohoku-oki earthquake (Terakawa *et al.*, 2013). This difference in mechanism between events occurring before and after the Tohoku-oki earthquake may reflect changes in pore fluid pressure, thus supporting a scenario involving fluid migration.

3.4.2. Seismicity by region

3.4.2.1. Swarm-like seismicity in the eastern area

In the eastern area, swarm-like seismicity began in the shallow crust within 1 h of the Tohoku-oki earthquake, during the passage of surface waves from the M_{JMA} 7.5 event offshore of Iwate Prefecture at 15:25 JST 11 March (Figure 6c, Tables 1 and 3). Such swarm-like seismicity clearly indicates that fluid flow caused the pore-fluid pressure to increase (e.g., Scholtz, 2002; Hainzl and Ogata, 2005). The depth of the seismicity in the eastern area apparently increased with time from about 2 km to more than 8 km. This depth increase, and tomographic results showing a high v_p/v_s structure in the shallow sedimentary layer in the entire northern Nagano hypocentral region (Sekiguchi et al., 2013), suggest the existence of a fluid source in the shallow crust in this area. Fluid diffusion and associated seismicity are often explained by the sudden connection of a relatively high-pressure source to its lower pressure surroundings (Ingebritsen and Manning, 2010), but fluids cannot diffuse from a depth of 2 km to a depth of more than 6 km (as would match the migration of the seismicity in the eastern area) because the confining pressure at 2 km depth is comparable to hydrostatic pressure at 6 km depth (assuming a general crustal density of 2.7 Mg/m^3 and gravitational acceleration of 9.8 m/s). Figure 13 is a time–distance plot of seismic events from the first event in the eastern area. From the time of the earliest event, the fluid diffusion front traces a parabolic curve, corresponding to D = 100–200 m^2/s, where D is the coefficient of diffusion. This diffusivity range is much higher than generally estimated in the crust, although a few studies have obtained higher values (e.g., Antonioli *et al.*, 2005; Noir *et al.*, 1997).

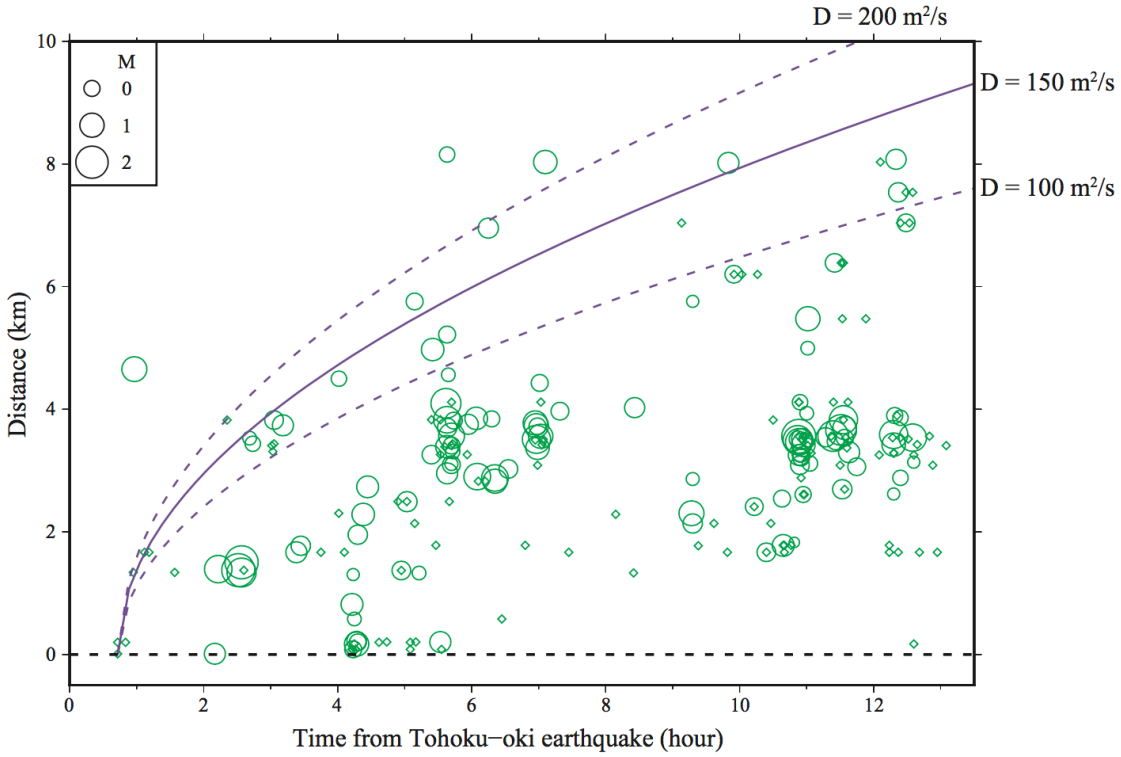

Figure 13. Distance versus time for the overall eastern cluster**.** Distances of events are relative to the first event occurred in the eastern area. Solid purple, upper dashed and lower dashed lines indicate the front of fluid diffusion (Shapiro et al., 1997) for a diffusivity, D, of 150, 200 and 100 (m^2/s), respectively.

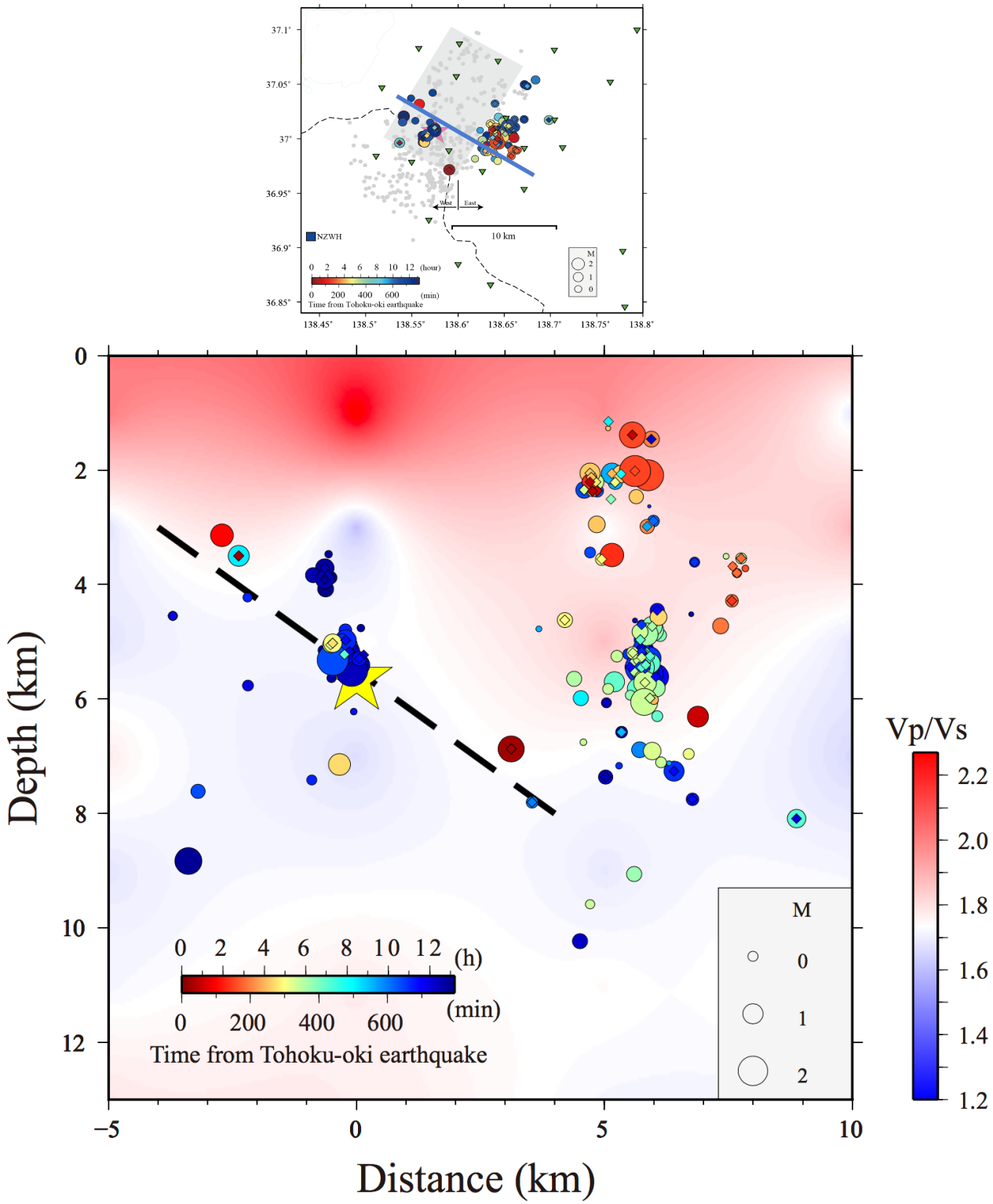

Figure 14. MFT-detected events overlapped with the Vp/Vs structure. (top) Same map as in Figure 6(a), with a solid blue line indicating the profile for the cross-section below; (bottom) Cross-section showing the seismicity distribution (same as Figure 8(a)) overlapped on the Vp/Vs structure (Sekiguchi et al., 2013).

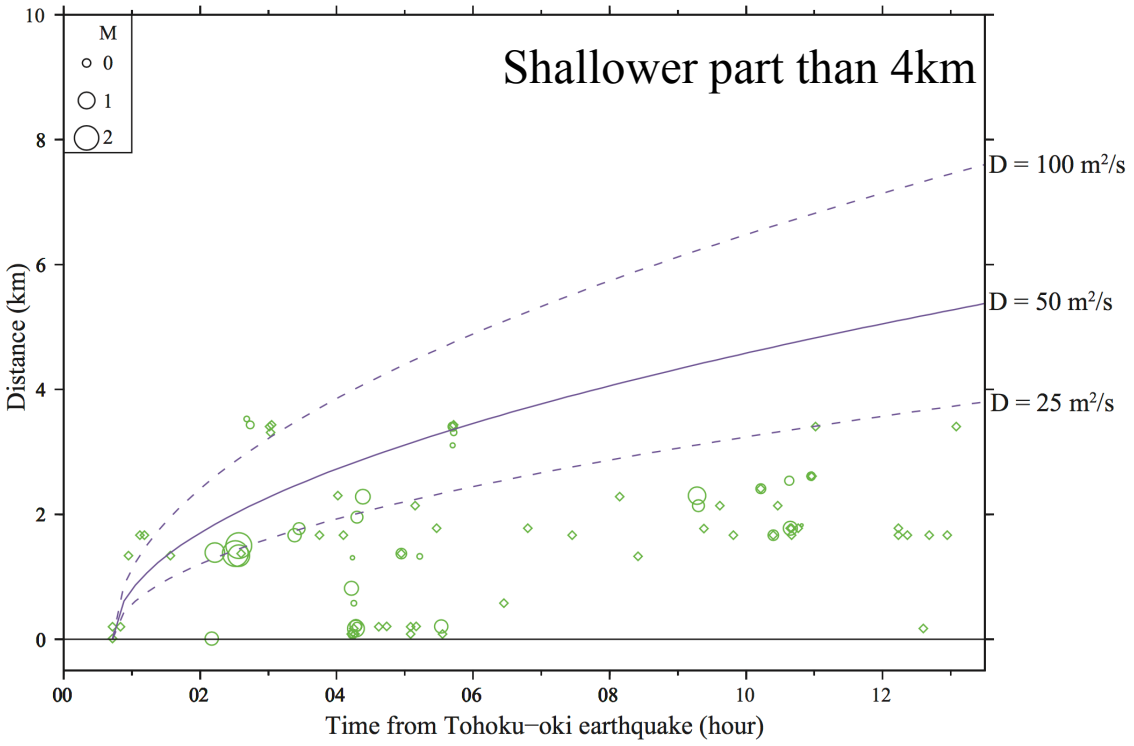

Figure 15. Migration of seismicity within the shallower sub-cluster in eastern region. Relative distances are measured relative to the first event of the shallower sub-cluster. Solid purple, upper dashed and lower dashed lines indicate the fluid diffusion front, for a diffusivity parameter, D, of 50, 100 and 25 (m^2/s), respectively.

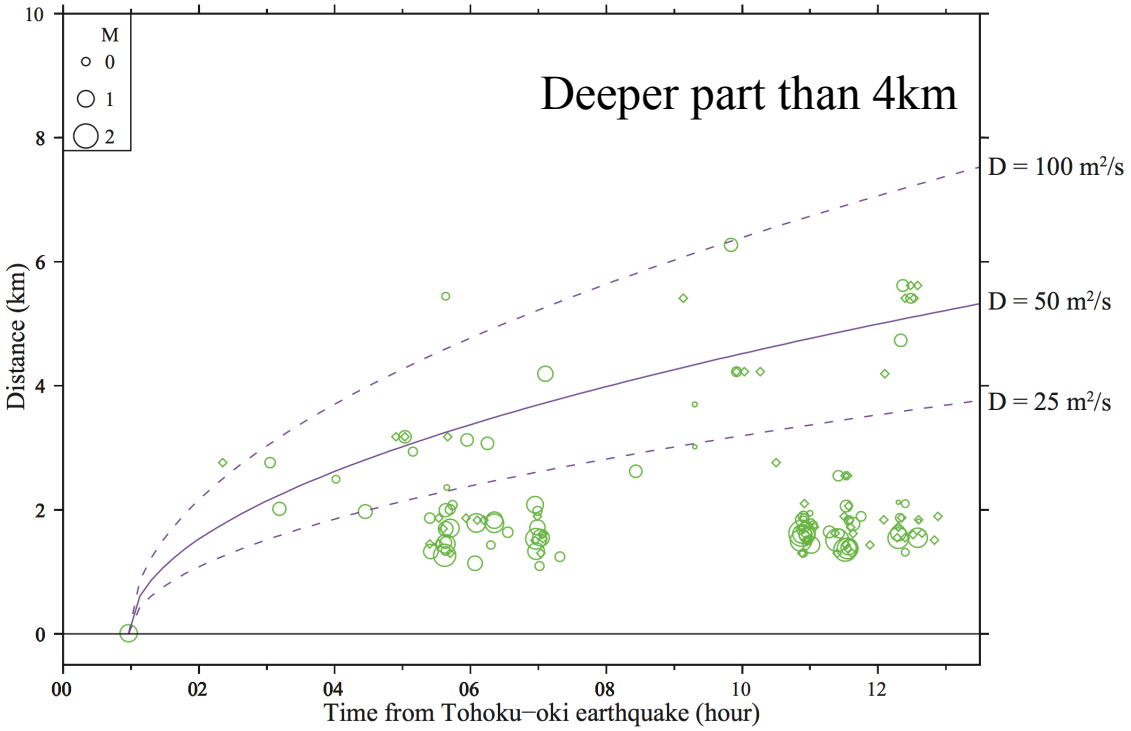

Figure 16. Migration of seismicity within the deeper sub-cluster in eastern region. Relative distances are measured relative to the first event of the deeper sub-cluster. Solid purple, upper dashed and lower dashed lines indicate the fluid diffusion front, for a diffusivity parameter, D, of 50, 100 and 25 (m^2/s), respectively.

On the other hand, there appear to be two sub-clusters of seismicity in the eastern area, one at about 2 km depth and the other at about 5 km depth (Figure 8). Figure 14 shows the event depth distribution superposed on the v_p/v_s distribution along the dip direction of the M_w 6.2 event fault. In the eastern area, v_p/v_s is high in the seismically active area at around 5 km depth, as well as in the shallower crust. This seismicity distribution may indicate that highly pressurized fluid sources existed close to both activity sub-clusters in the eastern area. This model is also expected to satisfy the condition of fluid pressure. In Figures 15 and 16, the time–distance distributions from the time of the earliest event in each subcluster are shown for events occurring at depths above and below 4 km. For both subclusters, D values were estimated to be on the order of 10 m^2/s; these are more realistic than the range obtained by assuming a single shallow fluid source (Figure 13).

Relatively early fluid diffusion in the shallow crust (<4 km depth) may be enhanced in the eastern area, because seismic activity in the shallower subcluster was initiated relatively earlier, within 1 h after the M_w 9.0 event and immediately after the M_{JMA} 7.5 aftershock, which was associated with dynamic stress changes of 26 - 44 kilopascals (Table 3), which is a bit less than the threshold for triggering seismicity in Japan (order of 90 kPa) (Van der Elst and Brodsky, 2010). Similarly, in Chapter 2, I found that in the shallow crust in the South area, swarm-like seismicity occurred immediately after the passing of surface waves from the Tohoku-oki mainshock (Figure 12 in Chapter 2). I speculate that the initiation of geofluid circulation along shallow fault-like structures by surface waves from the remote M_w 9.0 event, which would have had maximum amplitudes in the shallow crust, can explain the shallow swarm-like activity. Hence, especially in the shallow crust in the eastern area, dynamic stress changes caused by the remote M_w 9.0 event may have facilitated the early initiation of fluid flow, and the relatively small

dynamic stress changes caused by the M_{JMA} 7.5 event may have initiated fluid flow and seismic activation. In addition, the static stress regime within the continental crust in many areas of Japan changed from compressional to extensional after the Tohoku-oki megathrust event (GSI, 2011); this change may have resulted in the opening of cracks in the local crust, facilitating the mobilization of fluids.

In the eastern area, the surface structure of the northeast section of the Miyanohara fault, which is part of the western marginal fault zone of the Tokamachi tectonic basin, indicates a reverse-fault type displacement with a high dip angle to the northwest and an east–northeast strike (Ikeda *et al.*, 2002). Because detailed information about the subsurface structures on this fault is lacking, it is not possible to compare the seismicity distribution in the eastern area with such structures. Nevertheless, they may play a role in the development of channels permitting fluid flow. I assume that the relatively strong, swarm-like activity in the eastern area reflects the presence of fluids flowing along fault-like structures which create a favorable environment for fluid flow.

Several other aftershocks, excluding the M_{JMA} 7.5 event, were also associated with an increased number of local events above the background seismicity in the eastern area (Table 1). Slight dynamic stress changes due to these distant events may also have triggered successive seismicity by allowing further fluid flow.

As in Chapter 2, I calculated the static Coulomb stress changes (ΔCFS) due to slip on the Tohoku-oki earthquake fault plane (Yagi and Fukahata, 2011) for the mechanisms of three small local events in the eastern area with relatively high quality (B or C). The obtained ΔCFS values varied from –0.08 to 0.02 MPa, that is, below or close to the static stress threshold of 0.01 MPa,

above which earthquake triggering is usually observed (Parsons *et al.*, 2008). Therefore, it is doubtful that these static stress changes could have triggered the seismicity in the eastern area.

I speculate that dynamic stress changes or the static extensional stress regime due to the Tohoku-oki mainshock, or both, may have constructed the circumstance that facilitates fluid flow, and a large M 7.5 aftershock finally initiated fluid flow into the surrounding seismic crustal zone through fault-like structures in the eastern area and trigger swarm-like seismicity. This flow would have been from at least two sources, one at about 2 km depth and the other at about 5 km depth. Then, the repeated passage of surface waves from large or moderate Tohoku-oki aftershocks, and the associated slight dynamic stress changes could have both promoted further fluid flow into the surrounding crust and directly triggered seismicity.

3.4.2.2. Dynamically enhanced earthquake migration in the subcluster in the western area

In the western area, seismicity started in a tight subcluster at about 5km depth on the estimated fault plane of the M_w 6.2 event, with a delay of about 4 h after the M_w 9.0 event, and intense activity associated with earthquake migration occurred three times (Figure 9). Weak isolated seismicity started relatively early, after a delay of several tens of minutes or a few hours, deeper (about 7 km depth) or shallower (about 3km depth) than the subcluster, respectively.

In this subcluster, the first seismicity migration started about 1.5 km southwest along the fault strike from the M_w 6.2 epicenter during the passage of surface waves from a Tohoku-oki aftershock, and seismicity migrated at a speed of ~1 km/h (Figure 9a2 and 9b). The second migration started about 0.7 km southwest of the epicenter, near the place where the first migration

terminated, and the migration speed was ~2 km/h (Figure 9a3 and 9b). Thus, the observed migration speeds were mostly consistent with the values of ~1 km/day to ~1 km/h estimated for aseismic slip (e.g., Yagi *et al.*, 2014; Kato *et al.*, 2016; Lohman and McGuire, 2007). I fitted a migration front curve predicted by a fluid diffusion model, according to which the distance $r = \sqrt{4\pi Dt}$, where D = 25–60 m^2/s. In general, estimated diffusivities for crustal fluids are on the order of 0.01 to 10 m^2/s (e.g., Sholtz, 2002; Ingebritsen and Manning, 2010), though lower values, on the order of 0.01 to 0.1 m^2/s, have been observed in Japan (Okada *et al.*, 2015). Therefore, I inferred that either aseismic slip or fluid diffusion could drive this earthquake migration, and I interpreted the successive activations as due to the nucleation process of the moderate M_w 6.2 event.

As I pointed out above, the first and third activations in the subcluster started during the passage of surface waves from aftershocks. For the M_{JMA} 6.2 event offshore of Iwate Prefecture and the M_{JMA} 6.0 event offshore of Fukushima Prefecture, which were capable of triggering the first and third activations, respectively, I obtained maximum dynamic stress change values of 1.4 and 1.8 kPa, (Table 3). Surprisingly, these values are smaller than the threshold dynamic stress change values (several tens of kilopascals up to 100 kPa) for triggering earthquakes in Japan (e.g., van der Elst and Brodsky, 2010). Despite these low dynamic stress change values, the third activation occurred within several hundred meters of the *Mw* 6.2 local hypocenter (Figure 9a4) was well correlated with the surface waves from the M_{JMA} 6.0 event (Figure 12 and Table 1). Considering all of the above factors, I speculate that stress accumulation on the fault or weakening of the fault strength due to either aseismic slip or fluid flow along strike occurred before the third activation progressed to the critical state, thus allowing intense seismicity to be triggered by only

a slight dynamic stress disturbance in the area surrounding the source of the local M_w 6.2 event (gray rectangle in Figure 9).

Regardless of the driver of the earthquake migration, the relatively delayed initiation of activity in the subcluster appears to be result from a fluid-related process. Given tomographic results (Sekiguchi *et al.*, 2013), it is possible that a fluid source exists in or near the southwest part of the subcluster where the earthquake migration initiated. Figure 17 shows the depth–distance distribution of the western seismicity along the strike of the M_w 6.2 fault plane superposed on the v_p/v_s distribution. The seismic activity occurred at depths of less than 10 km. On the northeast side of the M_w 6.2 epicenter, the region with high v_p/v_s values is limited to depths shallower than about 3 km, whereas on the southwest side, high v_p/v_s values extend down to about 8 km depth. Thus, the southwest, not the northeast, part of the subcluster lies within the region of relatively high v_p/v_s values.

I also calculated the effect of static ΔCFS values due to the Tohoku-oki earthquake on the first-motion mechanisms of a small local event with quality C in the subcluster and of the local M_w 6.2 event with quality B. The ΔCFS values on both nodal planes of the event that occurred during the second activation about 0.7 km southwest along the fault strike from the M_w 6.2 epicenter (Figure 6a) were relatively large, about 0.14 and 0.06 MPa, which are significantly larger than the typical triggering threshold (on the order of 0.01 MPa; e.g., Stein, 1999). The ΔCFS values obtained for the M_w 6.2 event mechanism were negative or slightly positive (~0.06 MPa). Unfortunately, I have too little information on the obtained mechanisms to interpret static stress change interactions, so I cannot conclude the contribution of static stress changes from the Tohoku-oki earthquake from consideration with regard to initiation of activity in the subcluster.

Nevertheless, these calculations may imply that static stress changes in the southwest were also associated with the initiation of the first and second activations, whereas seismicity in the gray rectangle in Figure 9, mainly associated with the second and third activations, appears to be difficult to be explained by ΔCFS values alone.

Although the M_{JMA} 6.2 event offshore of Iwate Prefecture might have triggered the earliest event of the first activation, which started in the southwest within 200 s after the Love-wave arrival, this moderately distant event did not significantly increase the number of local events. Presumably, dynamically or statically prepared fluid flow resulting from the Tohoku-oki mainshock and subsequent aftershocks and relatively high ΔCFS could be responsible for the initiation of first activation, and the slight dynamic stress changes from this aftershock event may have provided only the final push required to trigger the activity.

Consequently, I interpreted the earthquake migration accompanying the aseismic slip or fluid diffusion in the subcluster as the nucleation process leading up to *Mw* 6.2 local event. The initiation of seismicity in the subcluster may be explained by not only flow from a fluid source located near the southwestern high v_p/v_s lobe but also relative higher values of ΔCFS in the southwestern part. Regarding the third activation, I assume that successive dynamic stress changes caused by the remote M_{JMA} 6.0 aftershock contributed to the acceleration of the source nucleation process in northern Nagano, culminating with the M_w 6.2 earthquake.

In contrast, in the deeper or shallower part than subcruster, some isolated weak seismicity started relatively early, after a delay of only several tens of minutes from the origin time of the M_w 9.0 megathrust event. Although a few of the earliest local events occurred at about 7 km depth after or during the passage of surface waves from the M_{JMA} 6.5 and M_{JMA} 7.4 aftershocks, which

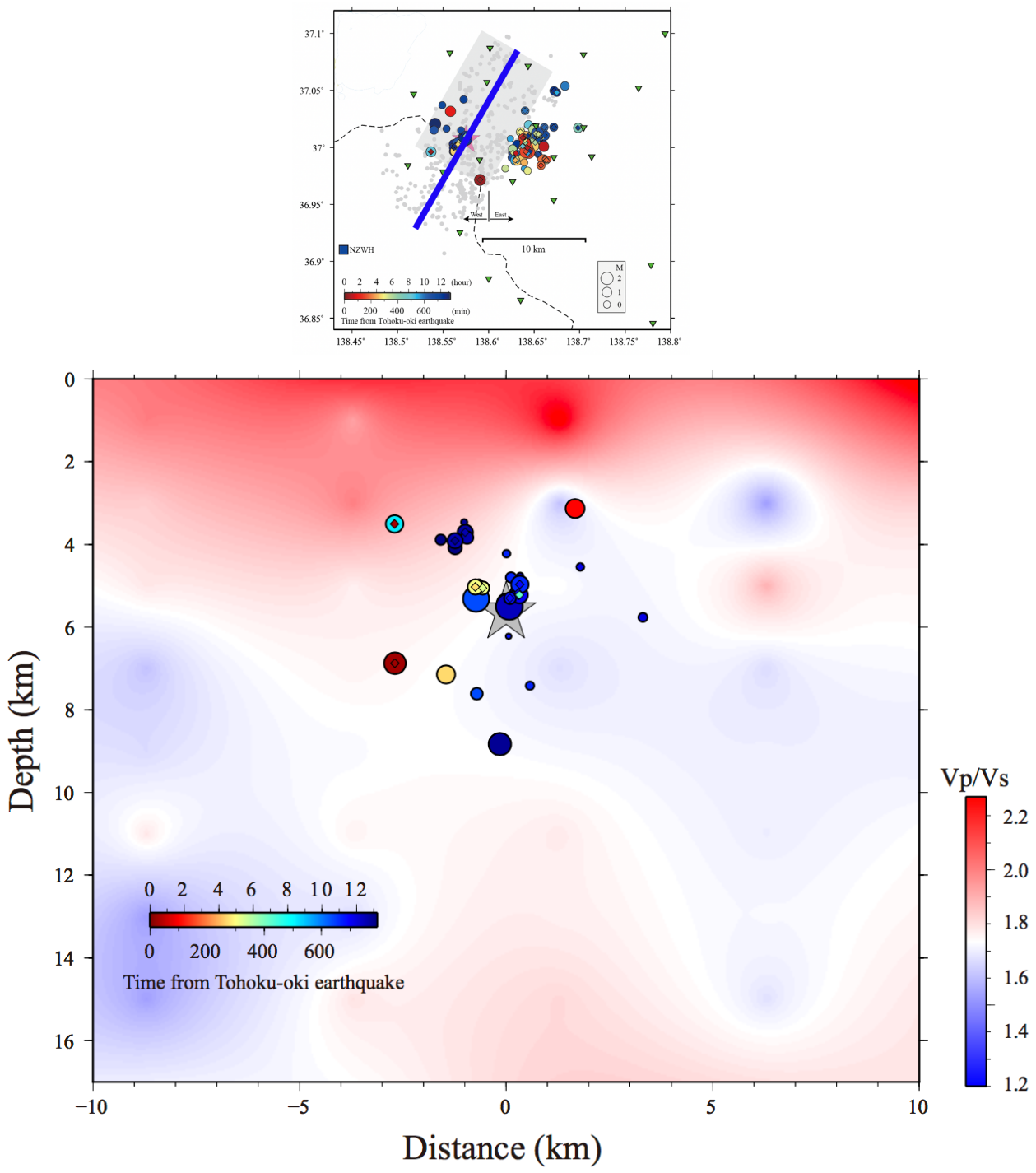

Figure 17. MFT-detected events (western area) overlapped with the Vp/Vs structure. (top) Same map as in Figure 6(a), with a solid blue line indicating the profile for the cross-section below; (bottom) Cross-section showing the seismicity distribution (western area) overlapped on the Vp/Vs structure (Sekiguchi et al., 2013).

caused small dynamic stress changes on the order of a few tens of kilopascals (Figure 11 and Table 3), subsequent activity was relatively sparse, unlike in the western subcluster and eastern area. Such relatively early triggering followed by an absence of activity appears to reflect immediate fluid flow and the lack of subsequent flowing further into the surrounding area. As shown in Figure 17, some of the earliest events in the deepest part and some relatively early events in the shallowest part were in or near high-v_p/v_s regions. If individual isolated diffusible fluid sources were located in these regions, then fluid could flow and elevate the pore-fluid pressure sufficiently to cause failure at some points in the shallowest or deepest parts; however, considering the subsequent sparseness of activity, the available fluid may have been insufficient to flow further into the surrounding area.

As another model, it might be possible to explain the greater delay of activity in the subcluster, compared with that in the shallower or deeper part, by the diffusion of geofluids from some sources located at the shallower or deeper part to medium depth, where the subcluster seismicity occurred, along the dip of the M_w 6.2 event fault plane. However, the seismicity distribution along the dip of the fault plane (Figure 8a) shows no evidence of swarm-like seismicity that would indicate active fluid flow, unlike in the eastern area, where I interpreted the seismic swarm to result from diffusion of crustal fluids through fault-like structures. Although it is possible that flow along the dip may have occurred aseismically, because the physical properties of the fault plane differed from those of the fault-like structures in the eastern area, it is more reasonable to consider a different fluid source and flow path as mentioned above.

3.4.3. Observed high permeability values in both areas

I estimated diffusivity values of ~10 m^2/s for earthquake migration or expansion in both the western and eastern areas. I assumed that the permeability K is proportional to $D\varepsilon\gamma C_T$ (Noir *et al.*, 1997), where D is diffusivity, ε is porosity, γ is viscosity, and C_T is the isothermal compressibility coefficient. Using nominal values $\varepsilon = 0.05$, $\gamma = 2.0\times10^{-4}$ Pa·s, and $C_T = 4.0\times10^{-10}$ Pa^{-1} for water under temperature and pressure conditions of around 5 km depth, I estimated the permeability to be $4.0\times10^{-14} - 4.0\times10^{-13}$ m^2. This permeability is 0–5 orders of magnitude larger than expected at depths of 1–10 km in typical brittle crust (Ingebritsen and Manning, 2002) and is roughly consistent with the relatively high values sometimes associated with earthquake migration or expansion involving the flow of highly pressurized fluids (Ingebritsen and Manning, 2010). In addition, large earthquakes often cause the permeability of the local crust to be temporarily enhanced through the static or dynamic processes (e.g., Rojstaczer *et al*., 1995; Elkhoury *et al.*, 2006) discussed in section 3.4.1. In other regions of Japan, studies that analyzed changes in water levels in wells also reported permeability changes after the Tohoku-oki earthquake (Kitagawa and Koizumi, 2011; Kinoshita *et al.*, 2015). I speculate that the relatively high permeability values in this study indicate fluid diffusion from highly pressurized source areas to lower pressure areas, which may have resulted from temporarily enhanced permeability due to the influence of the Tohoku-oki earthquake.

Chapter 4

Conclusion

In Chapter 2, the Matched Filter Analysis, applied using event-templates and continuous Hi-net waveform data, revealed 17 times more earthquakes than in the JMA catalog. I have also scrutinized continuous waveforms recorded by a local network to identify small and early local events.

The results show distinctive seismicity activation patterns. The seismicity about 10 km to the south, however, is shallower and shows a significantly stronger and early activation, while the epicentral region of the M_w6.2 earthquake is characterized by very sporadic activation during the 13 hours span, with two small foreshocks within one hour before the moderate event.

In particular, the southern locations where seismicity was activated during the passage of surface waves from the megathrust event are nearby a high fluid-temperature and fluid-flux geothermal hotspot. Other areas of early activation in the south are mildly geothermal. These observations, together with the overall episodic character of seismicity in the southern region, suggest geothermal fluid excitation as the underlying physical mechanism.

In Chapter 3, I obtained a detailed history of microseismicity in the hypocentral area of the M_w 6.2 event in the northern Nagano area by applying the MFT to data from a temporary dense network, which revealed 47 times more earthquakes than application of the MFT to the Hi-net dataset (see Chapter 2). I also searched Tohoku-oki aftershocks that triggered local events in the research area.

I identified two distinctive seismicity activation patterns. On the fault plane of the M_w 6.2 local event, most events were distributed along the dip or in a tight subcluster along strike in the immediate vicinity of the M_w 6.2 hypocenter. In particular, seismic migration occurred in a subcluster along strike toward the hypocenter, and intense activity was initiated during the passage of surface waves from a remote moderate earthquake that occurred about 40 min before the M_w 6.2 event and continued until the origin time of this local moderate event. This activity reflects the nucleation process of the M_w 6.2 local event. In contrast, about 5 km to the east, seismicity away from the fault of the M_w 6.2 event was relatively strong and swarm-like; the activity occurred in two depth regions, at depths of about 2 and 5 km, which coincide with high v_p/v_s regions. This activity is interpreted to have resulted from the diffusion of fluid through another fault system from at least two fluid sources, one at each depth.

In both areas, seismicity started after some delay from the origin time of the Tohoku-oki earthquake and immediately after the passage of surface waves from remote moderate-to-large aftershocks; sometimes activation occurred repeatedly during or immediately after subsequent remote aftershocks. Fluid flow which could induce these activations may have been facilitated dynamically or statically by the Tohoku-oki mainshock, but slight dynamic stress changes from remote aftershocks would have acted as the final trigger initiating local seismic activity by allowing to initiate fluid flow.

To summarize, I have analyzed the seismicity activated after the Tohoku-oki earthquake in Northern Nagano region in these chapters. I understood that the fluid drives the local earthquake activity of this area as a result of the flow prepared by the influence of Tohoku-oki earthquake and subsequent aftershocks. While I focused on a time scale of about half a day from the Tohoku-

oki earthquake and a specific local area located at Nagano-Niigata prefecture boundary, a previous study showed that remote triggering of seismicity widespread all over Japan and followed the occurrence of the 2011 M9.0 Tohoku-oki earthquake, at regions as far as Kyushu, at more than 1300 km distance from the Tohoku-oki epicenter (Miyazawa, 2011), and many of these epicenters are distributed in the volcanic and geothermal zones where the fluid excitation process seems to be dominant like the Northern Nagano area. Brenguier *et al.* (2014) showed that volcanic fluids have been pressurized in wide areas of NE Japan after the 2011 Tohoku-oki earthquake. Analyzing continuous waveforms recorded by Hi-net stations within 6 months before and after Tohoku-oki earthquake, they mapped crustal seismic velocity perturbations following M9.0 event and showed the remarkable velocity decrease in volcanic and geothermal regions, correlated to the amplitudes of seismic waves from Tohoku-oki mainshock. Given the above, the favorable condition for flowing fluid might be adjusted in the local crust by the impact of the Tohoku-oki earthquake, not only in Northern Nagano region but also in more wider areas in Japan.

For verifying the above-mentioned hypothesis, one question is how long favorable condition for flowing fluid lasts since the Tohoku-oki earthquake. Considering the possibility of local moderate- or large-scale earthquakes, or seismic swarms caused by fluid flow in local crust, investigating this matter is also important in estimating future seismic hazards all over Japan. The answer may be obtained by analyzing dynamically triggered seismic activity spreading over a wide area due to other distant large earthquakes occurring in several years after the Tohoku-oki earthquake.

Here, as an excellent opportunity to search for remote dynamic triggering in Japan, I briefly report on a relatively widespread activation of remote seismicity following the 2016 M7.3

Kumamoto earthquake, which occurred on the active strike-slip Futagawa fault, in the western part of Kyushu Island, Japan, at relatively shallow depth (12 km). By visually inspecting continuous waveform data at more than 1000 seismic stations all-over Japan, I detected locally triggered events and I correlated the observed remote triggering with the passage of surface waves from the Kumamoto earthquake.

In Figure A1 (Appendix), I show the location of seismic stations where remote earthquake triggering has been detected following the 2016 Kumamoto earthquake. The P-wave and S-wave arrivals of locally triggered events have been confirmed for most of the stations plotted in the figure. Most of the remotely triggered events in the Tohoku and Hokkaido regions, as well as close to Izu Peninsula, occur at or close to volcanoes, which suggests that the excitation of crustal fluids, by the passage of Rayleigh waves, played an important triggering role (Figure A2). Nevertheless, remote activation in other regions, like Noto Peninsula, occurred away from volcanoes. The relatively large-amplitude Love waves, enhanced by a source directivity effect during the Kumamoto earthquake, may have triggered seismicity on local active faults. The dynamic stresses in the areas where remote activation has been observed range from several kPa to tens of kPa, the thresholds being lower than in previous dynamic triggering cases for Japan (Harrington and Brodsky, 2006; Van der Elst and Brodsky, 2010); This might relate to the change in the local crustal conditions following the 2011 M9.0 Tohoku-oki earthquake in a wide range of Japan island and such changed condition might continue for several years at least.

However, to fully verify this hypothesis, more detailed studies are necessary. The occurrence of other similar large inland earthquakes in the future may help understand whether the “trigger-ability” in Japan has changed due to the 2011 Tohoku-oki earthquake.

Acknowledgements

I'm greatly indebted to Associate Professor Bogdan Enescu (Kyoto University) and Associate Professor Yuji Yagi (University of Tsukuba) for continuous support, guidance through the course of this study, preparing the thesis and related manuscript. I would like to thank Professor Kenichiro Hayashi and Associate Professor Koutaro Ujiie (University of Tsukuba) for valuable and constructive comments and for reading the manuscript. I'm grateful to Drs. Tetsuya Takeda (Ministry of Education, Culture, Sports, Science and Technology) for providing the data of 3D-velocity model in Northern Nagano region and his sincere comments. I am grateful to Senior Lecturer Toshiko Terakawa (Nagoya University), Professor Zhigang Peng (Georgia Institute of Technology), Professor Shinji Toda (Tohoku University) and Professor Xiaofeng Meng (University of Washington) for useful comments and advice. Professor Toshiaki Tsunogae (University of Tsukuba) and Dr. Akiko Tanaka (National Institute of Advanced Industrial Science and Technology) helped with the geothermal data. I'm grateful to Anca Opris (Graduate school of Life and Environmental sciences of Tsukuba) for checking the JMA earthquake catalog immediately after Kumamoto earthquake and contributing to the examination of the results. I gratefully acknowledge the work of past and present members of our laboratory. I used the earthquake catalogs provided by JMA and Hi-net, as well as the waveform data of Hi-net and F-Net networks. This study was supported by JSPS KAKENHI Grant Number 16J00635 (K. Shimojo). The text of this thesis was edited by English editing service operated by ELSS Co., Ltd.

Reference

Reference for Chapter 1

Brodsky, E. E., Roeloffs, D, Woodcock., I. Gall, and M. Manga (2003), A mechanism for sustained groundwater pressure changes induced by distant earthquakes, *J. Geophys. Res., 108, B82390, doi:10.1029/2002JB002321.*

Doi, I., and H. Kawakata (2012), A non-accelerating foreshock sequence followed by a short period of quiescence for a large inland earthquake, Geophys. Res. Lett., 39, L11308, doi:10.1029/2012GL051779.

Enescu, B., J. Mori, and M. Miyazawa (2007), Quantifying early aftershock activity of the 2004 mid-Niigata Prefecture earthquake (M_w6.6), J. Geophys. Res., 112, B04310, doi:10.1029/2006JB004629.

Enescu, B., Mori, J., Miyazawa, M., and Y. Kano (2009), Omori-Utsu law c-values associated with recent moderate earthquakes in Japan, Bull. Seismol. Soc. Am., 99, 2A, 884-891, doi: 10.1785/0120080211.

Enescu, B., S. Aoi, S. Toda, W. Suzuki, K. Obara, K. Shiomi, and T. Takeda (2012), Stress perturbations and seismic response associated with the 2011 M9.0 Tohoku-oki earthquake in and around the Tokai seismic gap, central Japan, *Geophys. Res. Lett., 39*, *L00G28, doi:10.1029/2012GL051839.*

Gomberg, J., P. A. Reasenberg, P. Bodin, and R.A. Harris (2001), Earthquake triggering by seismic waves following the Landers and Hector Mine earthquakes, Nature 411, 462-465

Harrington, R. M., and E. E. Brodsky (2006), The absence of remotely triggered seismicity in Japan, Bull. Seismol. Soc. Am., 96(3), 871–878, doi:10.1785/0120050076.

Hill, D. P., et al., Seismicity remotely triggered by the magnitude 7.3 Landers, California, earthquake, &'ience, 260, 1617-1623, 1993

Hirose, F., K. Miyaoka, N. Hayashimoto, T. Yamazaki, and M. Nakamura (2011), Outline of the 2011 off the Pacific coast of Tohoku Earthquake (Mw 9.0) — Seismicity: foreshocks, mainshock, aftershocks, and induced activity —, *Earth, Planets, Space, 63*, 513-518.

Ishibe, T., K. Shimazaki, K. Satake, and H. Tsuruoka (2011), Change in seismicity beneath the Tokyo metropolitan area due to the 2011 off the Pacific coast of Tohoku Earthquake, *Earth Planets Space, 63*, 731–735.

Kagan, Y. Y. (2004), Short-term properties of earthquake catalogs and models of earthquake source, *Bull. Seismol. Soc. Am.*, **94**, 1207–1228.

Kato, A., Obara, K., Igarashi, T., Tsuruoka, H., Nakagawa, S., and N. Hirata (2012), Propagation of Slow Slip Leading Up to the 2011Mw 9.0 Tohoku-Oki Earthquake, *Science*, *335*, 6069, 705--708, 2012.

Kato, A., J. Fukuda and K. Obara (2013), Response of seismicity to static and dynamic stress changes induced by the 2011 M9.0 Tohoku-Oki earthquake, Japan, *Geophys. Res. Lett., 40*, doi:10.1002/grl.50699.

Lengliné, O., B. Enescu, Z. Peng, and K. Shiomi (2012), Decay and expansion of the early aftershock activity following the 2011, Mw9.0 Tohoku earthquake, *Geophys. Res. Lett., 39*, L18309, doi:10.1029/2012GL052797.

Marsan, D. and B. Enescu (2012), Modeling the foreshock sequence prior to the 2011, MW9.0 Tohoku, Japan, earthquake, *J. Geophys. Res.*, 117, B06316, doi:10.1029/2011JB009039.

Miller, S. A., Collettini, C., Chiaraluce, L., Cocco, M., Barchi, M., Kaus, B.J.P., 2004. Aftershocks driven by a high-pressure CO2 source at depth. *Nature* 427, 724-727.

Miyazawa, M. (2011), Propagation of an earthquake triggering front from the 2011 Tohoku-Oki earthquake, Geophys. *Res. Lett., 38*, *L23307, doi:10.1029/2011GL049795.*

Miyazawa, M., and J. Mori (2005), Detection of triggered deep low-frequency events from the 2003 Tokachi-oki earthquake, Geophys, *Res. Lett.,* 32, L10307, doi:10.1029/2005GL022539

Muir-Wood, R. and King, G.C.P., 1993. Hydrologic signatures of earthquake strain, *J. Geophys. Res.*, 98, 22035-22068.

Nur, A., Booker, J. R, 1972. Aftershocks caused by pore fluid-flow. *Science* 175, 885-887

Obara, K. (2003), Time sequence of deep low-frequency tremors in the southwest Japan subduction zone: Triggering phenomena and periodic activity (in Japanese with English abstract), *J.Geogr*., 112, 837-849

Peng, Z., J. E. Vidale, and H. Houston (2006), Anomalous early aftershock decay rate of the 2004 Mw6.0 Parkfield, California, earthquake, Geophys. Res. Lett., 33, L17307, doi:10.1029/2006GL026744.

Peng, Z., and P. Zhao (2009), Migration of early aftershocks following the 2004 Parkfield earthquake, *Nature Geoscience*, 2, 877 – 881, doi:10.1038/ngeo697.

Prejean, S. G., Hill, D. P., Brodsky, E. E., Hough, S. E., Johnston, M. J. S., Malone, S. D., Oppenheimer, D. H., Pitt, A. M. and Richards-Dinger, K. B. 2004 Remotely triggered seismicity on the United States west coast following the Mw 7.9 Denali Fault earthquake Bull. Seismol. Soc. America, 94, S348-S359.

Sawazaki, K., and B. Enescu (2014), Imaging the high-frequency energy radiation process of a main shock and its early aftershock sequence: The case of the 2008 Iwate-Miyagi Nairiku earthquake, Japan, J. Geophys. Res., 119, 4729–4746, doi:10.1002/2013JB010539.

Shelly, D. R., G. C. Beroza, S. Ide, and S. Nakamula (2006), Lowfrequency earthquakes in Shikoku, Japan, and their relationship to episodic tremor and slip, Nature, 442, 188 – 191, doi:10.1038/nature04931

Sibson, R. H., Rupture nucleation on unfavorably oriented faults, Bull. Seismo!. Soc. Ant., 80, 1580-1604, 1990.

Terakawa, T., C. Hashimoto, and M. Matsu'ura (2013), Changes in seismic activity following the 2011 Tohoku-oki earthquake: Effects of pore fluid pressure, *Earth Planet. Sci. Lett., 365*, 17-24, doi: 10.1016/j.epsl.2013.01.017.

Yukutake, Y., R. Honda, M. Harada, T. Aketagawa, H. Ito, and A. Yoshida (2011), Remotely-triggered seismicity in the Hakone volcano following the 2011 off the Pacific coast of Tohoku Earthquake, *Earth Planets Space, 63*, 737-740.

References for Chapter 2

Bouchon, M., H. Karabulut, M. Aktar, S. Özalaybey, J. Schmittbuhl, and M.-P. Bouin (2011), Extended nucleation of the 1999 Mw7.6 Izmit earthquake, Science, 331, 877 − 880, doi:10.1126/science.1197341.

Brodsky, E. E., Roeloffs, D, Woodcock., I. Gall, and M. Manga (2003), A mechanism for sustained groundwater pressure changes induced by distant earthquakes, *J. Geophys. Res., 108, B82390, doi:10.1029/2002JB002321.*

Das, S., and C. H. Scholz, Theory of time-dependent rupture in the Earth, J. Geophys. Res., 86, 6039-6051, 1981.

Dieterich, J. (1994), A constitutive law for rate of earthquake production and its application to earthquake clustering, J. Geophys. Res., 99(B2), 2601–2618, doi:10.1029/93JB02581.

Enescu, B., J. Mori, and M. Miyazawa (2007), Quantifying early aftershock activity of the 2004 mid-Niigata Prefecture earthquake (M_w6.6), J. Geophys. Res., 112, B04310, doi:10.1029/2006JB004629.

Enescu, B., T. Takeda, Y. Asano, K. Obara and S. Sekiguchi (2011), Estimation of a feasible initial velocity model and earthquake locations for seismic tomography in the Niigata region, Japan Geoscience Union Meeting, Makuhari, Chiba, May 22-27.

Fukutomi, T. (1961), On the possibility of volcanic hot springs of meteoric and magmatic origin and their probable life span, Journal of the Faculty of Science, Hokkaido University, Series 7, Geophysics, 1, 223-266.

Geological Survey of Japan (2009), Geothermal potential map of Japan, CD-ROM version. Digital Geological Map GT-4.

Hill, D.P. (2012), Dynamic stresses, Coulomb failure, and remote triggering – corrected, Bull. Seismol. Soc. Am., 102, 2313-2336, doi:10.1785/0120120085.

Hill, D.P., and S. Prejean (2007), Dynamic triggering, in H. Kanamori (ed.) V. 4 Earthquake Seismology, pp. 258-288, Treatise on Geophysics (G. Schubert, Editor in chief), Elsevier, Amsterdam.

Jaeger, J. C., and N. G. W. Cook (1979), *Fundamentals of Rock Mechanics*, 3rd ed., Chapman and Hall, New York.

Kato, A., Obara, K., Igarashi, T., Tsuruoka, H., Nakagawa, S., and N. Hirata (2012), Propagation of Slow Slip Leading Up to the 2011Mw 9.0 Tohoku-Oki Earthquake, *Science*, *335*,

6069, 705--708, 2012.

King, G. C. P., R. Stein, and J. Lin (1994), Static stress changes and the triggering of earthquakes, *Bull. Seismol. Soc. Am.*, 84, 935-953.

Kiser, E., and M. Ishii (2013), Hidden aftershocks of the 2011 Mw 9.0 Tohoku, Japan earthquake imaged with the backprojection method, *J. Geophys. Res.*, 118, 5564–5576, doi:10.1002/2013JB010158.

Kumazawa, T., and Y. Ogata (2013), Quantitative description of induced seismic activity before and after the 2011 Tohoku-Oki earthquake by nonstationary ETAS models, *J. Geophys. Res.*, 118, 6165–6182, doi:10.1002/2013JB010259.

Lengliné, O., B. Enescu, Z. Peng, and K. Shiomi (2012), Decay and expansion of the early aftershock activity following the 2011, Mw9.0 Tohoku earthquake, *Geophys. Res. Lett., 39*, L18309, doi:10.1029/2012GL052797.

Maeda, T., K. Obara, T. Furumura, and T. Saito (2011), Interference of long-period seismic wavefield observed by the dense Hi-net array in Japan, *J. Geophys. Res.*, 116, B10303, doi:10.1029/2011JB008464.

Marsan, D. and B. Enescu (2012), Modeling the foreshock sequence prior to the 2011, MW9.0 Tohoku, Japan, earthquake, *J. Geophys. Res.*, 117, B06316, doi:10.1029/2011JB009039.

Meng, X., X. Yu, Z. Peng, and B. Hong (2012), Detecting earthquakes around Salton Sea following the 2010 Mw7.2 El Mayor-Cucapah earthquake using GPU parallel computing, *Procedia Comput. Sci.*, *9*, 937–946, doi:10.1016/j.procs.2012.04.100.

Okada, T., K. Yoshida, S. Ueki, J. Nakajima, N. Uchida, T. Matsuzawa, N. Umino, A. Hasegawa, and Group for the aftershock observations of the 2011 off the Pacific coast of Tohoku Earthquake (2011), Shallow inland earthquakes in NE Japan possibly triggered by the 2011 off

the Pacific coast of Tohoku Earthquake, *Earth Planets Space*, 63, 749-754, doi:10.5047/eps.2011.06.027.

Parsons, T., C. Ji, and E. Kirby (2008), Stress changes from the 2008 Wenchuan earthquake and increased hazard in the Sichuan basin, Nature, 454, 509−510, doi:10.1038/nature07177

Peng, Z., J. E. Vidale, and H. Houston (2006), Anomalous early aftershock decay rate of the 2004 Mw6.0 Parkfield, California, earthquake, Geophys. Res. Lett., 33, L17307, doi:10.1029/2006GL026744.

Peng, Z., J.E. Vidale, A.G. Wech, R.M. Nadeau, and K.C. Kreager (2009), Remote triggering of tremor along the San Andreas Fault in Central California, J. Geophys. Res., 114, B00A06, doi:10.1029/2008JB006049.

Peng, Z., and P. Zhao (2009), Migration of early aftershocks following the 2004 Parkfield earthquake, *Nature Geoscience*, 2, 877 – 881, doi:10.1038/ngeo697.

Pollitz, F. F., R. Bürgmann, and P. Banerjee (2011), Geodetic slip model of the 2011 M9.0 Tohoku earthquake, *Geophys. Res. Lett.*, 38, L00G08, doi:10.1029/2011GL048632.

Sawazaki, K., and B. Enescu (2014), Imaging the high-frequency energy radiation process of a main shock and its early aftershock sequence: The case of the 2008 Iwate-Miyagi Nairiku earthquake, Japan, J. Geophys. Res., 119, 4729–4746, doi:10.1002/2013JB010539.

Sekiguchi, S., T. Takeda, Y. Asano, B. Enescu, K. Shiomi, M. Matsubara, H. Kimura, T. Matsumoto, T. Saito, T. Matsuzawa, H. Kawabata, and T. Koda, (2013), Onshore earthquake observations, *The Annual Report of the Multidisciplinary Research Project for Investigations in the High Strain Rate Zone of Japan*, Research and Development Bureau of MEXT, Japan, and NIED, (Eds.), 11-49.

Shearer, P. (2009), Introduction to Seismology, 2nd Edition, *Cambridge University Press*.

Sturtevant, B., H. Kanamori, and E.E. Brodsky (1996), Seismic triggering by rectified diffusion in geothermal systems, *J. Geophys. Res.*, 101, B1125269-25282, doi:10.1029/96JB02654.

Tanaka, A. (2004), Geothermal gradient and heat flow data in and around Japan (II): Crustal thermal structure and its relationship to seismogenic layer, *Earth Planets Space*, 56, 1195-1199.

Suzuki, W., S. Aoi, H. Sekiguchi, and T. Kunugi, Rupture process of the 2011 Tohoku-Oki mega-thrust earthquake (M9.0) inverted from strong-motion data, *Geophys. Res. Lett.*, 38, L00G16, doi:10.1029/2011GL049136, 2011.

Tanaka, A., M. Yamano, Y. Yano, and M. Sasada (2004), Geothermal gradient and heat flow data in and around Japan (I): Appraisal of heat flow from geothermal gradient data, *Earth Planets Space*, 56, 1191-1194.

Terakawa, T., C. Hashimoto, and M. Matsu'ura (2013), Changes in seismic activity following the 2011 Tohoku-oki earthquake: Effects of pore fluid pressure, *Earth Planet. Sci. Lett., 365*, 17-24, doi: 10.1016/j.epsl.2013.01.017.

Yagi, Y., and Y. Fukahata (2011), Rupture process of the 2011 Tohoku-oki earthquake and absolute elastic strain release, *Geophys. Res. Lett.*, 38, L19307, doi:10.1029/2011GL048701.

Zhang, H., and C. H. Thurber (2003), Double-Difference tomography: the method and its application to the Hayward fault, California, *Bull. Seismol. Soc. Am, 93*, 1875-1889.

References for Chapter 3

Aiken, C., and Z. Peng (2014), Dynamic triggering of microearthquakes in three geothermal/volcanic regions of California, J. Geophys. Res. Solid Earth, 119, 6992–7009, doi:10.1002/2014JB011218.

Antonioli, A., D. Piccinini, L. Chiaraluce, and M. Cocco (2005), Fluid flow and seismicity pattern: Evidence from the 1997 Umbria-Marche (central Italy) seismic sequence, Geophys. Res. Lett., 32, L10311, doi:10.1029/2004GL022256.

Bower, D.R. and Heaton, K.C.（1978）: Response of an aquifer near Ottawa to tidal forcing and the Alaskan earthquake of 1964. Canadian Journal of Earth Sciences, 15, 331-340.

Brodsky, E. E., E. Roeloffs, D. Woodcock, I. Gall, and M. Manga (2003), A mechanism for sustained water pressure changes induced by distant earthquakes, J. Geophys. Res., 108(B8), 2390, doi:10.1029/2002JB002321

Das, S., and C. H. Scholz (1981), Theory of time-dependent rupture in the Earth, J. Geophys. Res., 86(B7), 6039–6051, doi:10.1029/JB086iB07p06039.

Dieterich, J. (1994), A constitutive law for rate of earthquake production and its application to earthquake clustering, *J. Geophys. Res.*, **99**(B2), 2601–2618, doi:10.1029/93JB02581.

Elkhoury, J. E., E. E. Brodsky, and D. C. Agnew (2006), Seismic waves increase permeability, *Nature*, **441**(7097), 1135–1138, doi:10.1038/nature04798.

Enescu B, Shimojo K, Opris A, Yagi Y (2016) Remote triggering of seismicity at Japanese volcanoes following the 2016 M7.3 Kumamoto earthquake. Earth Planets Space 68:165. doi:10.1186/s40623-016-0539-5

Geological Survey of Japan (2009), Geothermal potential map of Japan, CD-ROM version. Digital Geological Map GT-4.

Geospatial Information Authority of Japan, 2011a. Crustal deformation associated with the 2011 Off the Pacific Coast of Tohoku Earthquake on March 11, 2011. 〈http://www.gsi.go.jp/chibankansi/chikakukansi40005.html〉 (in Japanese)

Hainzl, S., and Y. Ogata (2005), Detecting fluid signals in seismicity data through statistical earthquake modeling, J. Geophys. Res., 110, B05S07, doi:10.1029/2004JB003247.

Hill, D. P., et al., Seismicity remotely triggered by the magnitude 7.3 Landers, California, earthquake, &'ience, 260, 1617-1623, 1993

Ikeda, Y., Imaizumi, T., Hirakawa, K., Miyauchi, T. and Sato, H. (2002): *Atlas of Quaternary Thrust Faults in Japan*. University of Tokyo Press.

INGEBRITSEN, S. E. and MANNING, C. E. (2010), Permeability of the continental crust: dynamic variations inferred from seismicity and metamorphism. Geofluids, 10: 193–205. doi:10.1111/j.1468-8123.2010.00278.x

Jaeger, J. C., and N. G. W. Cook (1979), *Fundamentals of Rock Mechanics*, 3rd ed., Chapman and Hall, New York.

Kato, A., J. Fukuda, S. Nakagawa, and K. Obara (2016), Foreshock migration preceding the 2016 M_w 7.0 Kumamoto earthquake, Japan, Geophys. Res. Lett., 43, 8945–8953, doi:10.1002/2016GL070079.

Katsumata, K., M. Kosuga, H. Katao, T. Yamada, A. Kato and the Research Group for the Joint Seismic Observations the Research Group for the Joint Seismic Observations, Focal mechanisms and stress field in the Nobi fault area, central Japan, Earth Planets Space, 67, 99, doi 10.1186/s40623-015-0275-2, (2015).

King, C.-Y., S. Azuma, G. Igarashi, M. Ohno, H. Saito, and H. Wakita (1999), Earthquake-related water-level changes at 16 closely clustered wells in Tono, central Japan, J. Geophys. Res., 104(B6), 13073–13082, doi:10.1029/1999JB900080.

Kinoshita, C., Y. Kano, and H. Ito (2015), Shallow crustal permeability enhancement in central Japan due to the 2011 Tohoku earthquake, Geophys. Res. Lett., 42, 773–780, doi:10.1002/2014GL062792.

Kitagawa, Y. and Koizumi, N. (2011) Changes in groundwater levels, groundwater pressures and discharge rates a day after the 2011 Off the Pacific Coast of Tohoku Earthquake(M9.0) : Report on Active Fault and Paleoearthquake Researches, AISTGSJ, 11, 309-318. (in Japanese).

L Hardebeck, Jeanne & M Shearer, Peter. (2002). A New Method for Determining First-Motion Focal Mechanisms. Bulletin of the Seismological Society of America. 92. 2264-2276. 10.1785/0120010200.

Liu, W., and M. Manga (2009), Changes in permeability caused by dynamic stresses in fractured sandstone, Geophys. Res. Lett., 36, L20307, doi:10.1029/2009GL039852.

Lohman, R. B., and J. J. McGuire (2007), Earthquake swarms driven by aseismic creep in the Salton Trough, California, J. Geophys. Res., 112, B04405, doi:10.1029/2006JB004596.

Muir-Wood, R. and King, G.C.P., 1993. Hydrologic signatures of earthquake strain, *J. Geophys. Res.*, 98, 22035-22068.

Noir, J., E. Jacques, S. Bekri, P. M. Adler, P. Tapponier, and G. C. P. King (1997), Fluid flow triggered migration of events in the 1989 Dobi earthquake sequence of central Afar, Geophys. Res. Lett., 24, 2335 – 2338.

Okada, T., K. Yoshida, S. Ueki, J. Nakajima, N. Uchida, T. Matsuzawa, N. Umino, A. Hasegawa, Group for the aftershock observations of the 2011 off the Pacific coast of Tohoku

Earthquake, 2011, Shallow inland earthquakes in NE Japan possibly triggered by the 2011 off the Pacific coast of Tohoku Earthquake, Earth Planets and Space, **63**, 749-754, doi:10.5047/eps.2011.06.027.

Okada, T., T. Matsuzawa, N. Umino, K. Yoshida, A. Hasegawa, H. Takahashi, T. Yamada, M. Kosuga, T. Takeda, A. Kato, T. Igarashi, K. Obara, S. Sakai, A. Saiga, T. Iidaka, T. Iwasaki, N. Hirata, N. Tsumura, Y. Yamanaka, T. Terakawa, H. Nakamichi, T. Okuda, S. Horikawa, H. Katao, T. Miura, A. kubo, T. Matsushima, K. Goto, H. Miyamachi, Hypocenter migration and crustal seismic velocity distribution observed for the inland earthquake swarms induced by the 2011 Tohoku-Oki, Geofluids, 15(1-2), 293-309, 2015.

Peng, Z., and P. Zhao (2009), Migration of early aftershocks following the 2004 Parkfield earthquake, *Nature Geoscience*, 2, 877 – 881, doi:10.1038/ngeo697.

Rojstaczer, S., S. Wolf, and R. Michel (1995), Permeability enhancement in the shallow crust as a cause of earthquake-induced hydrological changes, *Nature*, **373**, 237–239.

Scholz CH (2002) The Mechanics of Earthquakes and Faulting (Cambridge Univ. Press, Cambridge, UK), 2nd Ed.

Sekiguchi, S., T. Takeda, Y. Asano, B. Enescu, K. Shiomi, M. Matsubara, H. Kimura, T. Matsumoto, T. Saito, T. Matsuzawa, H. Kawabata, and T. Koda, (2013), Onshore earthquake observations, *The Annual Report of the Multidisciplinary Research Project for Investigations in the High Strain Rate Zone of Japan*, Research and Development Bureau of MEXT, Japan, and NIED, (Eds.), 11-49.

Shelly, D. R., G. C. Beroza, S. Ide, and S. Nakamula (2006), Low frequency earthquakes in Shikoku, Japan, and their relationship to episodic tremor and slip, Nature, 442, 188 – 191, doi:10.1038/nature04931

Stein RS. The role of stress transfer in earthquake occurrence. Nature. 1999;402:605–609.

Sturtevant, B., H. Kanamori, and E.E. Brodsky (1996), Seismic triggering by rectified diffusion in geothermal systems, *J. Geophys. Res.*, 101, B1125269-25282, doi:10.1029/96JB02654.

Terakawa, T., C. Hashimoto, and M. Matsu'ura (2013), Changes in seismic activity following the 2011 Tohoku-oki earthquake: Effects of pore fluid pressure, *Earth Planet. Sci. Lett., 365*, 17-24, doi: 10.1016/j.epsl.2013.01.017.

Terakawa, T., Matsu'ura, M., 2010. The 3-D tectonic stress fields in and around Japan inverted from centroid moment tensor data of seismic events. Tectonics 29, http://dx.doi.org/10.1029/2009TC002626.

Uchide, T., K. Imanishi, and R. Matsushita (2015), Campaign seismic observation for estimation of crustal stress regime in northeastern Yamanashi prefecture, Japan, *Annual Report on Active Fault and Paleoearthquake Researches*, 15, 211-233 (*in Japanese with English abstract*).

Urabe, T., and S. Tsukada, win-A Workstation program for processing waveform data from microearthquake networks (abstract), Seismol. Soc. Jpn., 2, 1992

M. Ukawa, M. Ishida, S. Matsumura, K. Kasahara Hypocenter determination method of the Kanto-Tokai observational network for microearthquakesRes. Notes. Nat. Res. Cent. Disaster Prev., 53 (1984), pp. 1-88

van der Elst, N. J., and E. E. Brodsky (2010), Connecting near-field and far-field earthquake triggering to dynamic strain, J. Geophys. Res., 115, B07311, doi:10.1029/2009JB006681.

Yagi, Y., and Y. Fukahata (2011), Rupture process of the 2011 Tohoku-oki earthquake and

absolute elastic strain release, *Geophys. Res. Lett.*, 38, L19307, doi:10.1029/2011GL048701.

Yagi, Y., R. Okuwaki, B. Enescu, S. Hirano, Y. Yamagami, S. Endo, and T. Komoro (2014), Rupture process of the 2014 Iquique Chile Earthquake in relation with the foreshock activity, Geophys. Res. Lett., 41, 4201–4206, doi:10.1002/2014GL060274.

Zhang, H., and C. H. Thurber (2003), Double-Difference tomography: the method and its application to the Hayward fault, California, *Bull. Seismol. Soc. Am, 93*, 1875-1889.

Reference for Chapter 4

Miyazawa, M. (2011), Propagation of an earthquake triggering front from the 2011 Tohoku-Oki earthquake, Geophys. *Res. Lett., 38*, *L23307, doi:10.1029/2011GL049795.*

Brenguier, F., M. Campillo, T. Takeda, Y. Aoki, N.M. Shapiro, X. Briand, K. Emoto, and H. Miyake, Mapping pressurized volcanic fluids from induced crustal seismic velocity drops, Science, 345 (6192), 80-82, doi:10.1126/science.1254073, 2014

van der Elst, N. J., and E. E. Brodsky (2010), Connecting near-field and far-field earthquake triggering to dynamic strain, J. Geophys. Res., 115, B07311, doi:10.1029/2009JB006681.

Harrington, R. M., and E. E. Brodsky (2006), The absence of remotely triggered seismicity in Japan, Bull. Seismol. Soc. Am., 96(3), 871–878, doi:10.1785/0120050076.

Appendix

Visual inspection of locally triggered events immediately after Kumamoto earthquake

I have processed waveform data recorded at high-sensitivity Hi-net and broadband F-net stations, operated by the National Institute for Earth Science and Disaster Resilience (NIED), as well Japan Meteorological Agency (JMA) stations located at volcanoes throughout Japan. Moreover, we have also processed waveform data recorded by the V-net network, operated by NIED, at Japanese volcanoes. In total, I have downloaded and processed the continuous waveform data at more than 1000 seismic stations all-over Japan.

I have first downloaded waveform data recorded within one hour before and after the mainshock occurrence time (April 16, 2016; 01:25:05, Japan Standard Time) and corrected adequately for instrument response.

In order to detect locally triggered events, I use a two-way Butterworth band-pass filter in the frequency range 10 – 30 Hz. As I have experimented before (Chapter 2 and 3), such a filtering ensures good detection of locally triggered remote events, while avoiding at least in part high-frequency noise. In many cases, the remote detections were confirmed by identifying the P- and S-wave arrival times of the triggered events.

In order to correlate the observed remote triggering with the passage of surface waves from the

Kumamoto earthquake, I have used F-net and Hi-net data in the frequency range 0.01 – 0.2 Hz (5 – 100s). In this respect, the Hi-net data was processed using the approach of Maeda et al. (2011), who showed that the Hi-net waveforms can be successfully used to retrieve long-period ground motions after applying an appropriately designed recursive filter.

I show in Figure A1 the location of seismic stations where remote earthquake triggering has been detected following the 2016 Kumamoto earthquake. The P-wave and S-wave arrivals of locally triggered events have been confirmed for most of the stations plotted in the figure. Stations where I could not be sure on the P- and S-wave arrivals, due to a rather poor signal-to-noise ratio (S/N), are shown in light colors. The S/N for the unambiguous wave arrivals had a median of 7.5 and minimum of 1.6 (smaller values were considered unreliable after careful visual inspection of seismograms). I have also eliminated, after visual inspection, spike-like signals that were considered to be noise rather than locally triggered events. In addition, stations located in areas where the "background seismicity" was masking the correlation of local seismicity with the passage of the mainshock surface waves, were not considered in the analysis. In other words, all the selected cases correspond to visually sharp seismicity activations (at rates at least few times higher than the background). The (S-P) time is up to a few seconds for most of the remote events, which confirms that they occur in the vicinity of the seismic stations where the detection was made.

Further support for the dynamic character of the triggered seismicity comes from Figure A2.

Figure A2a shows the high-frequency (10 – 30 Hz) filtered waveforms recorded at selected, but representative stations in Figure A1. The gray reverse triangles show the approximate arrival time of Rayleigh waves assuming a nominal, typical phase velocity of 3.5 km/s (e.g., Aiken et al., 2013). Remotely triggered events can be identified as sudden increases of the high-frequency waveform amplitudes occurring at progressively later times, function of epicentral distance.

Figure A2b shows the low-frequency vertical seismograms (0.01 – 0.2 Hz) recorded at broad-band F-net stations (Figure A1). These F-net stations were the closest available from the Hi-net stations used in Figure A2a. The gray circles indicate events identified on the high-frequency seismograms in Figure A2a. Note that these events are plotted at the same epicentral distances as the recording Hi-net stations, at times corresponding to their P-wave arrival at the corresponding station. Since the (S-P) times of the detected events are mostly up to about 3 s (usually 1-2 s), the distance-related uncertainties are up to ~25 km. Most of the detected remote events occur only during the larger surface wave (Rayleigh) phases, but in some cases (station N.NKNH, Figure 2a) the activation continues for longer times.

As one can notice in Figure A2b, there is a good agreement between the arrival of surface waves (Rayleigh waves) from the Kumamoto earthquake and the remotely triggered events. It is hard however to judge whether Rayleigh waves or Love waves (that can be identified on transverse-component, low frequency seismograms – figure not shown) or both are responsible for the triggering.

Reference

Aiken, C., and Z. Peng (2014), Dynamic triggering of microearthquakes in three geothermal/volcanic regions of California, J. Geophys. Res. Solid Earth, 119, 6992–7009, doi:10.1002/2014JB011218.

Maeda, T., K. Obara, T. Furumura, and T. Saito (2011), Interference of long-period seismic wavefield observed by the dense Hi-net array in Japan, *J. Geophys. Res.*, 116, B10303, doi:10.1029/2011JB008464.

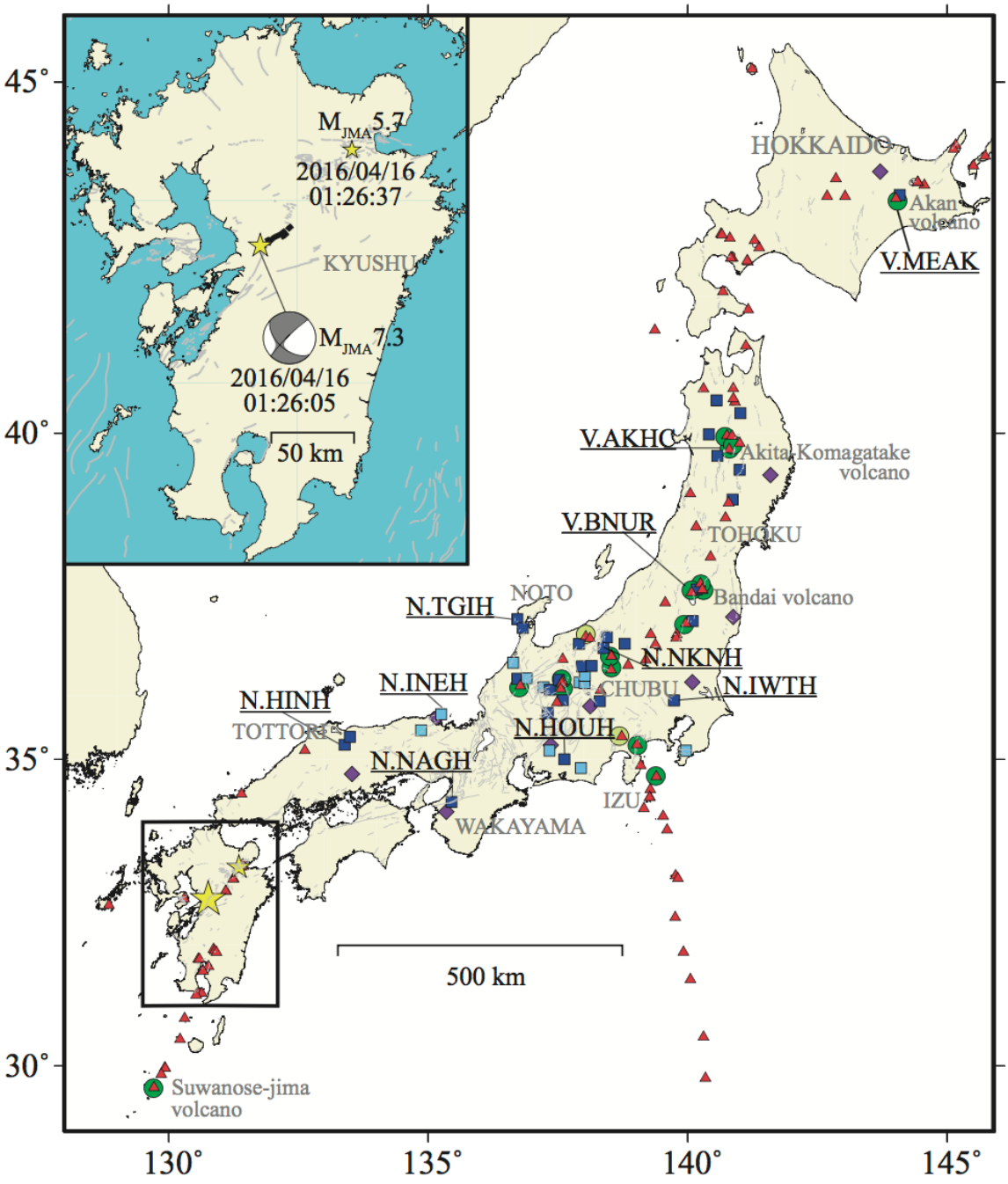

Figure A1. Map showing the seismic stations where remote triggering has been observed after the Kumamoto earthquake. The stations of JMA network located at Quaternary active volcanoes, are plotted as green circles, while the Hi-net (NIED) seismic stations are plotted as blue rectangles. Lighter colors indicate stations where the remote triggering occurred with less confidence (see text for additional explanations). The F-net stations used in Figure A2b are shown as purple diamonds. Stations with names written nearby, belonging to the Hi-net and JMA networks, are those used in Figure A2a. The red triangles and gray lines indicate volcanoes and active faults, respectively. The name of some regions in Japan is indicated in gray, upper-case letters; the name of volcanoes close to which remote earthquake triggering has been observed is also indicated (gray letters). The two yellow stars (in the map and inset) indicate the M7.3 earthquake and one of its immediate larger aftershocks in Oita prefecture, occurred towards NE. The inset indicates the mechanism of the mainshock (F-net, NIED), its occurrence time and magnitude, as well as its source fault.

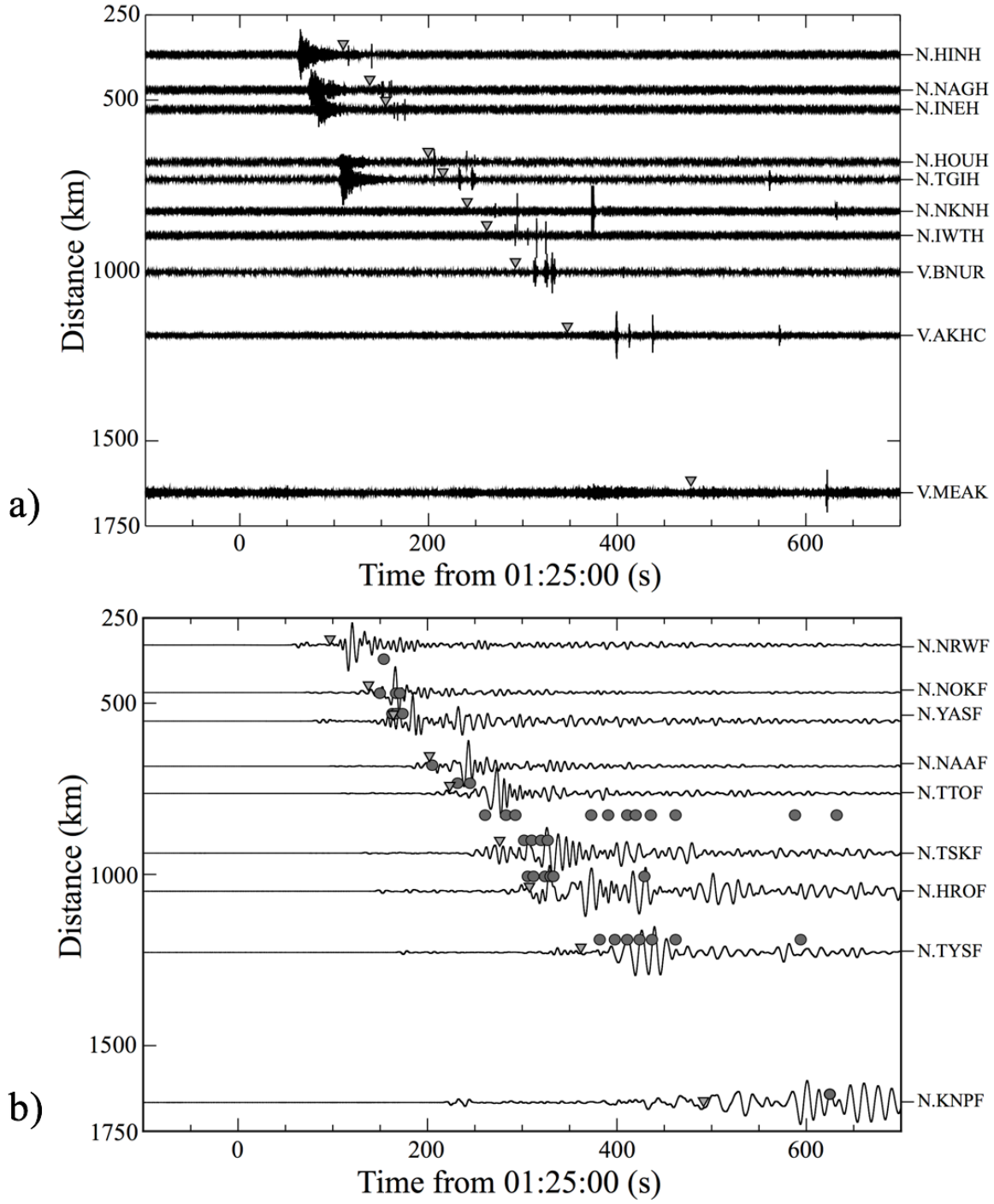

Figure A2. Remote earthquake triggering during the passage of surface waves. (a) Continuous velocity waveforms observed at Hi-net and JMA stations (vertical components), showing remote triggering due to the Kumamoto earthquake. The waveforms are band-pass filtered in the frequency-range 10 – 30 Hz and normalized to the maximum value on each seismogram. They are ordered function of epicentral distance, with distance increasing from up to down. Time is relative to the 01:25:00, on April 16, 2016 (i.e., the occurrence time of the Kumamoto earthquake). The name of each recording station is indicated on the right of the plot. (b) Low-frequency vertical-component seismograms (0.01 – 0.2 Hz) observed at F-net stations located closely to the Hi-net stations in (a), ordered function of epicentral distance and normalized. The gray circles indicate P-wave arrival times of remotely triggered earthquakes, as observed at the Hi-net stations shown in (a). Gray inverted triangles in both a) and b) indicate the arrival of Rayleigh waves, for a phase velocity of 3.5 km/s.